Friedrich-Alexander-Universität
Technische Fakultät

DLR

Shared Autonomy for an Intuitive Human-Robot Interface Assisting the Elderly in Activities of Daily Living

Comparing Shared Autonomy Control Modes to Identify Optimal Strategies for Grasping and Manipulation Tasks

at Friedrich-Alexander-Universität Erlangen-Nürnberg
at the Department of Artificial Intelligence in Biomedical Engineering
Assistive Intelligent Robotics Lab

in collaboration with the The German Aerospace Center (DLR)
(Institute of Robotics and Mechatronics)

Principal Supervisor:	Prof. Claudio Castellini (PhD)
Associate Supervisor:	Hannah Braun, Werner Friedl Silvana Miranda Montenegro, Marek Sierotowicz
Presented by:	Jonas Fischer jonas.f.fischer@fau.de 22650511
Submission:	1st May 2025

Declaration of Academic Integrity

Hiermit versichere ich, Jonas Fischer 22650511, die vorgelegte Arbeit selbstständig und ohne unzulässige Hilfe Dritter sowie ohne die Hinzuziehung nicht offengelegter und insbesondere nicht zugelassener Hilfsmittel angefertigt zu haben. Die Arbeit hat in gleicher oder ähnlicher Form noch keiner anderen Prüfungsbehörde vorgelegen und wurde auch von keiner anderen Prüfungsbehörde bereits als Teil einer Prüfung angenommen.

Die Stellen der Arbeit, die anderen Quellen im Wortlaut oder dem Sinn nach entnommen wurden, sind durch Angaben der Herkunft kenntlich gemacht. Dies gilt auch für Zeichnungen, Skizzen, bildliche Darstellungen sowie für Quellen aus dem Internet.

Mir ist insbesondere bewusst, dass die Nutzung künstlicher Intelligenz verboten ist, sofern diese nicht ausdrücklich als Hilfsmittel von dem Prüfungsleiter bzw. der Prüfungsleiterin zugelassen wurde. Dies gilt insbesondere für Chatbots (insbesondere ChatGPT) bzw. allgemein solche Programme, die anstelle meiner Person die Aufgabenstellung der Prüfung bzw. Teile derselben bearbeiten könnten.

Des Weiteren ist mir bekannt, dass die gemeinsame Bearbeitung der Aufgabenstellung mit anderen Personen in einem Raum oder mithilfe sozialer Medien eine unzulässige Hilfe Dritter im o.g. Sinne darstellt, wenn nicht ausdrücklich Gruppenarbeit vorgesehen ist. Jeder Austausch mit anderen Personen mit Ausnahme von Prüfenden und Aufsichtführenden während der Prüfungszeit über Aufbau oder Inhalte der Prüfung oder Informationen (z.B. Quellen) ist unzulässig. Gleiches gilt für den Versuch der jeweiligen Handlung.

Verstöße gegen die o.g. Regeln sind als Täuschung bzw. Täuschungsversuch zu qualifizieren und führen zu einer Bewertung der Prüfung mit nicht bestanden.

Erlangen, 16.04.2025

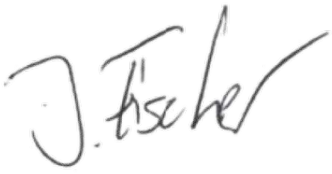

Jonas Fischer

Abstract

This thesis investigates shared autonomy as a key approach for intuitive human robot interaction to support elderly individuals in performing activities of daily living (ADL). The aim of the study was to find out which of the proposed control modes assists best for grasping and manipulation tasks.

After reviewing state of the art shared autonomy methods across various robotic interfaces, two shared autonomy approaches were developed, an active constraint (AC) and a weighted sum (WS) based framework.

Several subsystems were integrated into a unified system combining motion and hand pose intent detection. Therefore, inertial measurement units and surface electromyography were utilized respectively, as well as DLR grippers, DLR Fingertac for vibration feedback and the DLR light weight robot.

A user study with 12 participants (age of 27.3 ± 6.8 years) was conducted, evaluating three different modes, fully teleoperation (Teleop), AC and WS. Objective metrics were measured, such as task completion time, positioning accuracy, and traveled distances. Moreover, participants completed subjective measures using NASA Task Load Index and the Virtual Embodiment Questionnaire.

Objective and subjective results show that AC is the best suited form of shared autonomy assistance. AC significantly reduced mental and physical demand, especially in the demanding task compared to Teleop and AC. These findings highlight the advantages of AC, especially for the target group of elderly users.

Future work could include hardware and software improvements, further refinement of indexing and control robustness, and a focused user study with elderly participants. Overall, this thesis demonstrates the potential of shared autonomy to enhance robotic assistance in ADL for aging populations.

Abstract

Diese Arbeit untersucht geteilte Autonomie als einen vielversprechenden Ansatz für eine intuitive Mensch-Roboter-Interaktion, um ältere Menschen bei der Ausführung alltäglicher Aktivitäten zu unterstützen. Das Ziel der Studie war es herauszufinden, welche der vorgestellten Kontroll Modi, am besten für Greif- und Manipulaitonsaufgaben geeignet ist.

Nach einer Übersicht über den Stand der Technik im Bereich der geteilte Autonomie über verschiedene robotische Schnittstellen hinweg wurden zwei Ansätze entwickelt: ein aktiver Einschränkungsmodus (Active Constraint (AC)) und ein auf gewichteter Summe basierender Modus (Weighted Sum (WS)). Folgende Teilsysteme wurden in ein einheitliches System integriert, die Bewegungs- und Handposen-Erkennung mittels inertiale Messeinheiten und Oberflächen-Elektromyographie, DLR-Greifer, DLR Fingertac zur Vibrationsrückmeldung, sowie den DLR Leichtbauroboter. Die entwickelten Frameworks wurden zunächst in der Simulation getestet und auf das reale Robotersystem übertragen.

Eine Nutzerstudie mit 12 Teilnehmenden (im Alter von 27.3 ± 6.8 Jahren) wurde durchgeführt, in der die drei verschiedene Modi evaluiert wurden: vollständige Teleoperation (Teleop), AC und WS. Die Evaluation erfolgte anhand objektiver Metriken wie Aufgabenbearbeitungszeit, Positionierungsgenauigkeit und zurückgelegter Strecken sowie subjektiver Messungen mit dem NASA Task Load Index und dem Virtual Embodiment Questionnaire, um die am besten geeignete geteilte-Autonomie-Unterstützung für Greif- und Manipulationsaufgaben bei der entwickelten intuitiven Schnittstelle zu ermitteln.

Objektive und subjektive Ergebnisse zeigen, dass AC die am besten geeignete Form der Unterstützung mittels geteilter Autonomie darstellt. AC reduzierte die kognitiven und physischen Anforderungen signifikant, insbesondere bei der herausfordernden Aufgabe im Verlgeich zu Teleop und WS. Diese Befunde unterstreichen die Vorteile von AC, vor allem für die Zielgruppe älterer Nutzer.

Zukünftige Arbeiten könnten Hardware- und Softwareverbesserungen, eine weitergehende Verfeinerung der Indizierung und eine robustere Steuerung sowie eine gezielte Nutzerstudie mit älteren Teilnehmenden beinhalten. Insgesamt zeigt diese Arbeit das Potenzial von geteilter Autonomie auf, um robotische Assistenzsysteme zur Unterstützung älterer Menschen im Alltag zu verbessern.

Contents

Figures

Tables

1 Introduction

In this thesis shared autonomy frameworks are developed and evaluated to assist elderly in Activities of Daily Living (ADL), in particular in the kitchen for tasks like unloading a dishwasher or preparing a breakfast table.

Autonomy is a multifaceted concept that has been discussed across various fields, including morality, politics, psychology, and engineering. According to the Oxford English Dictionary, autonomy is defined as follows: "The condition or right of a state, institution, group, etc., to make its own laws or rules and administer its own affairs; self-government, independence. Occasionally also: an instance of this." [1]. In the context of robotics, this definition means that a fully autonomous robot can complete tasks by sensing, planning, and acting within an environment without any human involvement [2]. While the field of autonomous robotics has made significant strides in recent years, no robot has yet achieved full autonomy [2]. Semi-automated tasks are feasible, leading to the concept of shared autonomy. Considering the different concepts proposed by Patterson et al. [3] to control a system (see Fig. 1), shared autonomy falls in to the category of semi-autonomous systems. Both the user and the machine give command inputs and both are receiving feedback from the system.

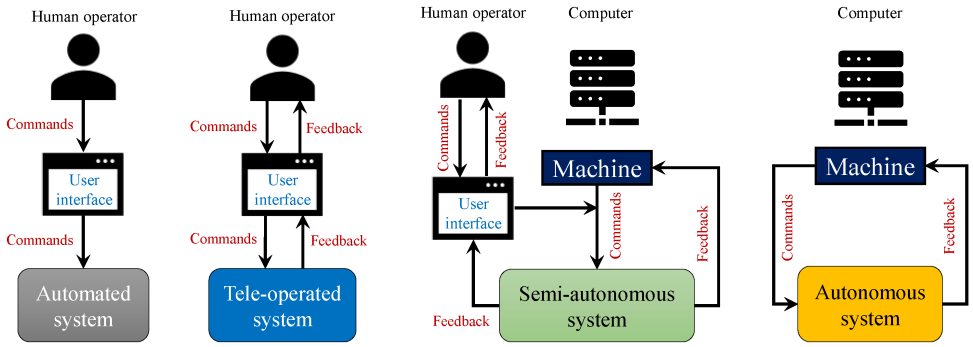

Figure 1. Controlling a system with automated, teleoperated, semi-autonomous and autonomous concepts [3]. This work aims to propose a semi-autonomous system where control is shared between an user and a machine.

1.1 Motivation

According to the United Nations, the number of people over 60 years will be doubled from 2015 to 2050 reaching almost 2.1 billion globally. Additionally, the number of people over 80 years old will triple by 2050 [4]. As the elderly population grows, the demand for long-term care services will also increase [5]. This underscores the importance of finding innovative and effective ways to assist the elderly that are tailored to their specific needs. Studies have demonstrated that assistive living technologies can help lower costs in certain situations [5]. In the literature, there is no exact age defined for the terms "older people" or "elderly." However, for the purposes of this thesis, individuals aged 60 and above are considered elderly.

Physical abilities decline with age, and this becomes especially important when it comes to managing household chores. As they age, many elderly prefer to stay in their own homes instead of living in a nursing home [5, 6], despite the physical challenges that aging brings. To achieve this, it is important for older adults to be able to perform ADL on their own [7]. According to Pashmdarfard et al., ADL are defined as follows: "The ADL refers to activities oriented toward taking care of ones own body. These activities are fundamental to living in a social world; they enable basic survival and well-being, such as bathing, toileting, dressing and eating." [7]. A common example of an ADL is housekeeping. Most household tasks require hand grasping and manipulation.

The main age-related declines that affect ADL, including grasping and manipulation, involve a physical decline in strength and dexterity. Decrease in flexibility is reflected in the following specific restrictions: a reduction in muscle mass of up to 45%, a decrease in hand-grip strength by 20-25%, significantly slower fine manipulation, reduced joint mobility and flexion power, a 25% loss of motor axons in hand muscles, and a significant reduction in motor units in the Thenar and Dorsal interossei muscles [6, 8–10]. One of the most significant declines in upper extremity function is in hand-force steadiness and the speed of hand-arm movements [8]. People over 70 experience an average reduction in wrist flexion by 12%, wrist extension by over 50%, and ulnar deviation by 22%, with these declines doubling in the following decade [8]. In most ADL, applying the right amount of pinch force, such as holding a glass of water, becomes harder due to diminished proprioception with age [11]. This also negatively impacts the speed and precision of placing small objects [9]. Apart from the reduction in physical power and coordination, the senses also deteriorate with age. Vision, crucial for detecting and identifying objects for manipulation, declines as well. Age-related macular degeneration is a leading cause of blindness in the United States [10]. This decline in vision increases the difficulty of tasks like opening bottles [8].

Rehabilitation robots have emerged as a promising solution to help elderly individuals continue living independently. To ensure that these systems are well accepted by the elderly, it is essential to understand their needs, desires, and preferences when performing ADL with assistance. Beer et al. [6] stress that assistive systems must be tailored to meet the specific needs of older adults. Additionally, it is important to maintain the user's autonomy for their well-being and to improve functionality of older adults [12]. In general, users of arm and hand manipulation systems prefer continuous in-the-loop control [13], and it is believed that this preference applies to older users as well.

Haltaufderheide et al. [14] propose the following seven key factors that should be considered to improve how elderly individuals perceive robots: promoting independence and safety, providing both physical and mental support, facilitating communication and social interaction, easing the burden on nursing staff, ensuring the individual's right to make decisions, protecting data privacy, and addressing liability concerns. Similarly, Jung et al. [15] highlight the importance of elderly individuals feeling safe when interacting with an assistive robot, which can be ensured through the robot's reliability.

Assistive devices must support in multiple tasks and needs [16]. To determine which specific ADL should be supported, Stanger et al. [16] surveyed individuals with limited arm and hand mobility. Tasks such as picking up objects from the floor or a shelf and carrying objects were rated as high priority, while tasks like eating/drinking, preparing food/drinks, personal hygiene, and leisure/recreational activities were rated as moderate to high priority [17].

Beer et al. [6] interviewed 21 older adults in the age between 65 and 93, to investigate their opinions and needs regarding assistive robots. Participants rated their preferences on a scale ranging from 1 to 5, where 1 meant only a human should perform the task, 3 indicated no preference, and 5 meant only a robot should perform the task. Fig. 2 shows their preferences for Fetching/Organizing Tasks. The majority of the users favored assistance from a robot, as indicated by the purple bar for the listed tasks and a mean value above 3.

Task	*M*	*SD*	Histogram
Fetching objects from floor or other room	3.75	0.94	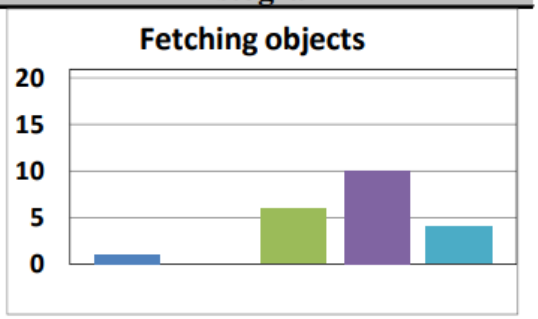
Picking up / moving heavy objects (e.g., furniture)	3.75	1.00	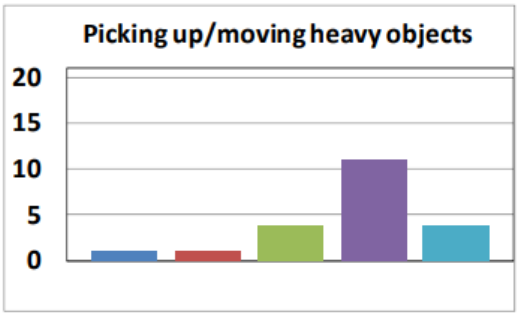
Reaching for objects	3.71	0.96	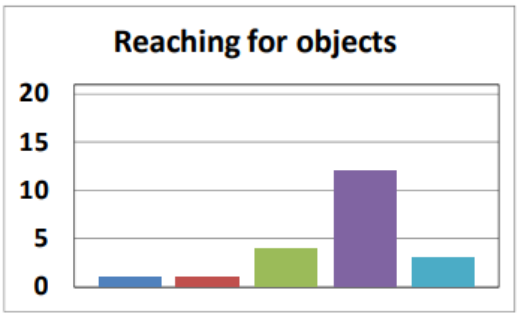
Finding / delivering items	3.62	0.92	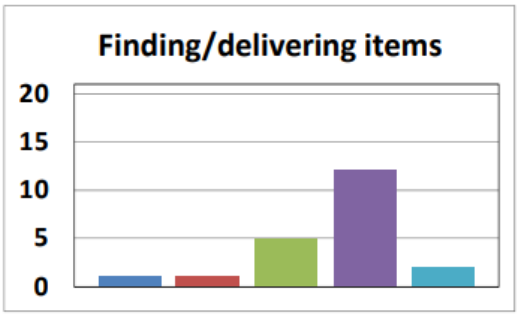

Figure 2. Rated preference for assigning fetching tasks, ranging from entirely human to entirely robot. [6]

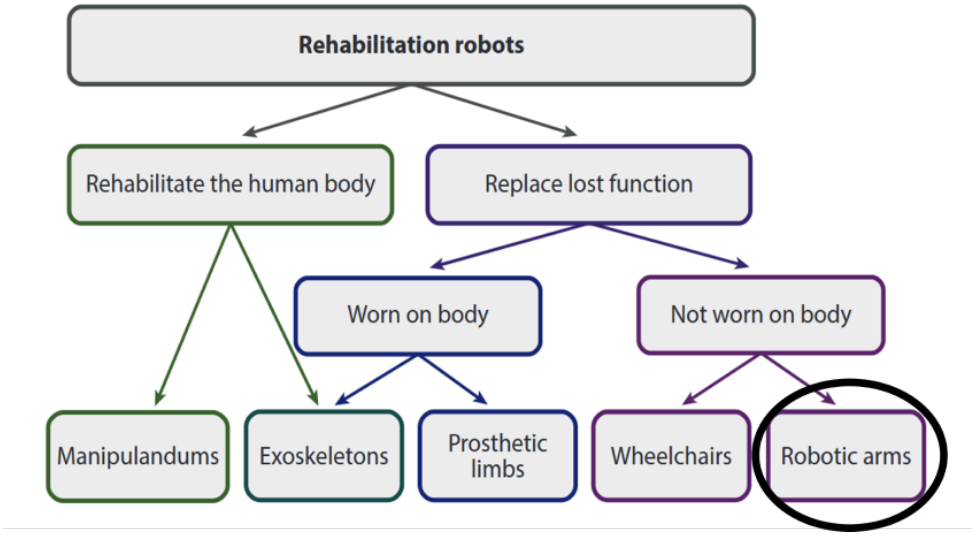

Figure 3. Categorization of rehabilitation robots [18]. The proposed approach relies on a robotic arm that is not worn on the body to replace lost functions.

Furthermore one participant said that a assistive robot would give a certain amount of independence in being in more control of their life. This study highlights the potential and wish of elderly to be assisted by a robot in ADL.

1.2 State of the Art of Shared Autonomy

Fig. 3 from the study by Argall [18] provides an overview of rehabilitation robots. This work examines how lost functions can be replaced by a robotic arm that is not worn on the body. Selvaggio et al. [2] differentiate between shared control and shared autonomy. Shared control means that the level of autonomy is adjusted manually by human, while in shared autonomy the level is adjusted automatically by the system. This thesis addresses shared autonomy and shared control, using the terms interchangeably throughout this work. Shared autonomy and shared control can be realized in various ways, as discussed in the following. One generic approach is to combine the user's and the autonomous control signals in a weighted sum:

$$h(u_h, u_a) = \alpha u_h + (1 - \alpha) u_a$$

In this Equation, u_h represents the human input, u_a the autonomous input and $\alpha \in [0, 1]$ indicates the level of autonomy [2]. Increasing α leads to a decrease of autonomy. This raises the question of how the optimal α can be determined. Most arbitration functions in the literature are structured in a way, where the arbitration of α depends on an independent variable, typically the robot's confidence in its interpretation, detection and recognition of the human user's goal. Leading to an increased α if the confidence

increases[19].
Gopinath et al. [20] propose to model α depending on user's verbal cues and the confidence. The confidence is modeled through the distance between the end effector of a robot and a inferred target location, and the nearness to the target. The results of this study showed that all participants were able to adapt to an optimal assistance model, and task performance improved. In the study by Dragan et al. [21] the users control a robot via a whole-body interface that detects their body and maps the user joint values onto the robots joints to enable a anthrophomorphic control scheme. The robots action is determined using a weighted sum that arbitrates the user input and the robots input depending on the confidence of a prediction of the users intent.

The autonomous component of a shared autonomous system can be modeled in different ways. One approach is for the robot to observe underlying patterns of task execution and learn from demonstrations, as shown in the following studies.
In the previous mentioned study by Gopinath et al. [20] the robot's autonomous policies are learned from human demonstrations through a method called Stable Estimator of Dynamical Systems (SEDS). In SEDS, the target poses are modeled as attractors in a dynamic system. The approach collects joint angle and velocity data from a set of demonstrations, then learns a time-independent dynamic system that models joint velocities as a function of joint angles. This enables the robot to generate trajectories that follow the general pattern of the demonstrations, ensuring the policy works across the entire workspace and the robots movements align with the demonstrated task.
In the study by Peternel et al. [22] human and robot work together in co-manipulation to accomplish a specific task. The robot initially acts as a follower, mimicking the human actions. As the collaborative task progresses under human guidance, the robot gradually learns the necessary movement patterns needed to perform the task. In parallel, the fatigue of the human is measured via EMG sensors. When the human shows signs of reaching a set level of fatigue, the robot applies learned skills to take over the more physically demanding parts of the task, allowing the human to regain strength.
Broad et al. [23] propose a model-based share control. The robot learns the user's interaction patterns and task dynamics by observing them and using a Koopman operator to analyze and model the behavior. By solving a predefined optimization problem, the autonomy of the robot is determined and dynamically adjusted by comparing it to the user's input. Experiments show that the model developed using the Koopman operator can be generalize across different users. Hence, it is not necessary to collect data from each individual user before the robot can provide assistance.

Another way to enable the robot's autonomous behavior is by predicting the user's real-time intent regarding the desired position first and then assisting in achieving that intended position effectively. Using a recursive Bayesian intent interference method to

combine multiple non-verbal observations to estimate and update the user's intended goal, has shown to directly affect shared autonomy performance [24].
Dragan and Siddhartha [21] presented a method to predict the users goal intention based on the trajectory data and in a second step predict how the user wants to approach the predicted target by optimizing a cost function.

Besides predicting the user's intend and letting the robot learn from demonstrations, virtual fixtures, also known as active constraints, also provide a reasonable approach to assist the users in ADL. According to Mehr et al. [25] the most challenging aspect for human operators, of many tasks is ensuring that the task constraints are consistently maintained. Virtual fixtures are high-level control algorithms that impose virtual constraints on the robot, rather than relying on physical constraints [26]. These virtual constraints can appear in various shapes, e.g. point, linear, paramatric curves, planar, parametric surface, or volumetirc primitive [27]. Quere et al. [26] propose using different active constraints based on the specific task. For example, when pouring liquid from one bottle to another, the constraint limits the maximum tilt angle to prevent spillage. Another example is a virtual cone aimed at a target, which ensures that the robot's end effector remains within the cone. Mehr et al. [25] address the two main challenges with regard to task constraints: Identifying which specific constraint the operator is trying to follow, and determining the best way to provide support once the constraint has been identified.
In [28], task constraints are used to assist users during bimanual teleoperation of a robot, resulting in higher task completion success compared to other approaches. The constraints of this study are tailored to the specific task that the user is performing. Hand positions were tracked using motion capture technology. For instance, when the user holds an object with both hands, the system provides assistance by maintaining a consistent distance between the robot's end effectors, ensuring the object does not fall. Rakita et al.[28] showed the effectiveness of the proposed method in two user studies.

In the context of this thesis, which focuses on assisting the elderly in the kitchen, it is implied that an assistive robot can handle certain low-level tasks but still requires user input for intentions and high-level planning.

To the best of current knowledge, no prior study has explored shared autonomy within a user interface that integrates motion tracking via inertial measurement units (IMU) and hand pose detection using surface electromyography (sEMG). Furthermore, no study has systematically compared significantly different shared autonomy approaches using the same interface within the same task. It is hypothesized that the optimal level of shared autonomy assistance is highly dependent on the control interface. Therefore,

this study closely examines existing shared autonomy approaches that employ similar user interfaces to the one proposed here.

As discussed in this chapter, various approaches exist for assisting with grasping and manipulation tasks during teleoperation. Dragan et al. [21] utilize a weighted sum approach to blend user and robot inputs, whereas Rakita et al. [28] investigate multiple assistance modes tailored to specific tasks, including active constraints. While Rakita et al. justify their shared control assistance by exploring how humans execute a certain task, no reasoning is provided in the study by Dragen et al. to make use of a weighted sum to mix the inputs of the user and the autonomous system.

The objective of this study is to determine whether a weighted sum-based approach (WS) or an active constraint-based approach (AC) is better suited for teleoperation in grasping and manipulation tasks or if fully teleoperation (Teleop) without assistance in terms of shared autonomy is preferred by users. Drawing on the aforementioned studies, two distinct shared autonomy frameworks were developed, both incorporating the following task decomposition: Reaching, Grasping, and Carrying.

Therefore the aforementioned AC and WS built the foundation of the frameworks presented in the following chapter. Shared autonomy can reduce the user's workload [2] and helps address the physical limitations discussed above.

2 Methods

This chapter explains the various methods used to achieve the objectives of this work. Firstly, it provides a detailed description the implementation of the proposed shared autonomy frameworks. Secondly, the used subsystems are presented and thirdly, the fusion of those subsystems into the overall systems are introduced. The overall setup consists of several subsystems: DLR light weight robot (LWR) [29], DLR Hybird Compliant Gripper (HCG) [30] /Compliant Low Cost Antagonistic Servo Hand (CLASH) [31], hand position tracking via IMU modules (BodyRig) [32], hand pose detection using a sEMG bracelet, and a M5Stick (M5Stack Technology Co., Ltd., China) with three vibration motors for vibrational feedback, namely Fingertac [33] (see Figure 4).

Figure 4. The overall setup with its subsystems LWR, HCG, hand position tracking via IMU moduls, hand pose detection using a sEMG bracelet and a M5Stick with three vibration motors for vibrational feedback

2.1 Mimicry-based Teleoperation of Robotic Arm

The robotic arm is controlled through an intuitive interface designed for Mimicry-based teleoperation. It refers to directly mapping the user's hand position and orientation to the robot's end effector in real time [34]. They represent a new type of telemanipulation that has proven to be effective, even for beginners [34].

The position and orientation of the user's hand are tracked using IMU. The position is tracked in Cartesian coordinates, and the orientation is represented using quaternions. To match the robots workspace (see Section 2.4.2) and optimize the mapping for the sensitivity of the robot's movements, the position data is rescaled by a constant factor of 0.3. This factor was determined experimentally during initial tests. Additionally, a shift

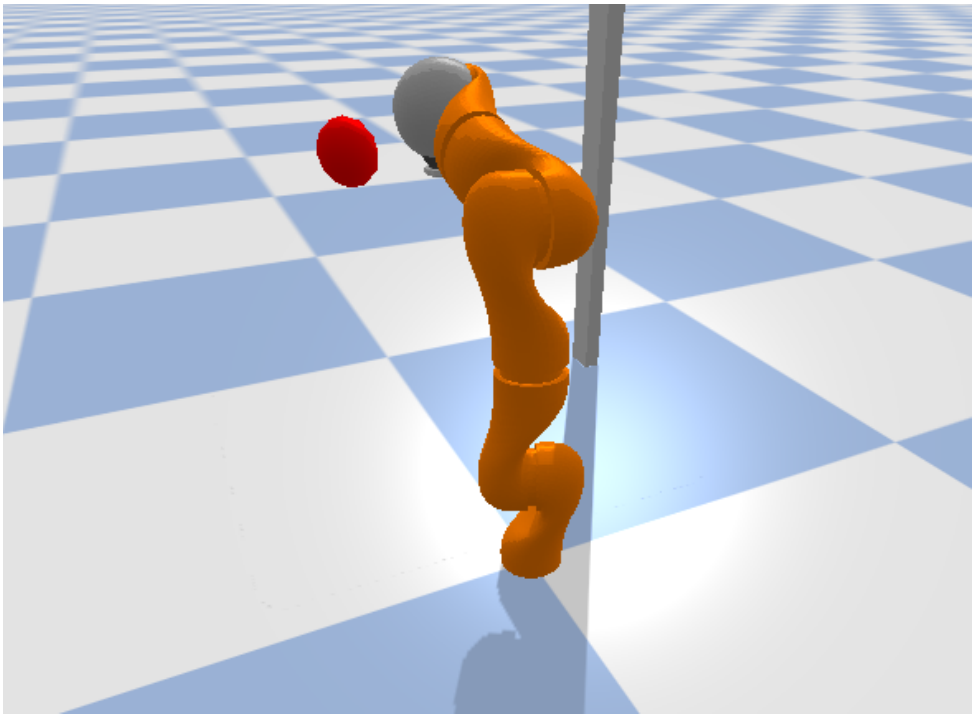

Figure 5. In the simulation, the user controls the LWR to move the TCP to the initial position of the real LWR, represented by a red dot.Once the offset between the user's hand position and the real robot's TCP position becomes sufficiently small, i.e. the simulated robot reaches the position of the red dot, the real robot begins to move.

of $+30\,\mathrm{cm}$ in the z-direction is applied to enhance user comfort, preventing the user from having to maintain an too high hand position, which could lead to arm fatigue.

Between the user's hand position and the robot's tool center point (TCP) position is a constant offset, greater than zero in all three directions. If this offset becomes too large, intuitive control may be compromised, especially during certain movements, such as those involving rotational offsets of the positions. To minimize this offset, a calibration procedure must be performed prior to teleoperating the robot. During this calibration phase, a digital twin of the robot is controlled in simulation. The user must align the simulated robot with the initial position of the real robot, which is illustrated in Pybullet [35] by a red dot (see Fig.5). Once the user's hand position and the robot's initial TCP position are within a $10\,\mathrm{cm}$ linear distance, control of the real robot is enabled.

IMU are known to experience signal drift over time, which could result in an uncomfortable arm configuration when the user attempts to reach certain positions in the robots workspace. To address this issue, an indexing method was implemented. By pressing the main button on the M5Stick control module (see Section 2.5 for more details on the M5Stick), the robot remains stationary, allowing the user to reconfigure their arm into a more comfortable position. Once the button is pressed again, the robot resumes following the user's hand, facilitating access to the entire robot workspace in a more

ergonomic manner. It should be noted that the use of this indexing method may result in an excessive offset, which could hinder intuitive control, as previously described.

The orientation offset between the user and the TCP is treated differently from the position offset and is always greater than zero. It is established at the end of the calibration phase as the difference between the initial orientation of the robot's TCP and the user's starting orientation. This offset remains constant throughout the teleoperation process and is only updated when indexing is performed.

Since the robot has a limited angular velocity, which the user can easily exceed, the user's orientation changes are smoothed before being commanded to the robot. The orientation computations are performed using quaternions to prevent the gimbal lock. Gimbal lock is a phenomenon that occurs in systems using Euler angles to represent three-dimensional orientation, particularly when two of the three rotational axes become aligned. This results in the loss of one degree of freedom, effectively reducing the system's ability to represent arbitrary rotations in 3D space. Equation (2.1) defines the orientation update q_{TCP}, incorporating the constant offset q_{offset}, the initial TCP orientation q_{initial}, and the user's new orientation q_{user}. After the calculation of the new desired orientation for the TCP, q_{TCP} is weighted with the previous orientation q_{prev} by making use of spherical linear interpolation and a constant factor $\alpha_{\text{robot control}}$ that determines the weighting between the previous and new orientations. In Fig. 6 the spherical linear interpolation is depicted. Point A for example represents the previous and B the new orientation and the weighting determines the final orientation (one of the red dots) on the sphere of the two original orientations. The weighting factor was experimentally determined to ensure that the robot's angular velocity limit is not exceeded. For LWR used in this work, $\alpha_{\text{robot control}}$ is set to 0.9, which keeps the TCPs orientation close to the previous one and avoiding exceeding the angular velocity.

$$q_{\text{TCP}} = q_{\text{user}} * q_{\text{offset}}^{-1} * q_{\text{initial}}; q = (i, j, k, w) \tag{2.1}$$

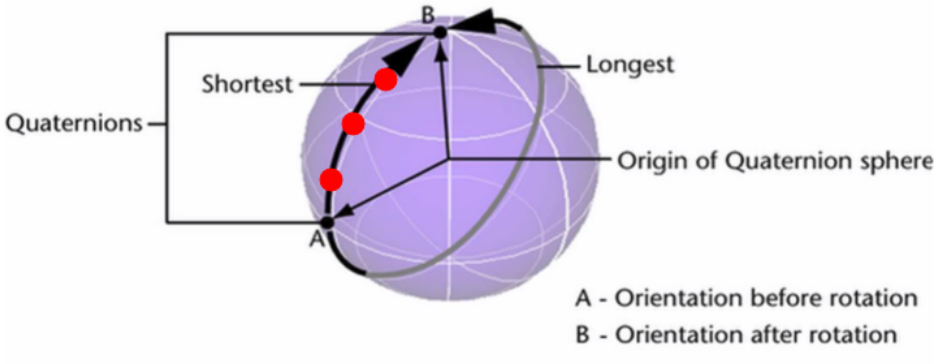

Figure 6. Spherical linear interpolation between point A and B and the intermediate orientations illustrated as red dots [36]

The gripper attached to the robots TCP is controlled via sEMG. sEMG signals are used to detect pretrained hand poses, which are then mapped onto corresponding actions of the robotic gripper. For instance, an open-hand gesture results in the opening of the gripper, while a power grasp gesture triggers the closing of the gripper. For further details, refer to Chapter 2.3.1.

2.2 Shared Autonomy Frameworks

The developed shared autonomy frameworks are designed to enhance both independence and safety while providing physical and cognitive assistance, all while respecting an individual's autonomy in decision-making. These frameworks built on the aforementioned Teleop approach.

- **Reaching**: This phase involves moving the TCP from its initial position to a pre-grasp position, which is critical for ensuring optimal object grasping.
- **Grasping**: The grippers fingers are opened to allow proper alignment with the object, ensuring that both fingers are positioned on opposite sides. The gripper then moves to the final grasp position and closes its fingers according to the predefined grasp modality described in Section 2.4.3.
- **Carrying**: This phase includes moving the TCP to a final position and placing the object as close as possible to the intended destination. Once the final position is reached, the fingers open, and the object is released from the gripper.

Depending on the specific subtask and the shared autonomy framework, different assistance is provided. In the following sections the two frameworks are explained in

detail with respect to the task of unloading a dishwasher, meaning grasping a plate or a cup from a drying rack and place it to a predefined position.

Active Constraints Framework

In this framework assistance is provided by making use of active constraints during teleoperation meaning that only certain actions are possible in certain states. The framework is depicted in Fig. 7. Fig 8 shows the implemented state machine and the corresponding transitions.

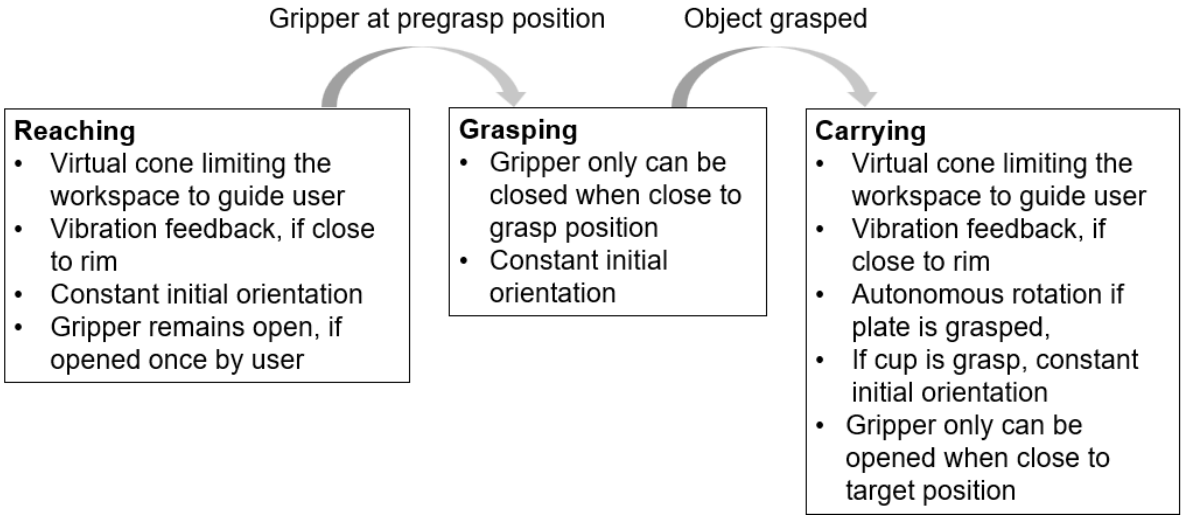

Figure 7. Active constraint based framework to assist the user in a grasping task

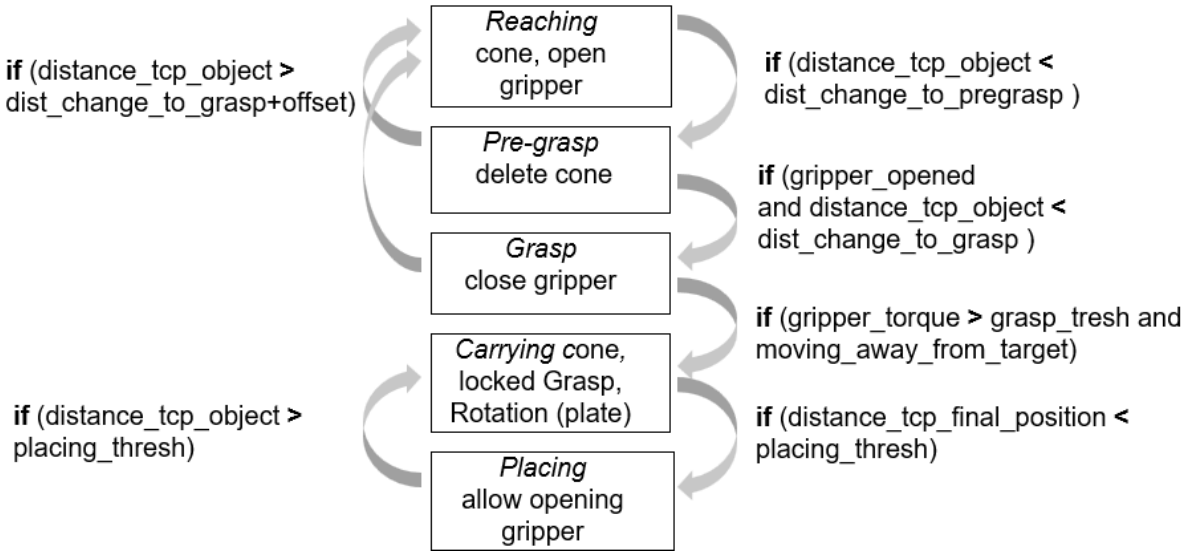

Figure 8. Active constraint based state machine to assist the user in a grasping task

In the reaching phase the workspace of the robot is limited to a virtual cone inspired by the study by Quere et al. [26]. The cone points to the pre-grasp position of the

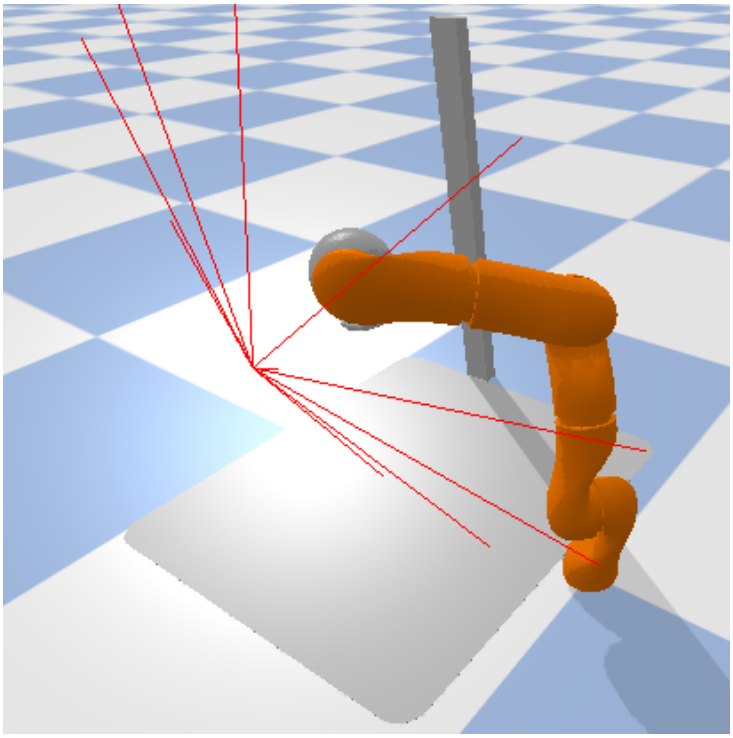

Figure 9. A virtual cone limits the workspace of the robot to guide the user towards a target.

desired object with its tip, see Fig.9. If the user teleoperates the TCP beyond the edge of the cone, it remains on the edge and restarts to follow the users hand movements again, if the user reenters the cone. Additionally, vibration feedback is provided as described in Section 2.5, if the TCP approaches the rim of the cone. This restriction of the workspace is intended to guide the user to the pre-grasp position. The TCP orientation is fully controlled by the autonomous system in all phases. During reaching and grasping it is kept constant to the initial orientation, meaning gripper is pointing downwards. To determine whether the user position is inside or outside the virtual cone, the cosine similarity between the vector that represents the middle axis of the cone $\mathbf{v}_{\text{middleaxis}}$ and direction vector pointing from the current user position to the pre-grasp position $\mathbf{v}_{\text{directionvector}}$ is employed, see Equation (2.2). $\mathbf{v}_{\text{middleaxis}}$ remains fixed throughout the reaching motion. If the resulting angle θ is smaller than the predefined angle θ_{cone}, the current user position is considered to be inside the cone. If it is greater, the position is outside the cone.

$$\theta = \arccos\left(\frac{\mathbf{v}_{\text{middleaxis}} \cdot \mathbf{v}_{\text{directionvector}}}{\|\mathbf{v}_{\text{middleaxis}}\|\|\mathbf{v}_{\text{directionvector}}\|}\right) \tag{2.2}$$

To improve the accessibility of the pre-grasp position, the tip of the virtual cone is positioned slightly behind the actual pre-grasp position in the x-y plane, relative to the initial position. Regarding the gripper, assistance is provided by keeping the gripper open if

the user opens it at any point during the reaching phase. Once the pre-grasp position is reached, the grasping phase begins. In this phase, shared autonomy is implemented by assisting the user in two ways: first, by keeping the gripper open as long as the TCP is above a specified distance; and second, by keeping the gripper closed if the TCP is below this threshold and the user has previously closed it. The threshold was evaluated during initial tests and is set to $3\,\mathrm{cm}$ below the pre-grasp position.

If the measured torque of the gripper exceeds the threshold of $0.8\,\mathrm{N\,m}$ for the plate or $0.5\,\mathrm{N\,m}$ for the cup, and the user teleoperates the TCP away from the grasp position, the carrying phase is initiated. To detect whether the TCP is being moved away from the grasp position, cosine similarity is used again. The comparison is made between two vectors: one representing the direction of the user's hand movement, obtained by subtracting the previous user position from the current user position, and the other pointing from the current user position to the grasp position.

During the carrying phase, another virtual cone is used in the same manner as in the reaching phase, with its tip pointing towards the predefined final position. Additionally, the user is unable to open the gripper to prevent the object from falling, as long as the TCP remains above a specified threshold distance ($7\,\mathrm{cm}$, as experimentally determined). Since the plate is grasped in a vertical orientation in the rack, the TCP must rotate around the x-axis to correctly position the plate. This rotation is performed autonomously if the user moves the TCP sufficiently away from the grasp position, ensuring that no collisions occur with the rack or other objects. If the object being handled is a cup, no rotation is performed.

Weighted Sums Framework

The second shared autonomy framework is based on the weighted sum and inspired by the study by Dragan et al. [21]. Similarly to the AC framework, this one also relies on task decomposition, with its phases Reaching, Grasping and Carrying. Each of the robotic subsystems (LWR and HCG) are controlled via weighted sums. Fig. 10 shows the WS framework and Fig. 11 the corresponding state machine.

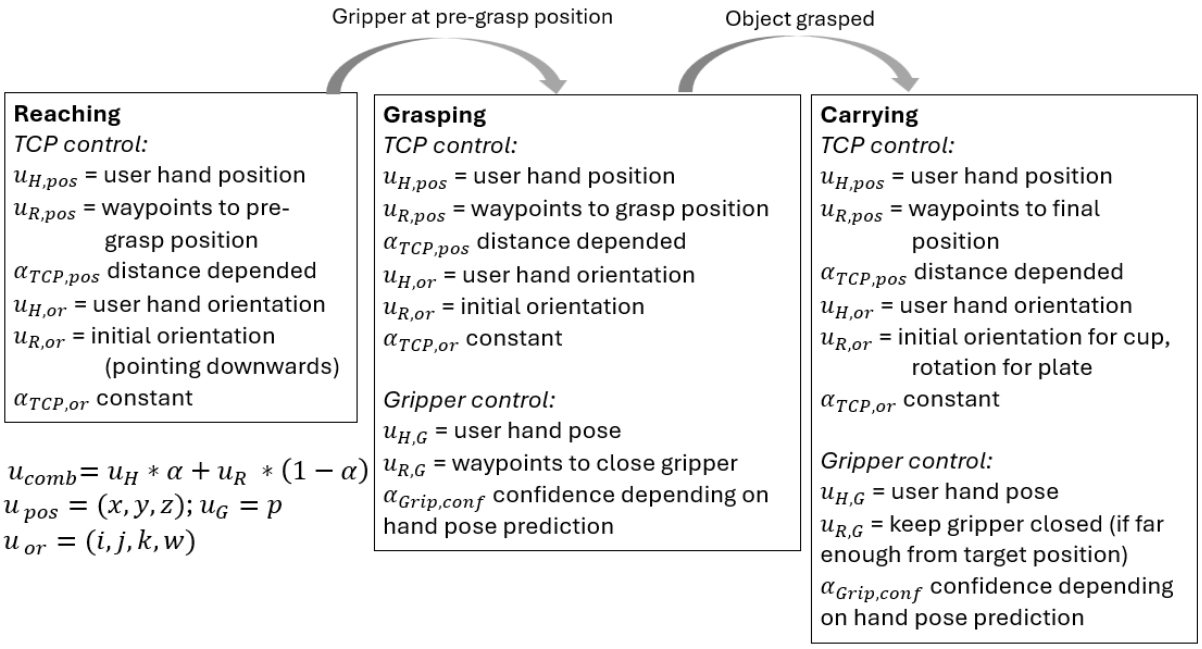

Figure 10. Weighted sum based framework to assist the user in a grasping task

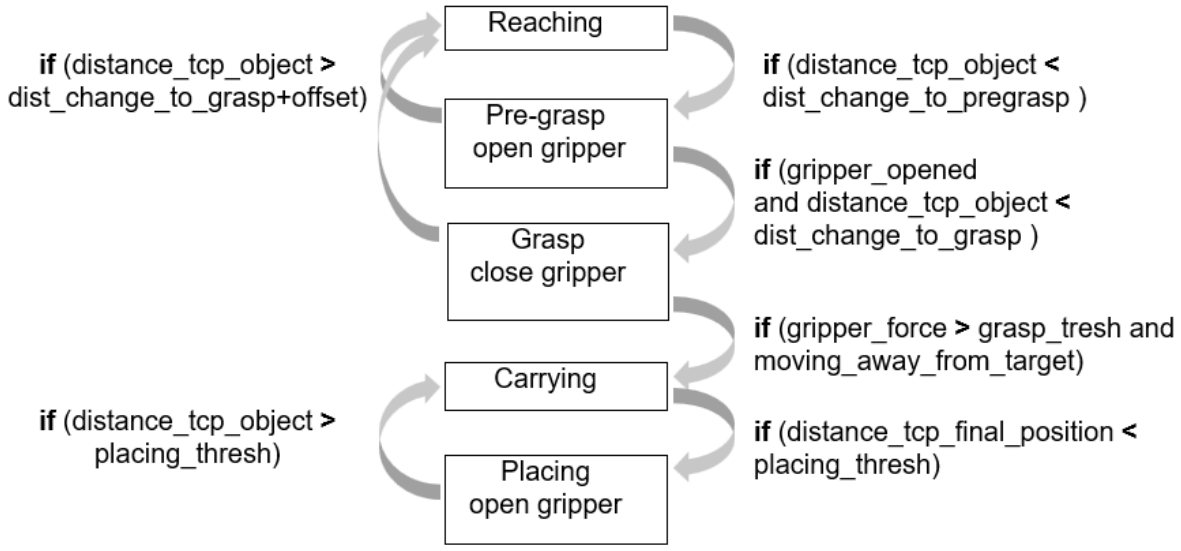

Figure 11. Weighted sum based state machine to assist the user in a grasping task

Equation 2.3 reflects the weighted sum for position control of the LWR. $\alpha_{\text{LWR, pos}}$ weights the position input by the user $u_{\text{user, pos}}$ with the inputs by the robot $u_{\text{robot, pos}}$. The robots input always follows an optimal path to the desired position based on workspace optimization. Therefore waypoints on a straight line are generated connecting the initial position with the pre-grasp position; for example in the reaching phase. The number of waypoints depend on the distance to the next desired position. The greater the distance, the more waypoints are generated. The red line in Fig. 12 illustrates the optimal

path from the initial position of the TCP to the pre-grasp position. The robots position input of the weighted sum is always the closest waypoint from its current position.

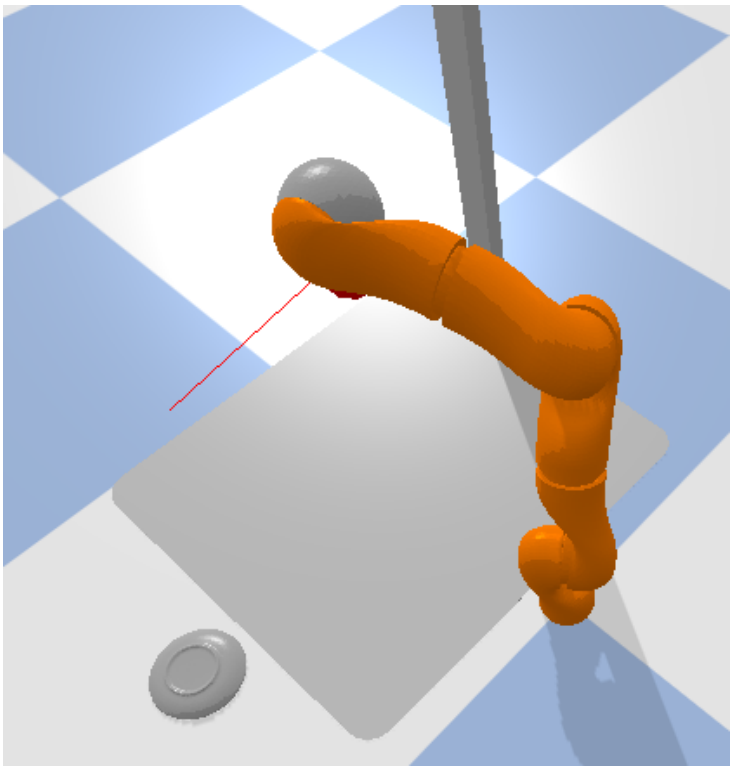

Figure 12. The red line indicates the optimal path from the robots current position to a desired position.

$\alpha_{\text{LWR, pos}}$ is distance-depended, meaning the closer the TCP is to the desired position, the smaller $\alpha_{\text{LWR, pos}}$ becomes in a linear fashion, leading to a stronger impact of the autonomous system. After an object is grasped $\alpha_{\text{LWR, pos}}$ is again set to 1 to give maximum freedom to the user. Approaching the final position it decreases to 0.2 to assist in placing the object as close to the final position as possible. Due to the rotation for the plate, the final TCP position differs slightly to the one, when the cup is grasped. Resetting $\alpha_{\text{LWR, pos}}$ to 1 requires to update the offset between user position and TCP position to avoid too fast linear motions of the TCP. From reaching to grasping the current $\alpha_{\text{LWR, pos}}$ is handed-over.

$$u_{\text{TCP}} = u_{\text{user, pos}} * \alpha_{\text{LWR, pos}} + (1 - \alpha_{\text{LWR, pos}}) * u_{\text{robot}}; u = (x, y, z) \tag{2.3}$$

The executed orientation of the robot around the x- and y-axis results from a spherical linear interpolation similar to Teleop, but with the additional optimal orientation of the autonomous system. The orientation around the z-axis is kept constant during the whole procedure. The autonomous orientation input depends on the phase. During

reaching and grasping it is the initial orientation (gripper pointing downwards). During Carrying it depends on the grasped object. For the cup the robots orientation input remains the same. Considering the plate, the autonomous orientation inputs lie on a sphere resembling an orientation around the x-axis and interpolating between the initial orientation and the final orientation that allows to position the plate properly. Fig. 6 based on the study by [36] illustrates the spherical linear interpolation on the shortest path between point A and B and the red dots show the intermediate orientations. The autonomous orientation input depends on the distance to the final position. The closer the TCP is to the final position, the closer the autonomous orientation is to the final orientation. $\alpha_{\text{LWR, or}}$ is kept constant during the whole procedure to avoid exceeding the maximum angular velocity of the robot.

The weighted sum for gripper control is shown in Equation 2.4. The autonomous input $u_{\text{R,G}}$ depends again on the phase of the task and the distance to a position. During reaching and grasping as long as the distance to the grasp position is greater than a certain threshold, it tries to open the gripper, if the user intents to open the gripper. To detect whether the user intents to open or close the gripper the current gripper command is compared with the previous gripper command. Increase of the commanded values meaning closing and vice versa. If the distance threshold is reached, the autonomous input aims to close the gripper according to the grasp pattern (see Section 2.4.3). In the carrying phase it keeps closing the gripper too, as long as the distance to the final position is greater than another distance threshold and opening if the TCP is close enough to the final positioning. The weighting factor for the gripper depends on the confidence of the prediction of the hand pose. The higher the confidence of the Ridge Regression Prediction (see Section 2.3.1), the higher $\alpha_{\text{Grip, conf}}$, giving more control to the user (user input $u_{\text{H,G}}$) and vice versa.

$$u_{\text{gripper}} = u_{\text{H, G}} * \alpha_{\text{Grip, conf}} + (1 - \alpha_{\text{Grip, conf}}) * u_{\text{R,G}}; u = [0, 1] \tag{2.4}$$

In the subsequent sections, the used hardware and the communication between them are described.

2.3 Motion Detection

The following two chapters explain the motion detection, meaning the user's hand movement in space and intent detection, meaning the user's hand pose. Fig. 13 shows a user wearing the Myo armband (black and white) for hand pose detection via sEMG, IMUs on each arm segment for the detection of the hand movement and the Fingertac for vibration feedback.

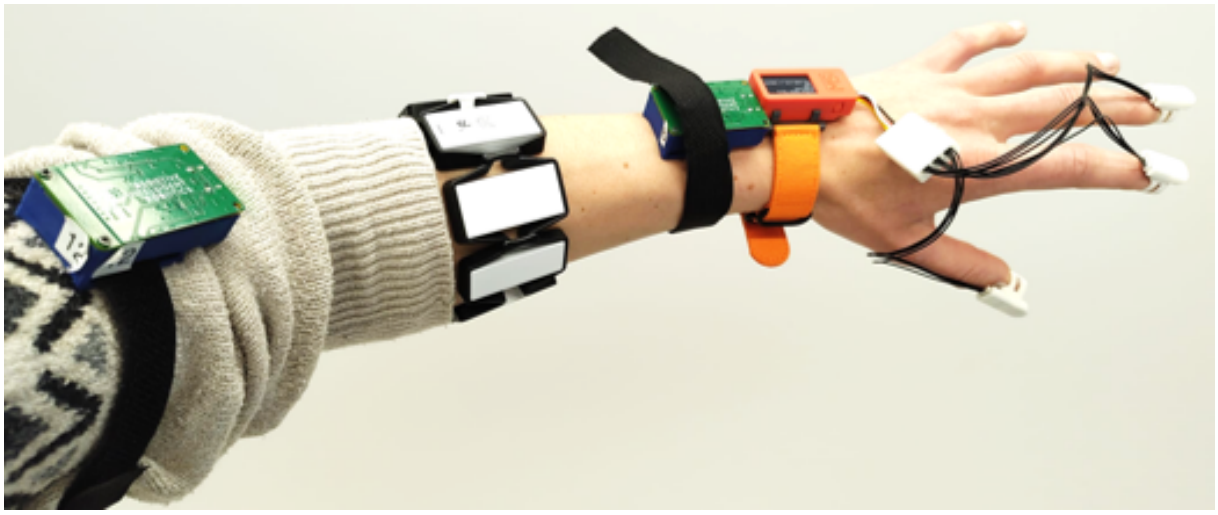

Figure 13. User wearing IMU on the upper and lower arm and on the hand (blue boxes with green cover), the Myo armband (black and white) on the lower arm and the Fingertac (orange device and vibration motors implemented in the white covers placed on the fingertips).

2.3.1 Intent Detection of hand pose using surface electromyography

sEMG, first introduced in the 1950's and 1960's [37], has been widely used in research since then in assistive and rehabilitation contexts. It is often employed to detect hand movements in amputees for controlling prosthetic devices or to operate robotic systems via teleoperation [38]. sEMG measures electrical signals generated by muscle activity on the skin's surface when muscles are activated by electrical or neurological impulses. The amplitude of sEMG signals typically falls between 0 to 10 mV (peak-to-peak) or 0 to 1.5 mV (RMS), with the main frequency range concentrated between 20 and 450 Hz [39]. The Myo armband (Thalmic Labs, Cananda) is used to capture muscle activities. Within this work the method developed by Gijsberts et al. [37] forms the basis of the sEMG-based control system for the gripper. This method makes use of a machine learning approach, namely Incremental Ridge Regression to translate the measured sEMG signals to hand poses. These poses are then mapped to the gripper's functions, enabling an intuitive way to control the gripper and grasp objects.

2.3.2 Position tracking of hand using IMU

To control the robot via Mimicry-based Teleoperation (see Section 2.3.2), the desired position of the user's hand must be tracked. This is achieved using the BodyRig, as proposed and developed by Sierotowicz et al. [32]. The BodyRig consists of independent modules, each equipped with an IMU, a battery, and a Wi-Fi module. For this study, the user wears modules on the upper arm, lower arm, and hand (see Fig. 13).

The modules transmit their orientations via Wi-Fi to a separate PC. The position and orientation of the user's hand are then determined based on a forward kinematic model, resampled and scaled and send to the robot (see Section 2.6 for detailed description of the network setup).

2.4 Robotic Platform

This section explains the robotic platform that is controlled by the user. It consists of the LWR proposed and developed by Albu-Schäffer et al. at the German Airospace Center (DLR) in 2007 [29] and HCG [30] attached to the robot's TCP. Before the implemented shared autonomy framework was evaluated at the real robotic system, it was developed and tested in simulation.

2.4.1 Simulation in Pybullet

For simulation the open source physics engine Pybullet [35] was used. Pybullet provides a set of functionalities to simulate a robot's behavior which is close to the real world. To control a robot within this environment, its physical characteristics need to be defined in terms of an Extensible Markup Language(XML) file. An open source available XML file of the robot is merged with a representation of the HCG as XML file to control both together in the simulation. Furthermore, XML files of objects like a plate, bowl, cup, and rack are generated and loaded into the simulation environment to enable to test grasping and positioning in the simulation.
The measured hand position via IMU of the user determines the position of the robots TCP. Therefore, position control is applied on the robot. To do so, the joint angles are computed via Inverse Kinematics (IK) using the functionalities of Pybullet. Moreover, some joints are restricted in their range of movements, leading to less solutions in the IK calculation and a smoother and less hectic movements of the robot. Furthermore, these restrictions keep the robot in a predefined configuration to provide a more intuitive control of the robot. The user's hand pose detected by sEMG is mapped on to the fingers of the HCG. An opened hand leads to opening the gripper and vice versa for closing. Both finger positions are controlled with the same control signal provided by the sEMG detection. Combining both position control of the robot and the gripper, the user is in full control of the system in the simulation.

In addition to the implementation that provides full control of the robot as described above, the assisting systems are also initially implemented and tested in the simulation. To verify the correct behavior of the autonomous part, Pybullet provides functionalities to visualize encoded control behaviors.

In Fig. 12 the red line indicates the waypoints from the TCP to the next target position. As described in Section 2.2, these waypoints represent the autonomous control input of the weighted sum. Similarly, active constraints can be visualized. Fig. 9 shows the virtual cone assisting the user to move the robots' TCP to the desired grasp position.

2.4.2 Lightweight Robot

Within this work a LWR was used. Despite classical industrial robots, which are designed for high positioning accuracy, high speed and robustness in well organized settings, the LWR is developed for human interaction for daily surroundings. It matches the requirements for human-machine interactions of a light weight mechanical structure for better mobility and injury risk avoidance. The robot has a total system weight of 15 kg. Moreover, it is equipped with torque sensors in every joint that enable a mass-spring-damper system for compliant robot human interaction and collision detection. Seven degrees of freedom (DoF) provide kinematic redundancy inspired by the human arm. The LWR workspace is up to 1.5 m. Within this work, the robot is used in a cartesian impedance control for compliance and a zero gravity mode that allows the robot to compensate its own weight and the grippers weight. For an intuitive control of the robot and to avoid collsions of the robot with the sourrounding (table, drying rack, dishes), some of its joints are restricted to keep the robots fourth joint ("ellbow") in an upper position.

The capability map of the LWR was investigated before initial control of the robot with the intuitive interface to ensure reachability of commanded cartesian positions. The 3D representation capability map is depicted in Fig. 14a and a 2D cross section in Fig. 14b. The colors refer to different reachability indices. The reachability index describes the local dexterity in the taskspace. Blue dots indicates a high (reachability index of 1) and red a low reachability (reachability index of 0) [40]. This later also influenced the location of the objects initial and final positions during the user study. The maximum dimensions for each axis are as follows: x- and y-axis: $1.55\,\mathrm{m}$ z-axis: $1.35\,\mathrm{m}$.

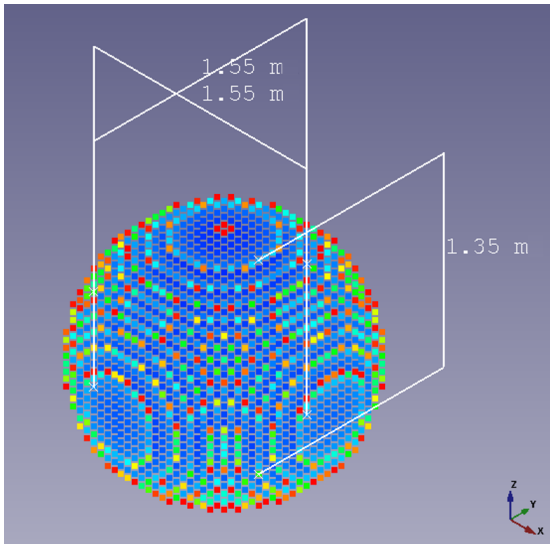

(a) 3D representation of the capability map and dimensions of the LWRs workspace, red indicates low reachability, blue high [40].

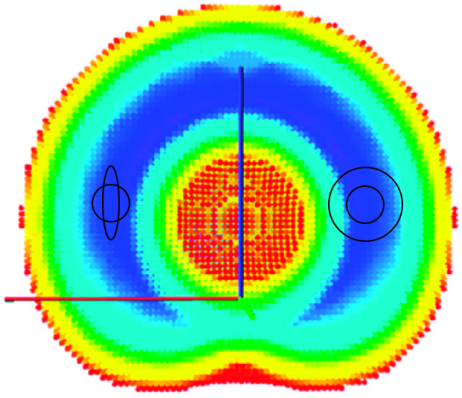

(b) 2D cross section of the capability map of LWRs workspace, red indicates low reachability, blue high [40]. Inital position (left) of objects and final position (right) of objects was choosen in a way that it is easly reachable for the robot and the proximal postilions are depicted as circles , see Fig. 18 and 19 for the experimental setup of plate and cup respectively.

Figure 14. Capability maps of the LWR

2.4.3 Hybrid Compliant Gripper and Grasp Modalities

The HCG features eight DoF, with each finger incorporating a suction cup at the fingertip and an electromagnet on its side. This enables four distinct grasping strategies. Each finger possesses three DoFs, one at the distal interphalangeal joint and two at the metacarpophalangeal joint, allowing independent control of finger stiffness regardless of position. Additionally, the fingers are mounted on a base that provides an extra DoF per finger, enabling them to tilt outward. The hand can support objects weighing up to 1.5 kg in a pinch grasp (for friction coefficients exceeding 0.75) and up to 500 g when using a single suction cup.

Exploring the Dofs of the gripper allows different grasp modalities for different objects. For this projects two grasp modalities, for grasping a cup and a plate, were developed. These modalities were inspired by a human grasp. Fig. 15 shows the two grasps. Fig. 15a depicts a human hand grasping the plate (middle, ring and little fingers are stretched away for better visualization of the grasp). The angles of the human hand are transferred to the fingers of the HCG as follows and shown in Fig. 15b: base joint of thumb $\alpha_1 = 40°$, distal interphalangeal of thumb $\alpha_2 = 0°$, base joint of index finger $\beta_1 = 50°$ and distal interphalangeal of index finger $\alpha_2 = -20°$. The grasp modality for the cup was developed similarly and is shown in Fig. 16 and with the following angles: base joint of thumb $\alpha_1 = 20°$, distal interphalangeal of thumb $\alpha_2 = 0°$, base joint of

index finger $\beta_1 = 20°$ and distal interphalangeal of index finger $\alpha_2 = 0°$. Since the cup is grasped from the top to lift it out of the rack, a grasp modality for round objects, which encloses the cup, could not be applied. In order to apply the necessary force on the objects to lift it without slippage, the stiffness of the fingers were adjusted accordingly.

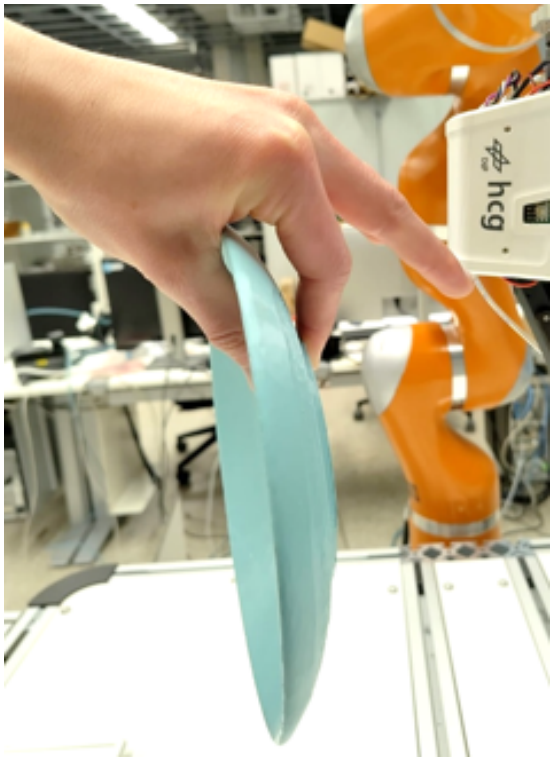

(a) Human hand grasping the plate.

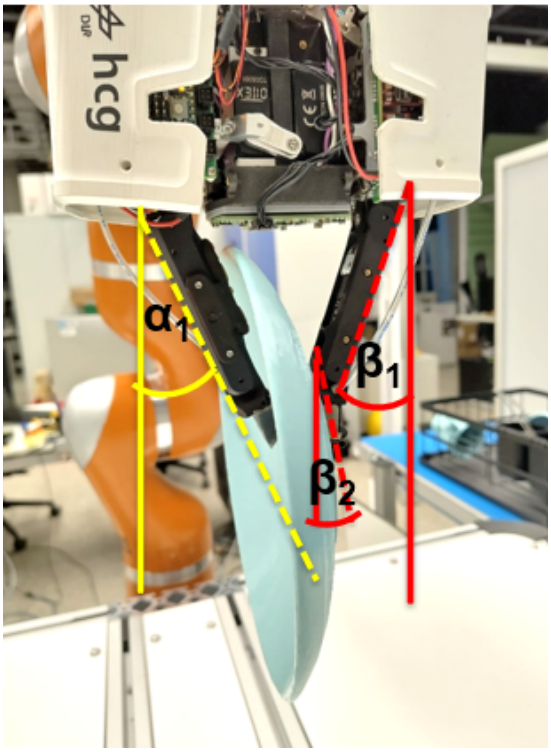

(b) Gripper grasping the plate inspired by the human grasp by applying the following angles on the fingers: base joint of thumb $\alpha_1 = 40°$, distal interphalangeal of thumb $\alpha_2 = 0°$, base joint of index finger $\beta_1 = 50°$ and distal interphalangeal of index finger $\alpha_2 = -20°$.

Figure 15. Human hand and gripper grasping the plate

Initially, the gripper was controlled using an interpolative approach, where the maximum and minimum values of the sEMG signal, corresponding to a fully open and fully closed hand, were linearly mapped onto the grippers fingers. However, due to the unreliability of the sEMG signal, users experienced difficulty in maintaining a stable grasp on objects. To address this issue, the control strategy was modified to a binary on/off mechanism, in which the gripper remains open below a predefined threshold and closes once the threshold is exceeded.

In addition to the HCG, CLASH was also utilized [31] and a best suited grasp pattern for each object was developed similarly to the procedure for the HCG described above.

(a) Human hand grasping the cup from above.

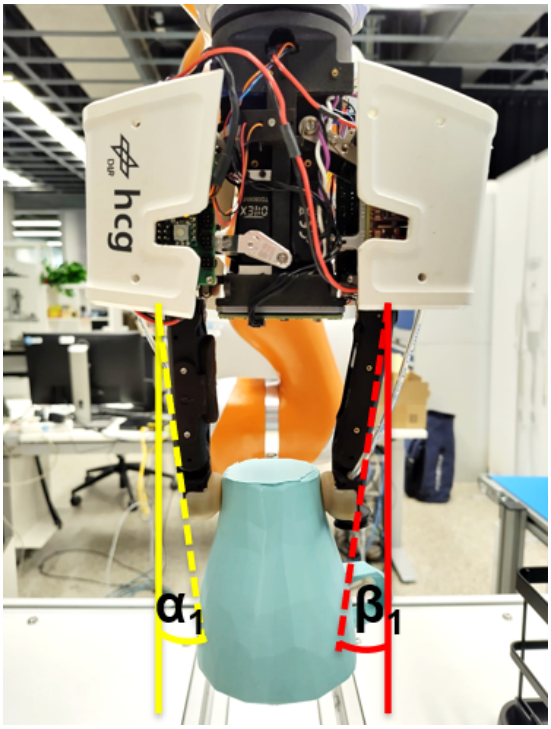

(b) Gripper grasping the cup inspired by the human grasp by applying the following angles on the fingers: base joint of thumb $\alpha_1 = 20°$, distal interphalangeal of thumb $\alpha_2 = 0°$, base joint of index finger $\beta_1 = 20°$ and distal interphalangeal of index finger $\alpha_2 = 0°$.

Figure 16. Human hand and gripper grasping the cup.

2.5 Vibration Feedback

The user receives two different kind of feedback, visual feedback, due to the fact that he or she stands next to the robot while teleoperating and vibrational feedback via the so called FingerTac proposed and develpoed by Hulin et al.[33]. It is a haptic wearable designed as a fingertip thimble that provides tactile feedback without covering the underside of the fingertip. It is funded by the German Research Foundation (DFG, Deutsche Forschungsgemeinschaft) as part of Germanys Excellence Strategy EXC 2050/1 Project ID 390696704 Cluster of Excellence Centre for Tactile Internet with Human-in-the-Loop (CeTI) of Technische Universität Dresden. FingerTac uses a unique technique where vibrations are applied simultaneously to both sides of the finger. This creates the illusion that the vibrations originate from the center of the fingertip rather than from the exact contact points. The vibrations are transmitted through mechanical linkages from actuators placed on the top of the device to the skin. User studies showed that users perceived the vibrations as if they were coming from the fingertip itself rather than from the actuators. Within this study vibration motors are placed on the thumb, index finger and middle finger each (see Fig. 13).

The control module for the vibration feedback is provided by an M5Stick, manufactured by M5Stack Technology Co., Ltd., Shenzhen, China. It is worn on the user's wrist (see Fig. 13) and receives command values via Wi-Fi (UDP) from a host PC. Upon receiving these command values, the system converts them into a corresponding vibration frequency, which activates the connected motors to produce the feedback.

FingerTac allows different feedback modalities depending on the subtask of the proposed shared autonomy frameworks. In the active constrained-based shared autonomy approach, FingerTac provides user feedback in two ways. During the subtasks of Reaching and Carrying, vibrational feedback is used to indicate when the user approaches the edge of the virtual cone detected using the cosine similarity (see Chapter 2.2). The frequency of vibration increases as the distance between the robot's TCP and the cone's edge decreases. The mapping between distance and vibration frequency is proportional. During the grasping subtask, FingerTac transfers the torque applied by the gripper's fingertips on an object to the user's fingertips through varying vibrational frequencies. The frequency of the vibrational feedback increases with the increase of the applied torque linearly. This also provides tactile feedback when the fingers of the gripper make contact with the object. In the weighted sum-based shared autonomy framework, feedback for the subtasks Grasping and Carrying is provided in a manner similar to the active constrained-based approach during Grasping. Vibrational feedback during the Reaching and Carrying subtasks was tested by increasing the vibrational frequency as the perpendicular distance between the TCP and the optimal

path increased. However, due to the absence of directional information, this feedback approach was not perceived as useful and instead caused confusion during the initial testing phase of the system. Hence, this method was not further developed or utilized. During full teleoperation, feedback is provided during the grasping and carrying phase, where the applied torque of the gripper's fingers is mapped into vibration cues, as described above.

2.6 Network Setup and Communication Architecture

The overall setup consists of several subsystems (LWR, HCG/CLASH, BodyRig, sEMG and Fingertac) as illustrated in Fig. 4. These subsystems communicate within a dedicated network, comprising both wireless (Wi-Fi and Bluetooth) and wired connections. The communication and software architecture is illustrated in Fig. 17.

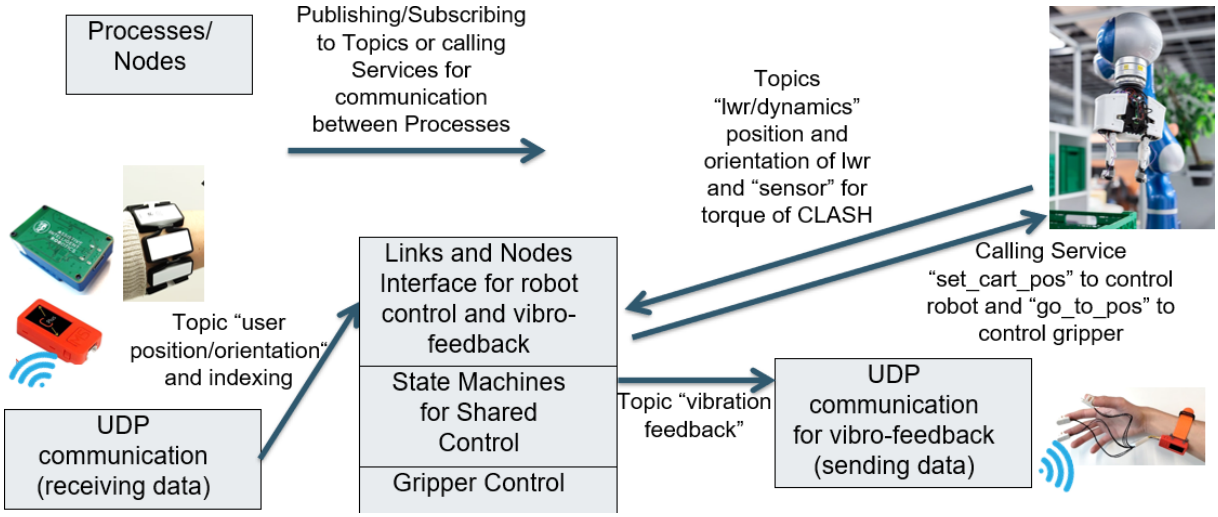

Figure 17. Data communication on DLR side using Links and Nodes. Boxes refer to the processes and the arrows to the topics or services that enable communication between processes.

The central component of the network is an access point, which receives position and orientation data from the IMU modules (see Section 2.3.2) via Wi-Fi and forwards this information to the laptop. The laptop then calculates the hand position and orientation using a C#-based software suite. Similarly, information regarding the indexing button press is transmitted to the access point via Wi-Fi, and from there, it is forwarded through a wired connection to the DLR-PC for further processing.

The determination of the hand pose is facilitated by muscle activity detected using the sEMG bracelet, which transmits data via Bluetooth to the laptop. The actual hand pose calculation is performed on the laptop using iM. Both the hand pose and hand

position/orientation data are then sent, via a wired connection through the access point, to the DLR-PC. On the DLR-PC, the data is processed using the DLR software and Nodes, an internal DLR software framework designed to facilitate parallel execution of multiple processes and enable inter-process communication, similar to the Robot Operating System (ROS), taking into account the desired teleoperation mode (fully teleoperation or one of the two shared autonomy control strategies) and the specific subtask within that mode. Subsequently, a movement command is sent to the robot and the gripper and the simulated robot (simulation running on the DLR-PC for the calibration phase (see Section 2.1)).

Data such as the position and orientation of the robots TCP and the gripper, along with the torque applied by the gripper, are streamed in the reverse direction, from the robot to the DLR-PC, through the access point, and to the M5Stick, providing vibrational feedback to the user. All Wi-fi connections are based on the User Datagram Protocol (UDP).

Inter-process communication is established through a publish-subscribe mechanism or service calls. The UDP communication process (receiving data) facilitates communication between the C#-based software suite and the DLR host PC, enabling the reception of position and orientation data from the so called BodyRig, as proposed and developed by Sierotowicz et al. [32] (see Chapter 2.3.2 for more details), as well as the desired gripper pose derived from the sEMG. This data is published to the user position/orientation topic within the Links and Nodes framework. The Links and Nodes interface manages internal communication within the DLR system, offering functionalities to retrieve the current robot position and orientation, as well as the torques applied to the gripper fingers, by subscribing to the corresponding topics. Additionally, it publishes data to the vibration feedback topic, which is subsequently received by the UDP communication process (sending data) and transmitted to the Fingertac [33] via UDP. Fingertac, developed and presented by Hulin et al. [33] is a haptic wearable device designed as a thimble that delivers tactile feedback while leaving the underside of the fingertip uncovered (see Chapter 2.5 for more details).

For each operational mode (Teleop, AC, and WS) dedicated processes were developed to implement distinct state machines (see Section 2.2 for the AC framework and 2.2 for the WS framework). These nodes invoke the required functions from the Links and Nodes interface to acquire necessary data or execute specific actions, such as robot and gripper movement or vibrational feedback delivery. During initial testing, it was observed that the gripper exhibited a latency in reaching the desired position, leading to a temporary halt in robot control. To mitigate this issue and prevent disruptions in the control loop, the gripper control was decoupled and managed by a dedicated node,

gripper control, allowing for parallel execution. Furthermore, a button on the M5Stick is employed to enable indexing. The corresponding UDP socket for this functionality is also implemented within the UDP communication process (receiving data) node.

3 User Study

The user study aims to determine the most suitable form of shared autonomy assistance for the proposed system. Prior to the experiment, the experimental procedure was thoroughly explained to participants in both oral and written form, and informed consent was obtained from each participant. The study protocol, including data collection procedures, was reviewed and approved by the DLR ethics committee.

A total of nine male and three female participants, with an average age of 27.3 ± 6.8 took part in the experiment. The study task involved grasping an object, either a plate or a cup and repositioning it to a predefined location. The task was divided into three phases: (1) reaching for the object using the robotic system and maneuvering the robots TCP close enough to the object. The object was placed in a predefined position within a drying rack. (2) grasping the object with the user-controlled gripper and (3) finally carrying and placing it at the predefined final position. In Fig. 18 the experimental setup for the task with the plate is depicted and in Fig. 19 the experimental setup for the task with the cup.

Participants were equipped with the described user interface, which included IMU on the upper and lower arm as well as the hand, a Myo armband on the lower arm, and the Fingertac on the fingertips see Fig. 13. The training of the hand pose for the Ridge Regression algorithm (see Section 2.3.1) was done as follows for rest and power grasp: First the inital position of the users hand for 9 seconds, second flexion, extension, supination and pronation for $5\,\mathrm{s}$ each and lastly in a dynamic manner for $5\,\mathrm{s}$ in which the user moves its hand wrist in a circular motion. Before engaging in teleoperation with the LWR, the participants performing the task with the plate were asked to do the task manually using their own hand while their movement data, including position and task completion time, were recorded. These data served as a ground truth reference for later analysis. Since the standard deviations of traveled distances and completion time was low ($0.5 \pm 0.07\,\mathrm{m}$. for traveled distance and $6.2 \pm 0.8\,\mathrm{s}$. for completion time) and due to the fact that the plate and cup are placed and grasped at the same positions, these data were only recorded for the group performing the task with the plate.

During initial tests performing the task before conducting the study, it was noticed that the plate could not be reliably grasped with the HCG or the CLASH even if the gripper is positioned perfectly to the object. To avoid falling of the object a wooden brick was attached on to the plate to ensure a safe grasp if commanded.

Before each trial, participants performed a calibration procedure as described in Chapter 2.1. Additionally, they were given the option to request retraining of the hand pose

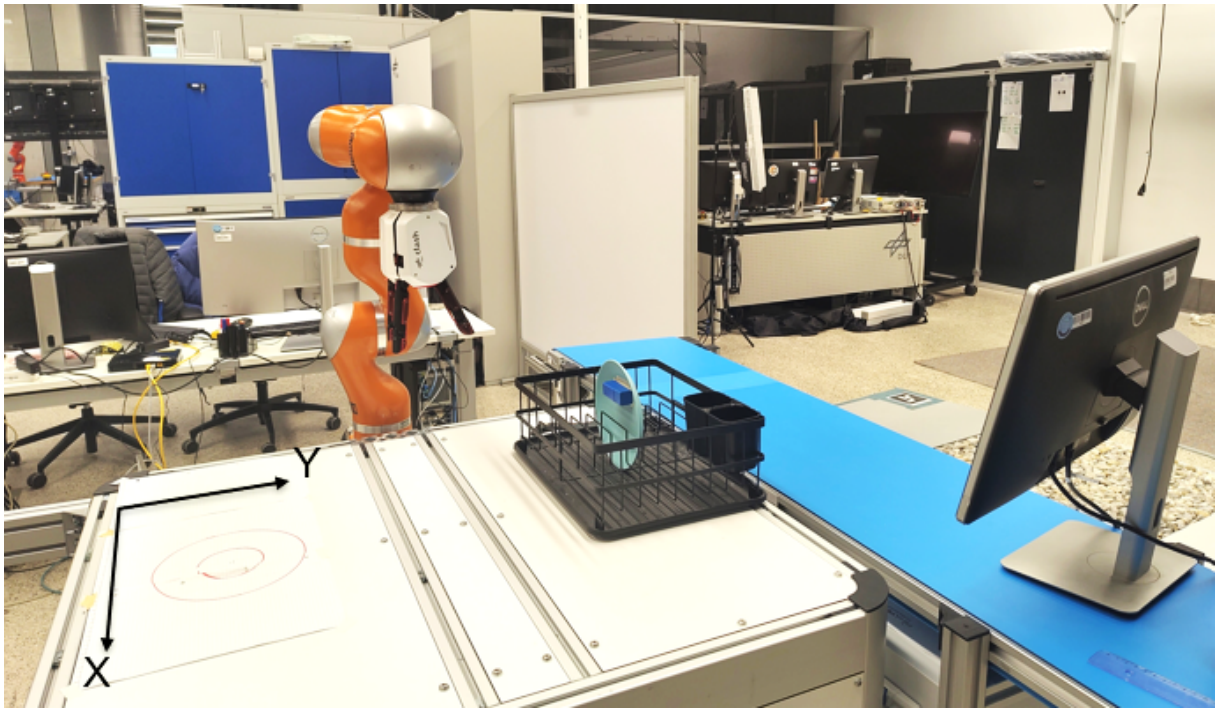

Figure 18. The photograph depicts the experimental setup with the robot and the CLASH mounted on the robots TCP, the drying rack and the plate, the final positions for plate and cup on the left marked with red circles and the corresponding coordinate system and a screen on the right for a convenient view during the calibration phase.

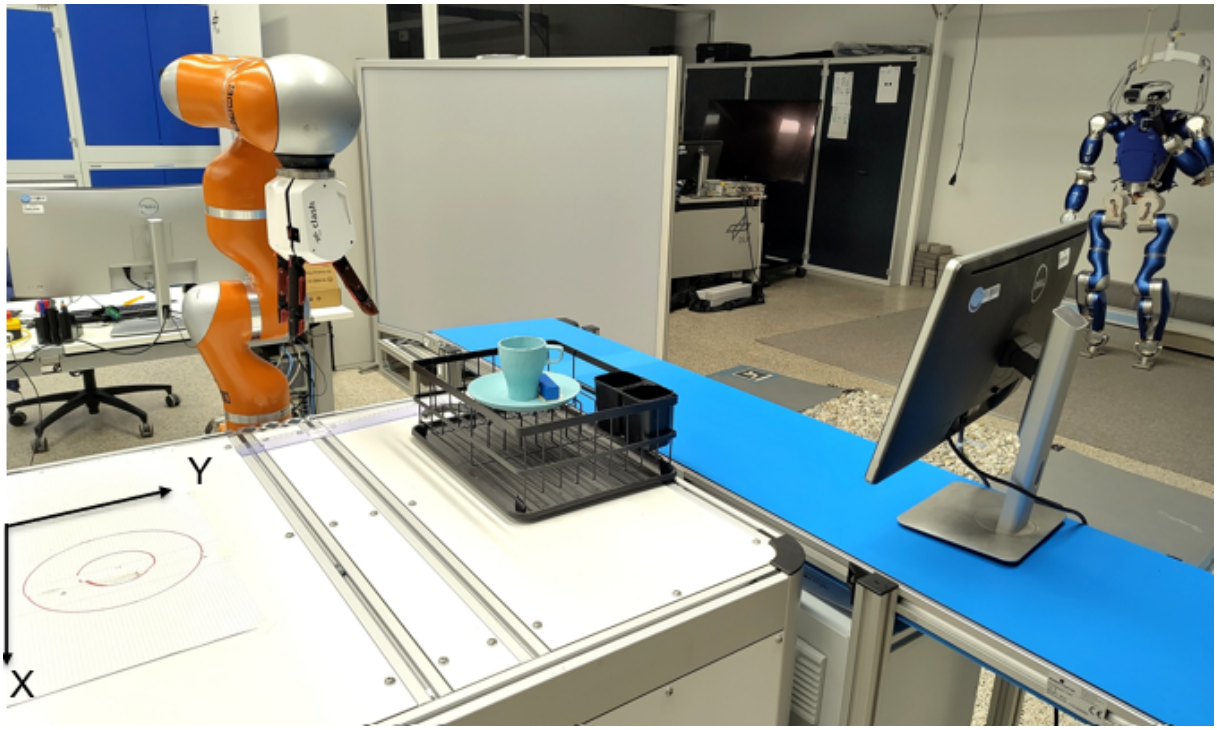

Figure 19. The photograph depicts the experimental setup with the robot and the CLASH mounted on the robots TCP, the drying rack and the cups initial position, the final positions for plate and cup on the left marked with red circles and the corresponding coordinate system and a screen on the right for a convenient view during the calibration phase.

at any point during the experiment. If drift occurred in the IMU sensors, a linear and rotational offset was adjusted for the user to ensure that the workspace could be fully utilized with the robot. The participants underwent a training phase to familiarize themselves with the system. They first controlled the robot and gripper in Teleop mode for six minutes, followed by three-minute trials in each of the two shared autonomy modes.

Following the training phase, the main experiment started. Each participant was assigned to a specific object, either a plate or a cup and performed the task under all three control modes for six minutes per mode, completing as many repetitions as possible within the time limit. After each trial, participants were required to complete two questionnaires: the NASA Task Load Index (NASA-TLX) [41] and the Virtual Embodiment Questionnaire (VEQ) [42]. Throughout the study, data were recorded, including the positions and orientations of the users hand, the robots TCP, the gripper's position, sEMG control signals, and task completion times. The different modes are the independed variables and the order of the modes was randomized to compensate for possible learning effects. The objective metrics include success rate, completion time, travelled distance of the TCP, and the displacement of the object from its final position. Subjective user assessments are evaluated using the NASA TLX and VEQ scales.

The statistical significance was assessed using the following analysis: First, the data was tested for normality using the Shapiro-Wilk-Test. If the data followed a normal distribution, significance was evaluated using mixed effects models. Since linear mixed models show advantages over repeated measures ANOVA [43] [44] [45] and due to their ability to account for random factors such as individual differences between users, linear mixed models were chosen as the preferred analysis method. If the data was not normally distributed, a Friedman test was performed. If a significant result was found in the Friedman test, pairwise comparisons between the modes were conducted using the Wilcoxon Signed-Rank test.

4 Results

This chapter presents the results of the user study. First, the results of the objective metrics are presented, revealing no statistically significance findings between the modes, except for the success rate. This is followed by the results of the subjective assessments, namely the NASA TLX and VEQ, where significant effects are described if they were found. It is not further stated, if no significance was found between any mode for any metrics. See Appendix A.2 for detailed results of the linear mixed models.

4.1 Objective Measurements

4.1.1 Success Rates

The success rates are evaluated in two different ways. First, they are calculated based on the sums of successes and failures independent from the users. The overall success rate across all modes, tasks, and users is 58.9%. Fig. 20 presents the corresponding plots for the different modes: overall (Fig. 20a) with success rates of 56.7% for Telepo, 65.7% for AC and 52.7% for WS, for tasks performed with the plate (Fig. 20b) with success rates of 39,2% for Telepo, 50% for AC, 42.3% for WS and an overall succes rate of 43.9%, and for tasks involving the cup (Fig. 20c) with success rates of 76% for Teleop, 76.9% for AC, 62.1% for WS and an overall succes rate of 71.6%. In general, descriptively, users achieved the highest success rates for the AC mode independent of the object. Teleop has a higher success rate for the tasks with the cup compared to WS, but for the plate tasks it is vice versa.

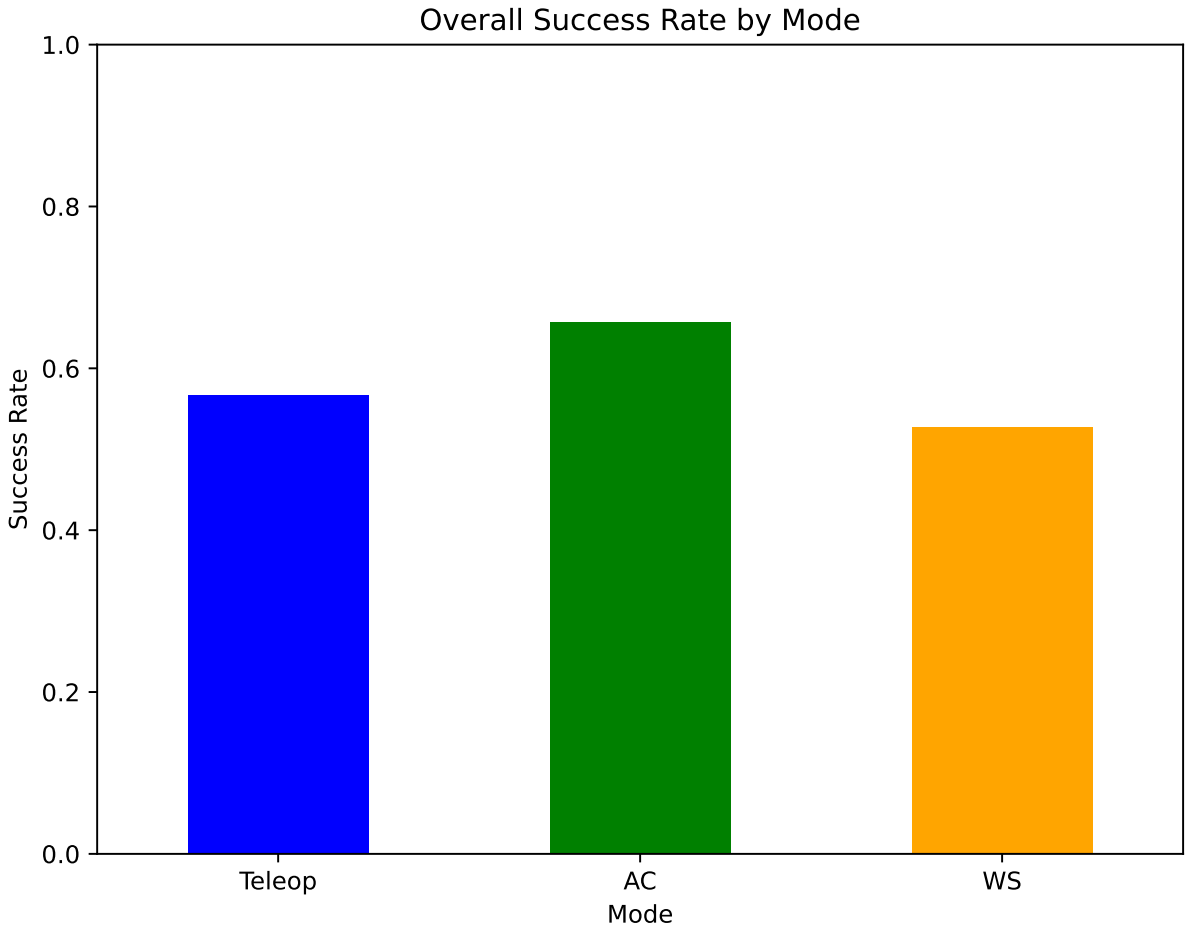

(a) The success rates per Mode for all objects. The mode AC has the highest success rate, while the success rate.

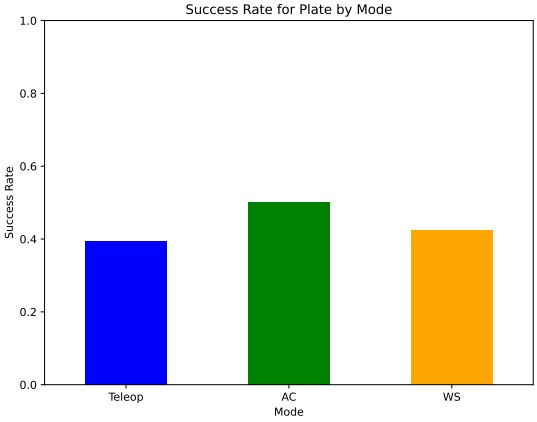

(b) The success rates per Mode for the tasks performed with the plate. AC has the highest success rate compared to the other modes.

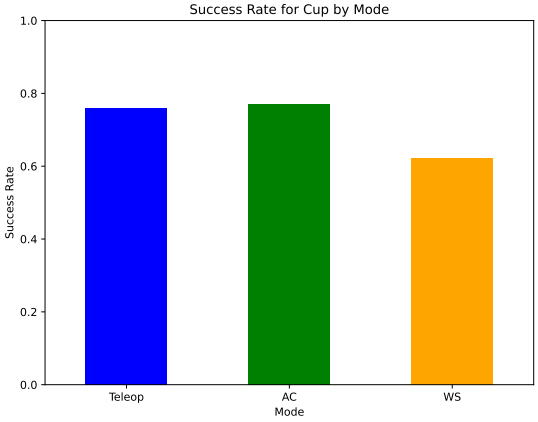

(c) The success rates per Mode for the tasks performed with the cup. AC has the highest success rate compared to the other modes.

Figure 20. Success rates over all modes and objects and over the tasks with plate and cup.

In addition to calculating the success rates based on the sums of all successes and failures, independent of the users, the bar charts in Fig. 21 displays the average success rates. In this case, the success rate for each user is calculated first, and then the averages are determined. This approach gives less weight to users who were able to perform the task more times, compared to those who were able to complete fewer repetitions within the six-minute time frame.

The average success rate across all modes, tasks and users is 54.2%. Fig. 21a presents the average success rates for different modes and tasks overall tasks and users for the different modes. AC has the highest average success rate of all modes with 63.3%, followed by Teleop with 52.4% and WS with 47%. The difference in success rates between AC and WS is significant (p=0.048).

Fig. 21b shows the average success rate overall attempts performed with the plate for each mode and Fig. 21c for the cup. The average success rate over all attempts and modes for the plate is 46.4% and for the cup 62,3%. The difference between the success rates of AC and WS for the task conducted with the cup is significant (p=0.0361).

Among the different modes, AC achieves the highest average success rates. The comparison between Teleop and WS is less straightforward. Overall, as well as in tasks involving the cup, Teleop outperforms WS. However, for plate-related tasks, the average success rates of Teleop and WS are nearly identical (43.9% for Teleop and 43.3% for WS).

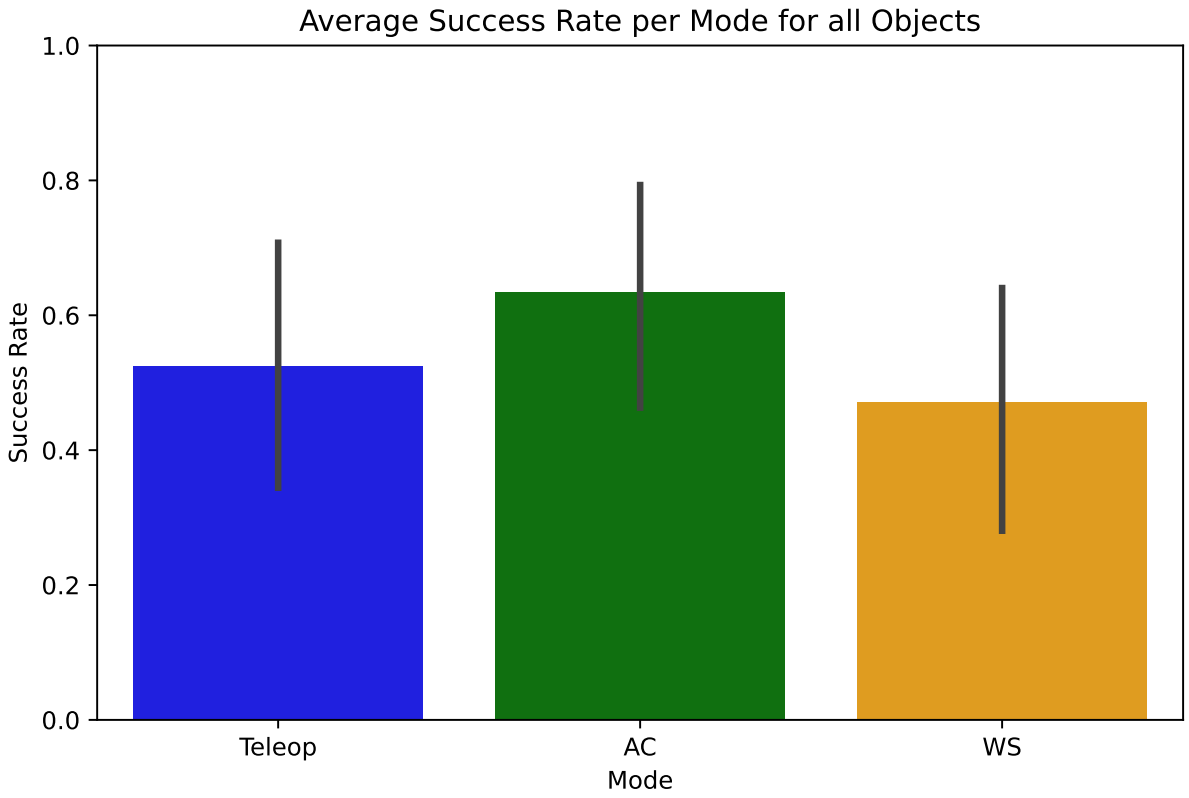

(a) The average success rates per mode for all objects. The mode AC has the highest success rate with over 60 %, while the success rate of Teleop and WS is at around 50%.

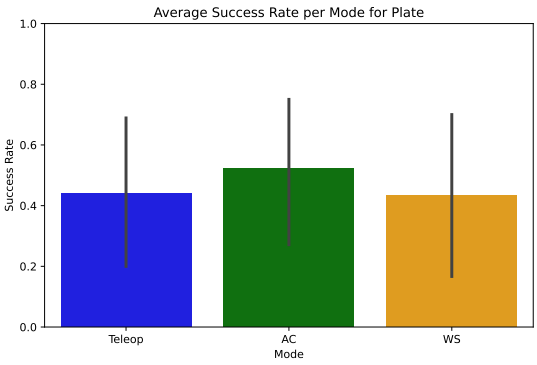

(b) The average success rates per mode for the tasks performed with the plate. AC has the highest success rate compared to the other modes.

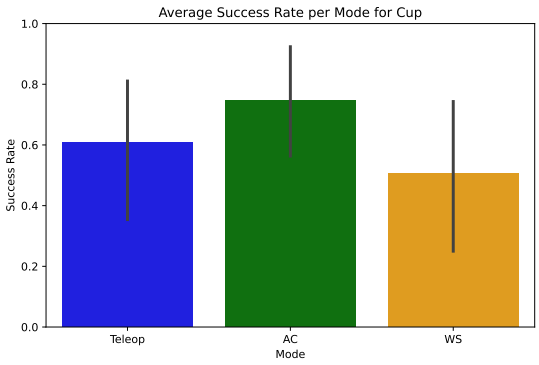

(c) The average success rates per mode for the tasks performed with the cup. AC has the highest success rate compared to the other modes.

Figure 21. Average success rates and standard deviations over all modes and objects and over the tasks with plate and cup.

4.1.2 Completion Times

The completion time is defined as the duration from the first movement of the real LWR until the user positioned the object. The average completion time over all modes and object (without considering the mode "without robot") is $45.954\,\mathrm{s}$. The bar charts in Fig. 22a illustrate the average completion time in seconds for the different modes, including Teleop, AC, WS, and without robot. The "without robot" mode exhibits the shortest completion time. The modes Teleop, AC and WS differ only slightly. Also for the object-dependend diagramms (Fig. 22b and Fig. 22c) the differences are less than 8% among the modes with the robot. The task with the cup (average completion time of $41.3\,\mathrm{s}$) could be accomplished $13.2\,\mathrm{s}$ faster in average, compared to the one with the plate (average completion time of $54.5\,\mathrm{s}$).

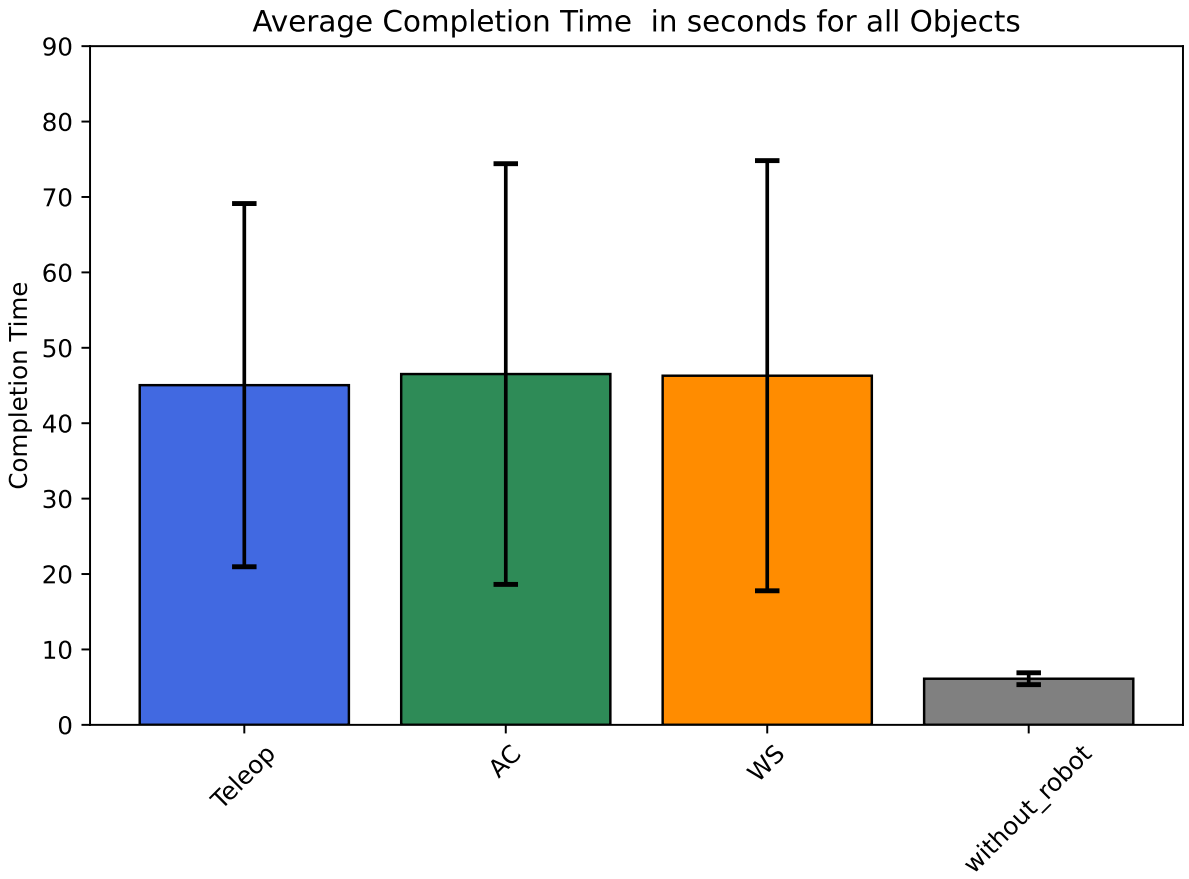

(a) Average completion times in seconds for all successful attempts over all objects.

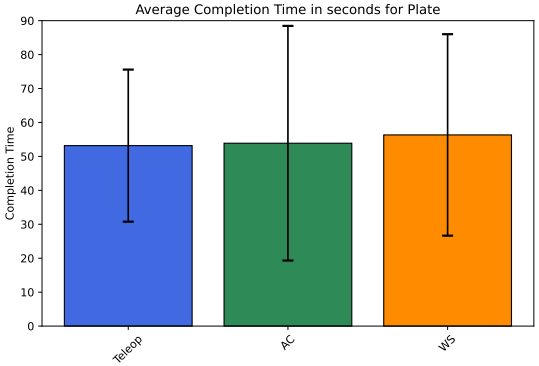

(b) Average completion times in seconds for the task performed with the plate.

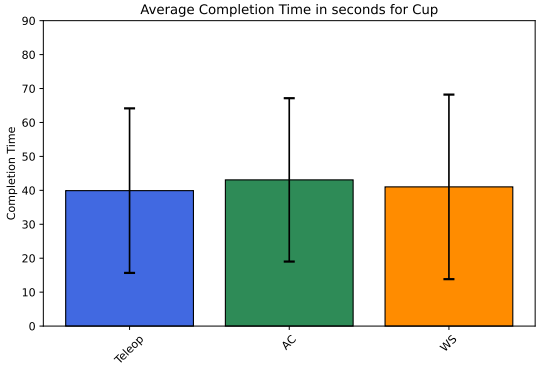

(c) Average completion times in seconds for the task performed with the cup.

Figure 22. Averages and standard deviations for the objective metrcies completion time in seconds.

4.1.3 Travelled Distances

The average travelled distance across all modes, tasks and users (without the catergory "without robot") is $2.2\,\mathrm{m}$. Fig. 23a presents the average traveled distances in m of the robot's TCP across the different modes, including Teleop, AC, WS, and without robot (where the traveled distance of the user's hand is measured and scaled according to the robot's control commands). The "without robot" mode exhibits the shortest traveled distance. The traveled distances in Teleop and AC are comparable, with only minor differences. Among the robot-assisted modes, WS results in the shortest traveled distance regardless of the handled object. Comparing travelled distance between the modes Teleop and AC for the different objects, the results are not as large as for the WS. For the task with the plate Teleop outperforms AC (Fig. 23b), but for the task with the cup it is the other way around (Fig. 23c). The tasks involving the cup has a lower average travelled distance ($1.9\,\mathrm{m}$) compared to the tasks with the plate ($2.65\,\mathrm{m}$).

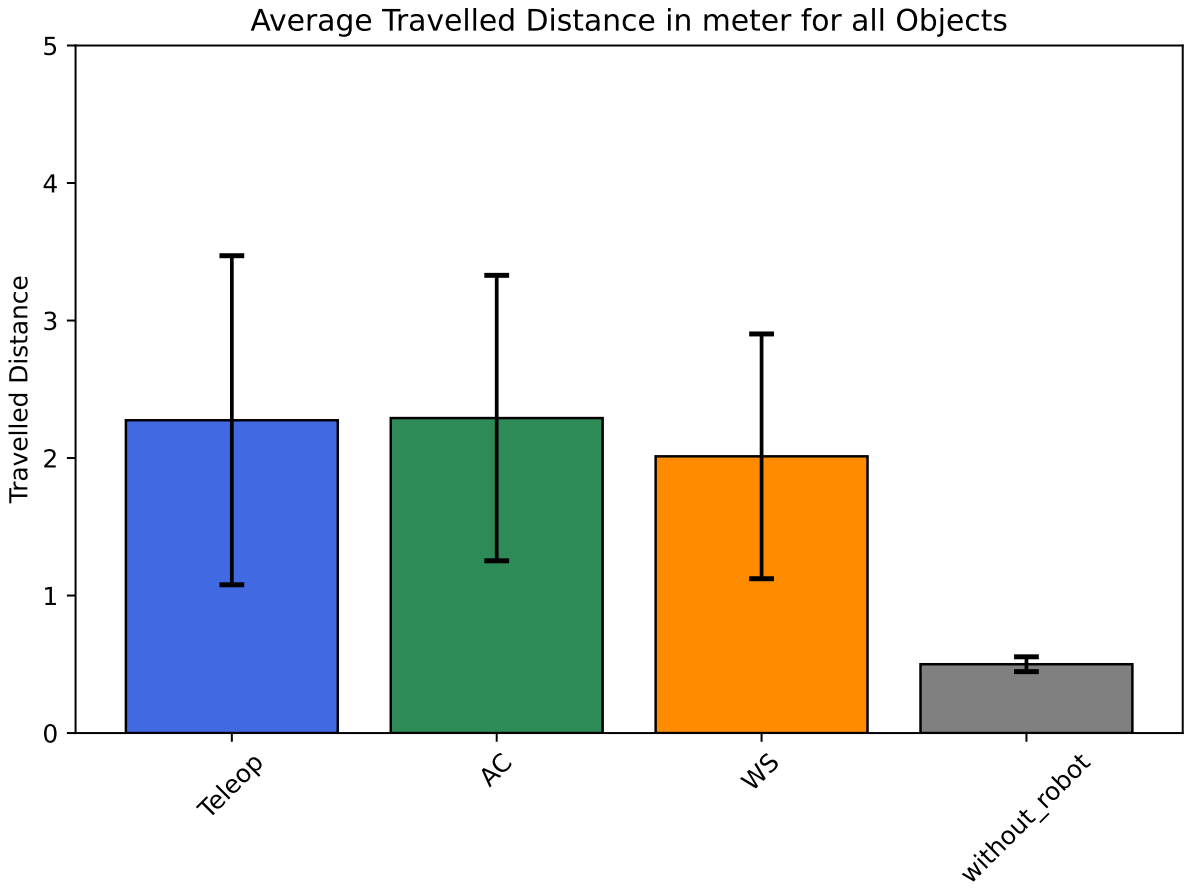

(a) Average traveled distances in m for all successful attempts over all objects.

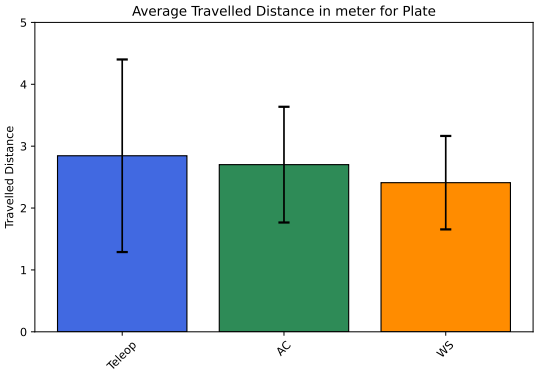

(b) Average Traveled distances in m for the task performed with the plate.

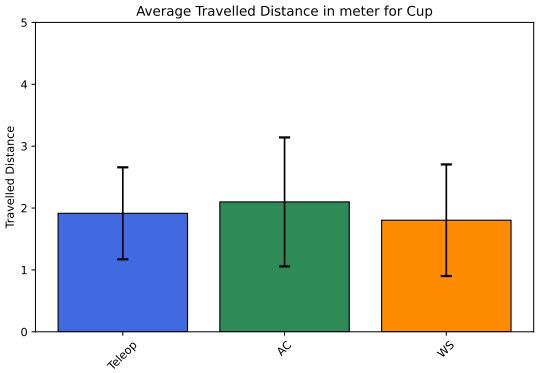

(c) Average Traveled distances in m for the task performed with the cup.

Figure 23. Averages and standard deviations for objective metrics traveled distances in m.

4.1.4 Displacements

The displacements were measured according to the coordinate systems shown in Fig.18 and Fig. 19 after the user placed the object. The diagram in Fig. 24a depicts the average displacement in the X and Y direction in cm for different modes, including Teleop, AC, and WS over all tasks. The average displacement over all modes and tasks is $4.7\,\mathrm{cm}$ in X direction. As all users successfully positioned the plate with a displacement below $1\,\mathrm{cm}$ when performing the task without the robot, this mode is omitted. Teleop exhibits the highest displacement in the X direction, whereas AC and WS facilitate more precise object placement. The average displacement over all tasks and modes in Y direction is $4.8\,\mathrm{cm}$. Teleop and WS show similar levels of accuracy, while AC enables more precise object placement in Y direction.

The average displacements for the plate are shown in Fig. 24b. AC has the lowest average displacement for these tasks in X direction, while Teleop exhibits the highest. In Y direction AC shows the lowest displacement over all modes, while for Teleop and WS the displacements are similarly. Considering the tasks with the cup (Fig. 24c), WS enabled the most precise positioning in X direction, while AC has the highest. The displacements are nearly identical across all modes in Y direction for the cup tasks. In average the users performing the tasks with the cup were able to place it closer to the final position (average displacement in X direction over all tasks with the cup $3.8\,\mathrm{cm}$ and $4.1\,\mathrm{cm}$ in Y direction) compared to the ones with the plate (average displacement in X direction over all tasks with the plate $6\,\mathrm{cm}$ and in Y direction $6.1\,\mathrm{cm}$)

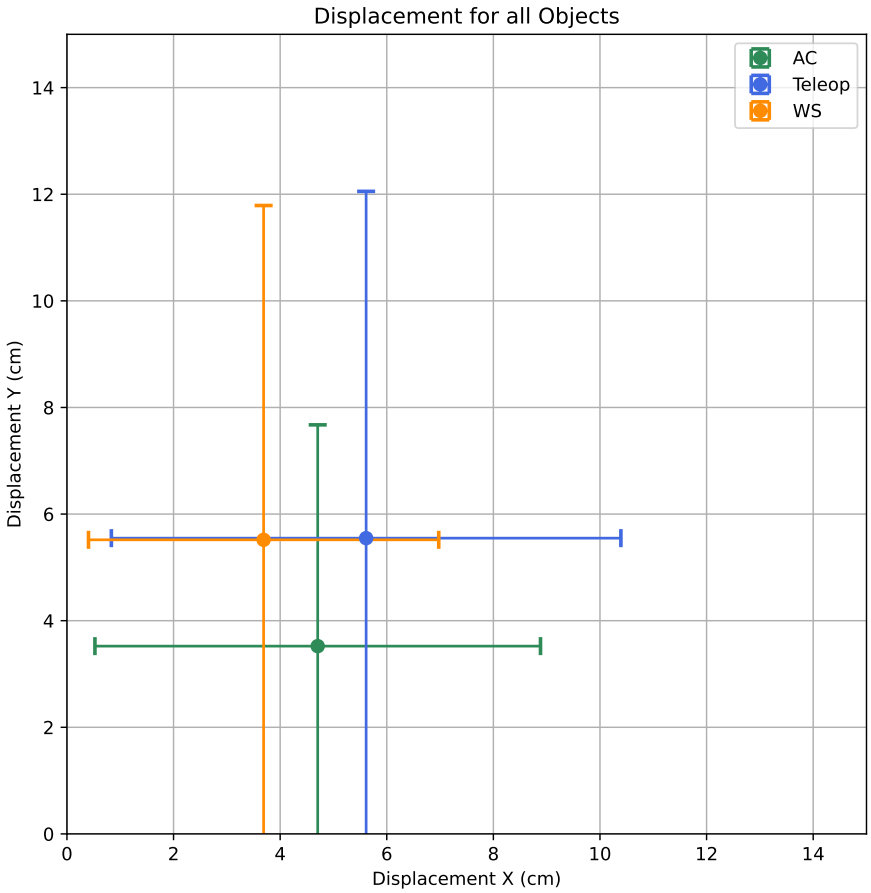

(a) Average displacements for all successful attempts over all objects from the predefined final position in X and Y direction.

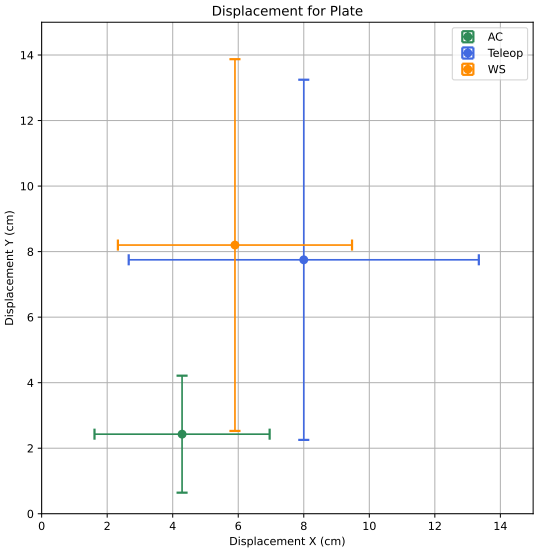

(b) Average displacements for all successful attempts with the plate from the predefined final position in X and Y direction.

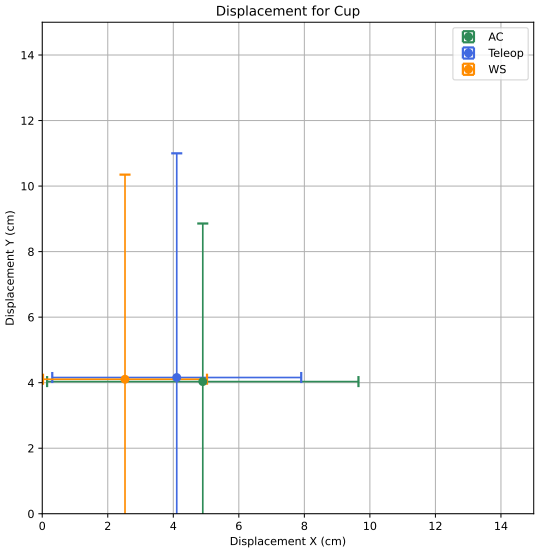

(c) Average displacements for all successful attempts with the cup from the predefined final position in X and Y direction.

Figure 24. Averages and standard deviations for the metrics displacement in X direction.

4.1.5 Learning Effects

The data was analyzed to determine whether users exhibited a learning effect. No learning effect was found when considering the success rates. The following diagrams suggest the presence of a learning curve for some metrics over multiple repetitions. Data was only included in this analysis if more than one user completed a given number of repetitions for a specific object and mode. Since the reliability of the results strongly depends on the number of successful attempts per repetition, Table 1 presents the number of successful trials for each metric and repetition across all modes. Additionally, Table 2 summarizes the data for the Teleoperation mode, Table 3 for the AC mode, and Table 4 for the WS mode. The higher the number of repetitions, the lower the number of successful attempts, meaning that the results are less reliable for many repetitions.

Considering all data without differentiating between modes, a learning trend can be observed for completion time (Fig. 25a for all objects, Fig. 25b for tasks with the plate and Fig. 25c for tasks with the cup) and traveled distance (Fig. 26a for all objects, Fig. 26b for tasks with the plate and Fig. 26c for tasks with the cup).

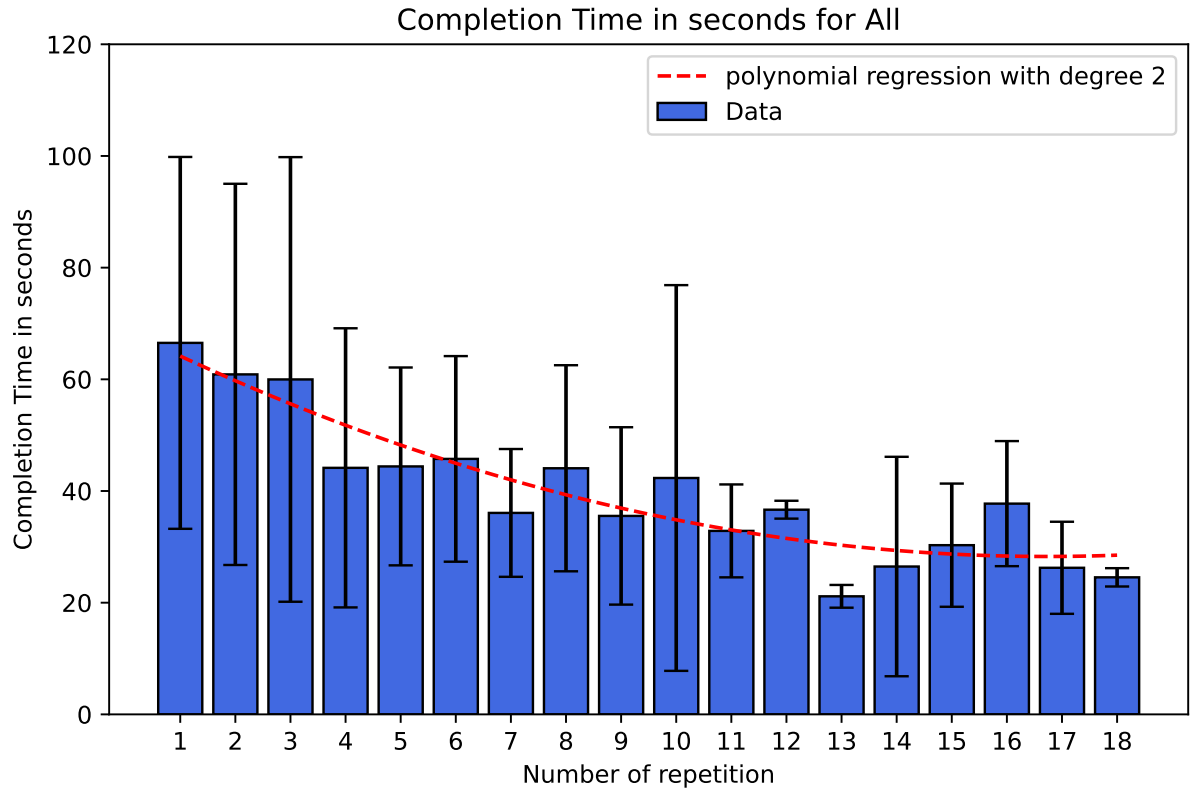

(a) Learning curve in dashed red of the completion time over all successful attempts based on a polynomial regression with degree two.

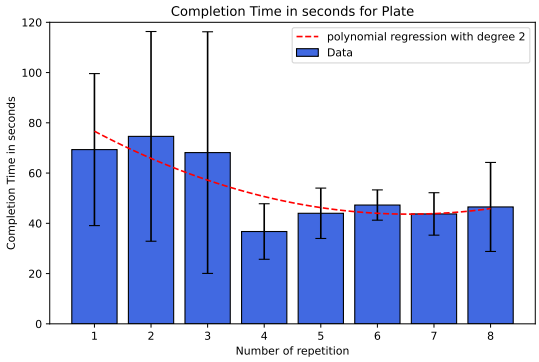

(b) Learning curve in dashed red of the completion time over all successful attempts with the plate based on a polynomial regression with degree two.

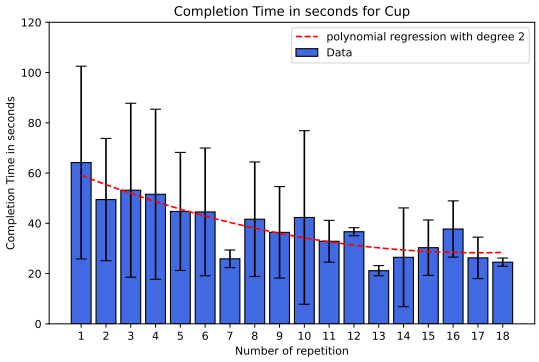

(c) Learning curve in dashed red of the completion time over all successful attempts with the cup based on a polynomial regression with degree two.

Figure 25. Learning curves for completion time are represented as dashed red lines across all successful attempts, as well as separately for attempts with the plate and the cup across all modes.

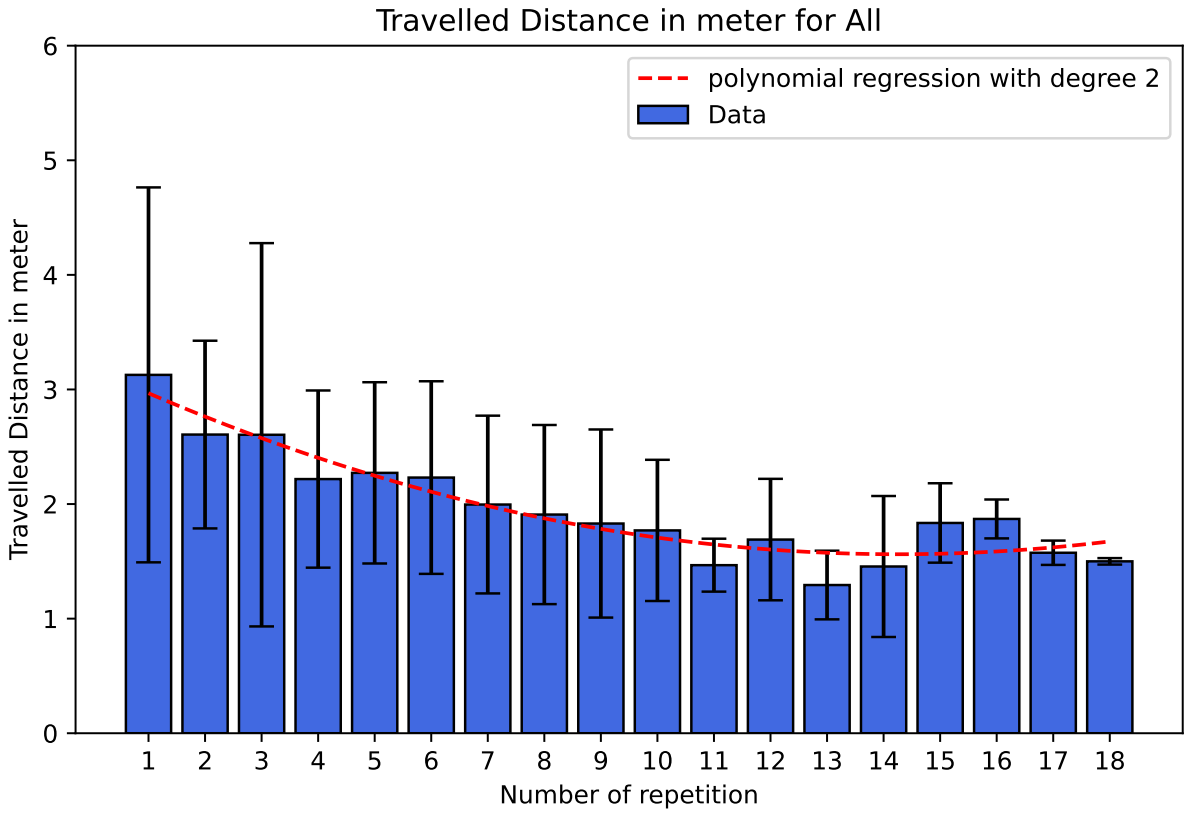

(a) Learning curve in dashed red of the metric traveled distance over all successful attempts based on a polynomial regression with degree two.

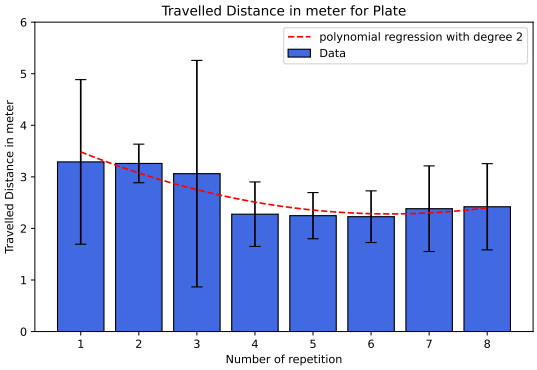

(b) Learning curve in dashed red of the metric traveled distance over all successful attempts with the plate based on a polynomial regression with degree two.

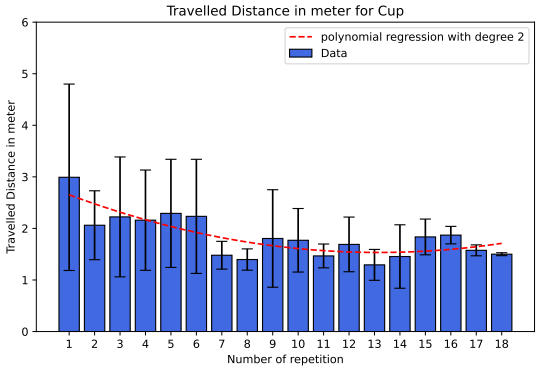

(c) Learning curve in dashed red of the metric traveled distance over all successful attempts with the cup based on a polynomial regression with degree two.

Figure 26. Learning curves for traveled distance are represented as dashed red lines across all successful attempts, as well as separately for attempts with the plate and the cup across all modes.

Repetition	Number of successful trials	Object
1	11	both
2	11	both
3	10	both
4	9	both
5	8	both
6	8	both
7	7	both
8	6	both
9	5	both
10	3	both
11	3	both
12	3	both
13	3	both
14	2	both
15	2	both
16	2	both
17	2	both
18	2	both
1	5	Plate
2	5	Plate
3	5	Plate
4	5	Plate
5	4	Plate
6	4	Plate
7	4	Plate
8	3	Plate
1	6	Cup
2	6	Cup
3	5	Cup
4	4	Cup
5	4	Cup
6	4	Cup
7	3	Cup
8	3	Cup
9	5	Cup
10	3	Cup
11	3	Cup
12	3	Cup
13	3	Cup
14	2	Cup
15	2	Cup
16	2	Cup
17	2	Cup
18	2	Cup

Table 1. Table showing the number of successful trials per repetition for all modes and all objects, as well as for tasks with the plate and the cup.

No learning effect is present in the Teleop mode. This is shown in the diagrams depicting completion time and traveled distance across all objects (Fig. 27a and Fig. 28a) as well as for tasks involving the plate (Fig. 27b and Fig. 28b) and cup (Fig. 27c and Fig. 28c). In these cases, performance deteriorated in the second and third repetitions.

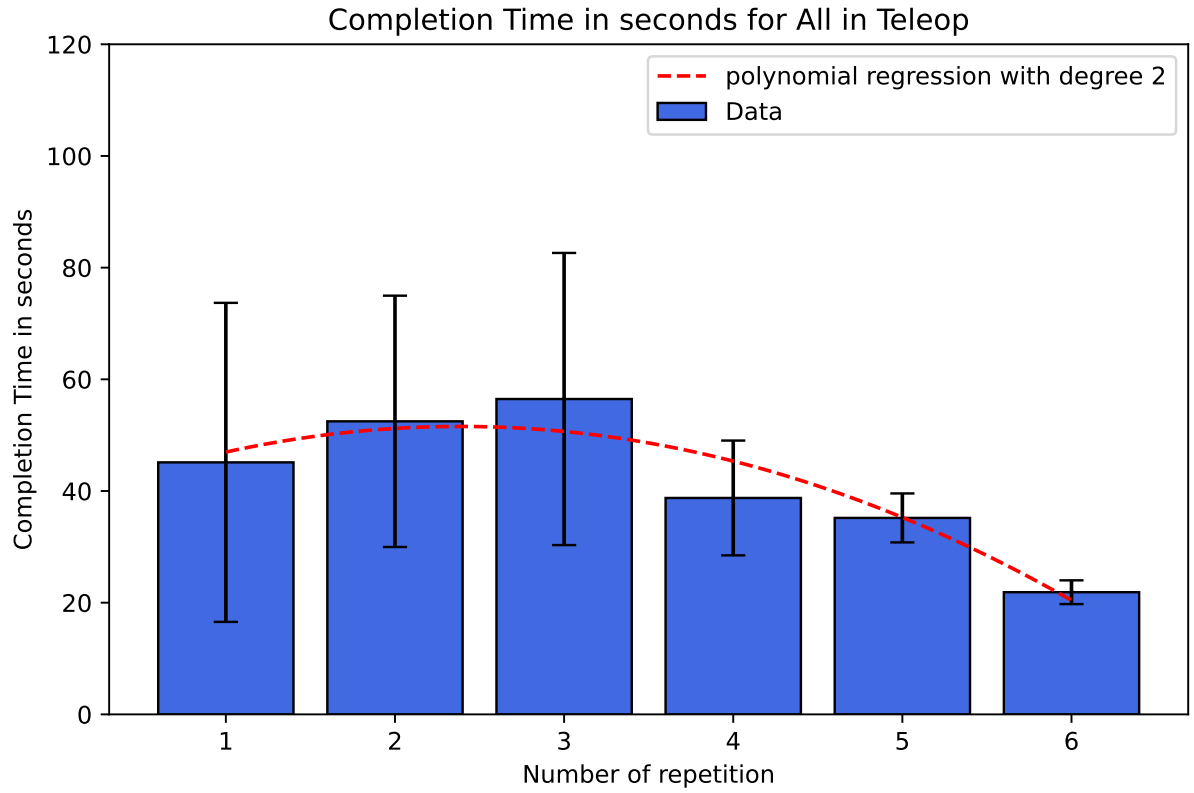

(a) The learning curve for completion time in the Teleop mode is depicted as dashed red line over all attempts.

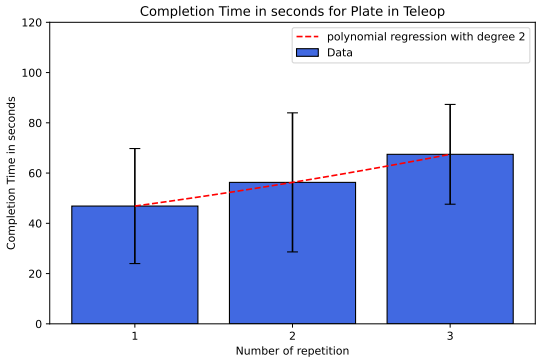

(b) The learning curve for completion time in the Teleop mode is depicted as dashed red line over the attempts performed with the plate.

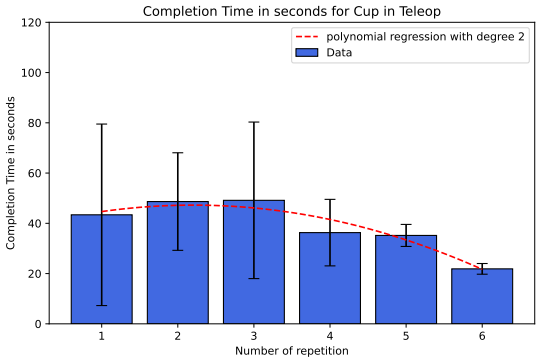

(c) The learning curve for completion time in the Teleop mode is depicted as dashed red line over the attempts performed with the cup.

Figure 27. The learning curves for completion time in the Teleop mode are depicted as dashed red lines, representing all successful attempts in this mode, as well as separately for attempts involving the plate and the cup.

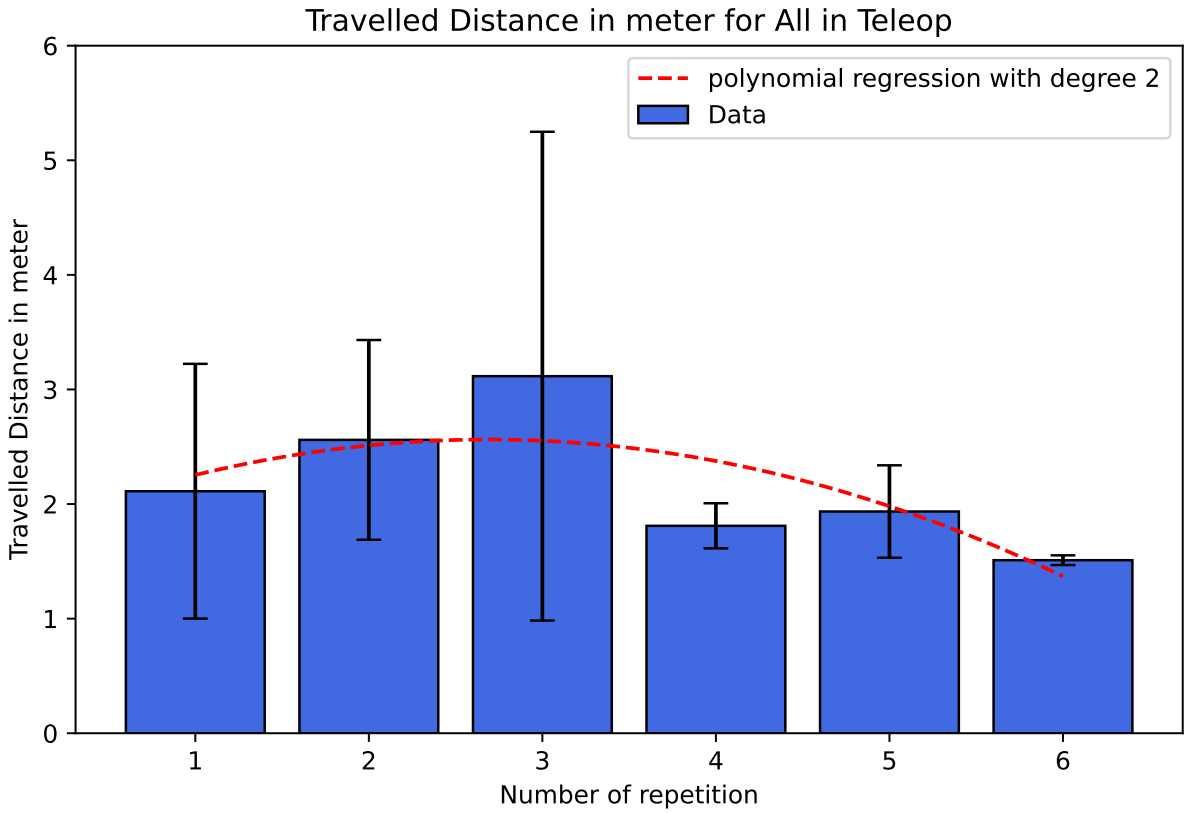

(a) The learning curve for traveled distance in the Teleop mode is depicted as dashed red line over all attempts.

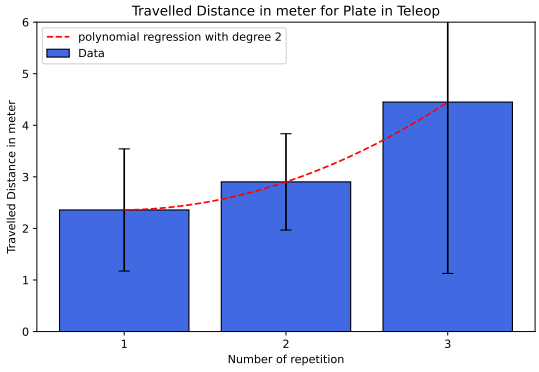

(b) The learning curve for traveled distance in the Teleop mode is depicted as dashed red line over the attempts performed with the plate.

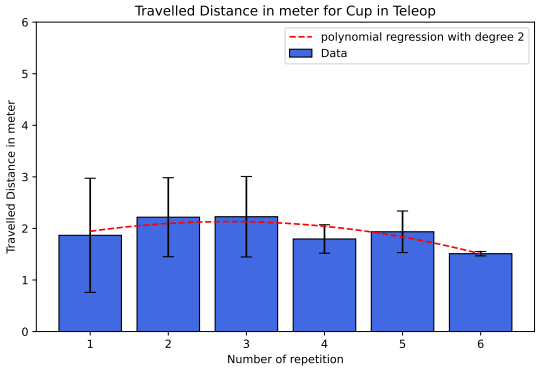

(c) The learning curve for traveled distance in the Teleop mode is depicted as dashed red line over the attempts performed with the cup.

Figure 28. The learning curves for traveled distance in the Teleop mode are depicted as dashed red lines, representing all successful attempts in this mode, as well as separately for attempts involving the plate and the cup.

Repetition	Number of successful trials	Object
1	10	both
2	8	both
3	5	both
4	3	both
5	2	both
6	2	both
1	5	Plate
2	4	Plate
3	2	Plate
1	2	Cup
2	3	Cup
3	2	Cup
4	3	Cup
5	2	Cup
6	2	Cup

Table 2. Table showing the number of successful trials per repetition for Teleop and all objects, as well as for tasks with the plate and the cup.

For the AC mode, a learning effect can be observed in both completion time and traveled distance when considering data from all objects (Fig. 29a and Fig. 30a).

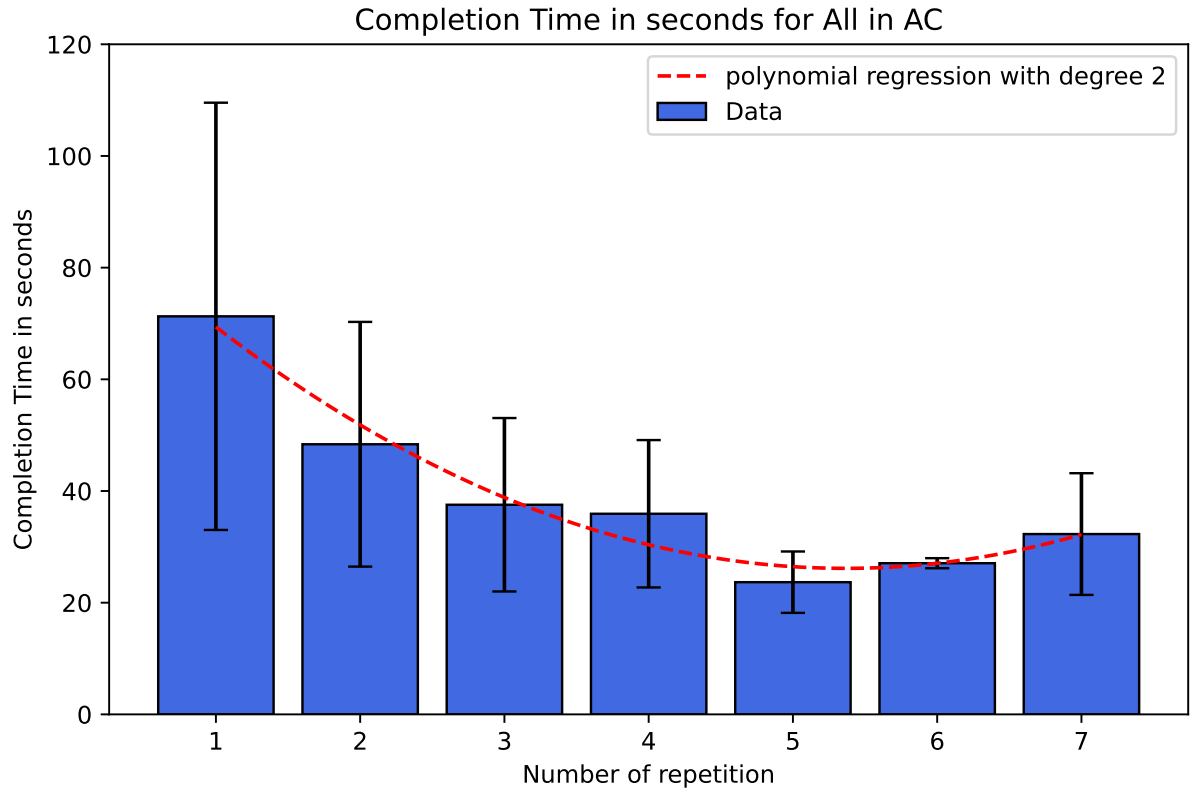

(a) The learning curve for completion time in the AC mode is depicted as dashed red line over all attempts.

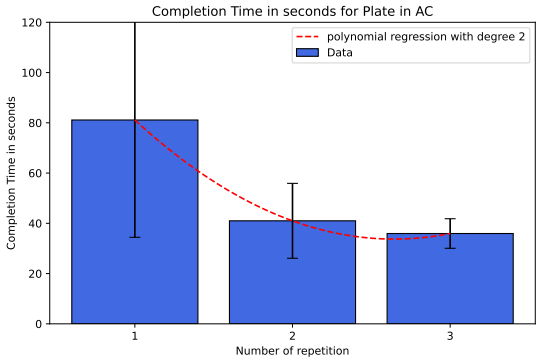

(b) The learning curve for completion time in the AC mode is depicted as dashed red line over the attempts performed with the plate.

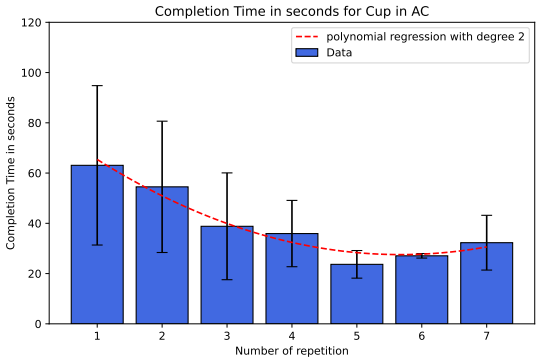

(c) The learning curve for completion time in the AC mode is depicted as dashed red line over the attempts performed with the cup.

Figure 29. The learning curves for completion time in the AC mode are depicted as dashed red lines, representing all successful attempts in this mode, as well as separately for attempts involving the plate and the cup.

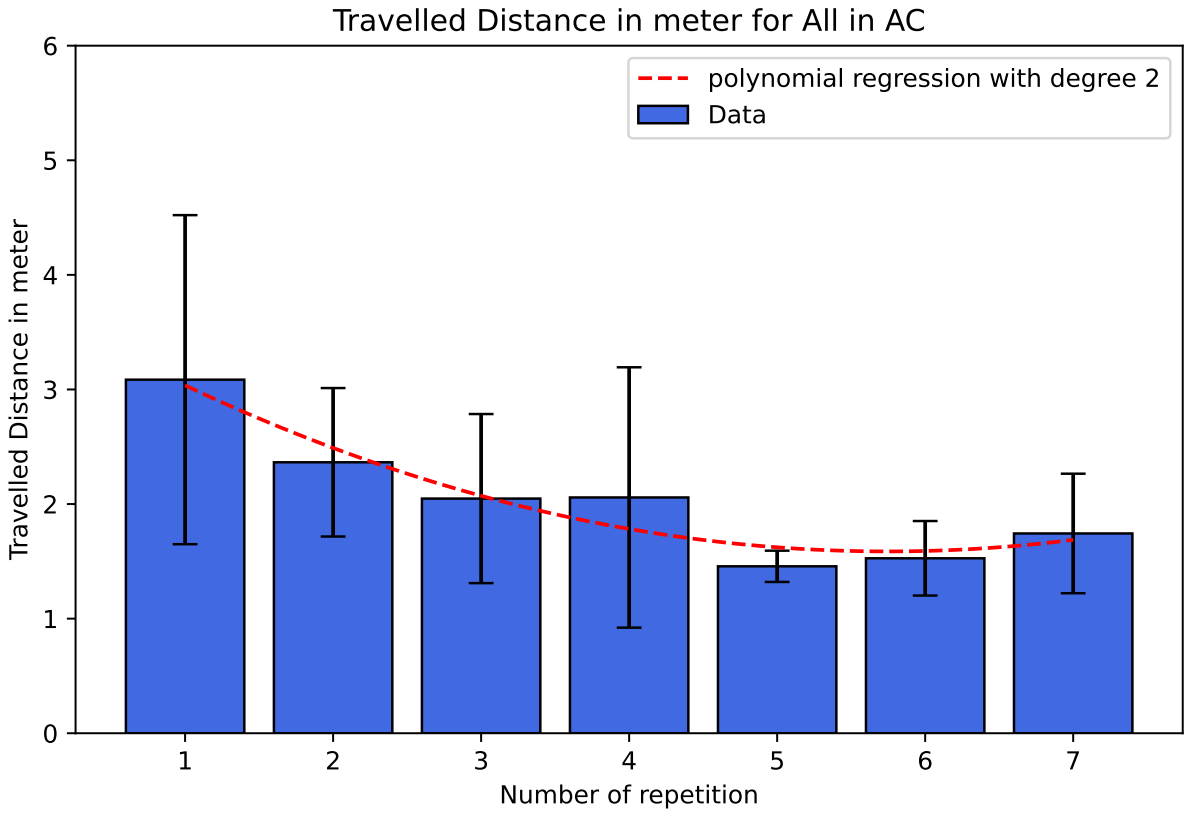

(a) The learning curve for traveled distance in the AC mode is depicted as dashed red line over all attempts.

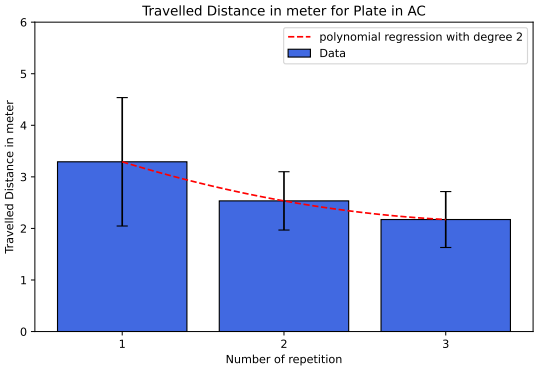

(b) The learning curve for traveled distance in the AC mode is depicted as dashed red line over the attempts performed with the plate.

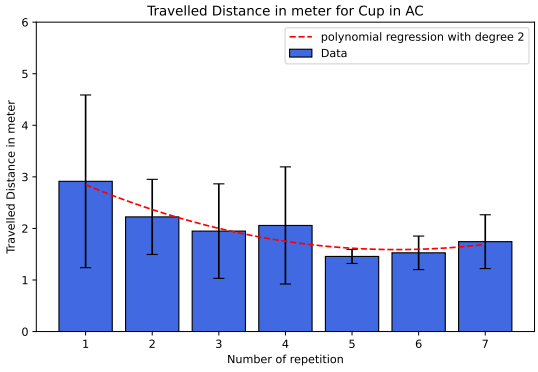

(c) The learning curve for traveled distance in the AC mode is depicted as dashed red line over the attempts performed with the cup.

Figure 30. The learning curves for traveled distance in the AC mode are depicted as dashed red lines, representing all successful attempts in this mode, as well as separately for attempts involving the plate and the cup.

Repetition	Number of successful trials	Object
1	9	both
2	9	both
3	7	both
4	4	both
5	3	both
6	3	both
7	3	both
1	5	Plate
2	5	Plate
3	4	Plate
1	4	Cup
2	4	Cup
3	3	Cup
4	4	Cup
5	3	Cup
6	3	Cup
7	3	Cup

Table 3. Table showing the number of successful trials per repetition for AC and all objects, as well as for tasks with the plate and the cup.

Similarly to AC, in the WS mode, a learning effect can be seen for these metrics across all objects (Fig. 31 and Fig. 32). However, for tasks involving the plate in WS mode, no learning effect are observed (Fig. 31b and Fig. 32b), as the second repetitions show worse performance than the initial attempts.

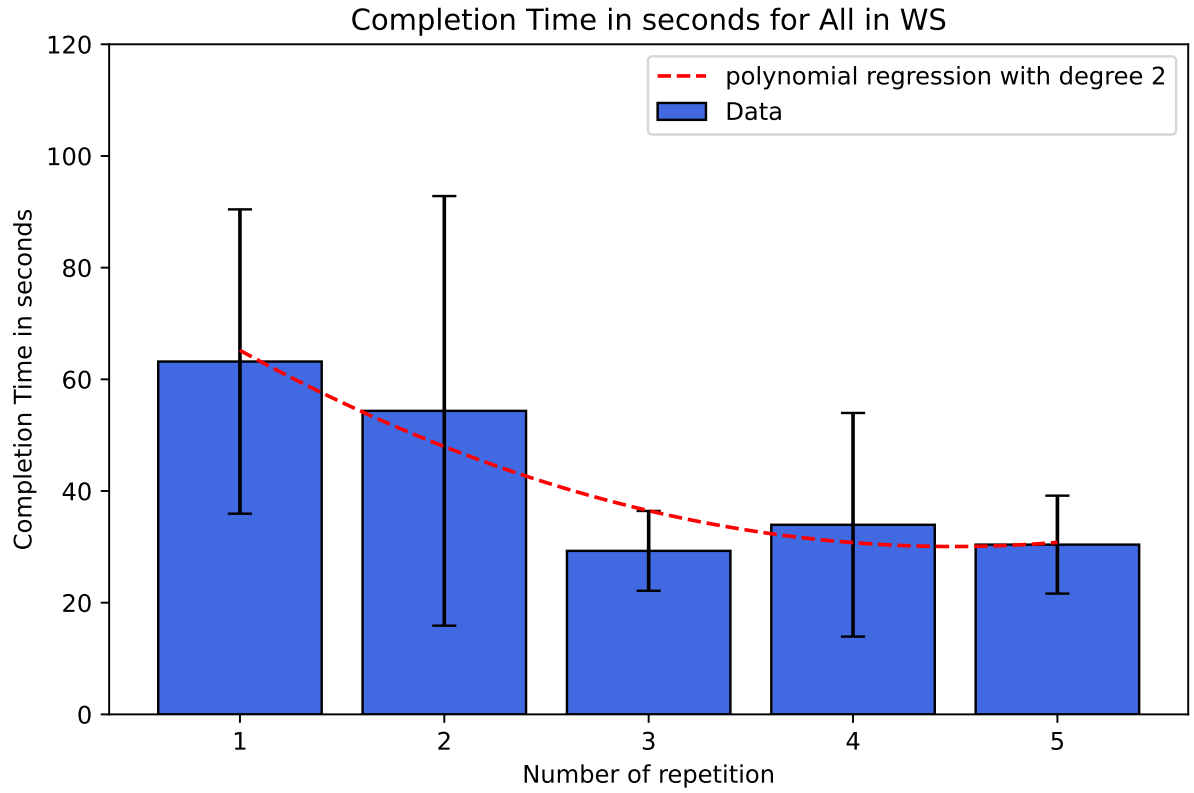

(a) The learning curve for completion time in the WS mode is depicted as dashed red line over all attempts.

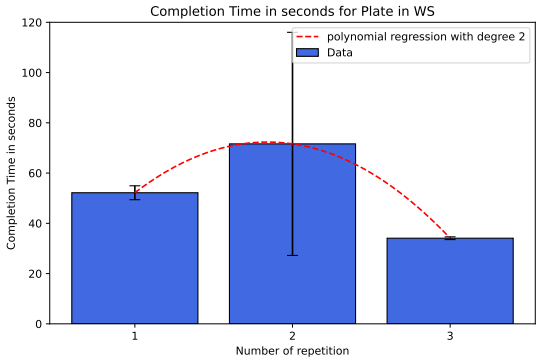

(b) The learning curve for completion time in the WS mode is depicted as dashed red line over the attempts performed with the plate.

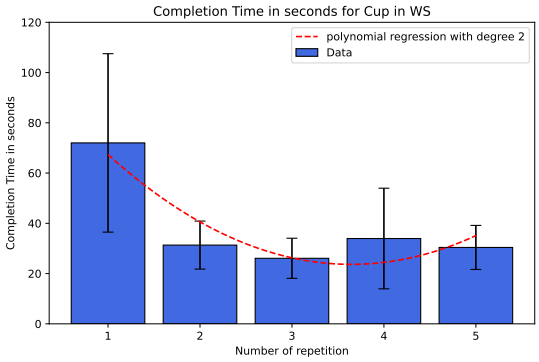

(c) The learning curve for completion time in the WS mode is depicted as dashed red line over the attempts performed with the cup.

Figure 31. The learning curves for completion time in the WS mode are depicted as dashed red lines, representing all successful attempts in this mode, as well as separately for attempts involving the plate and the cup.

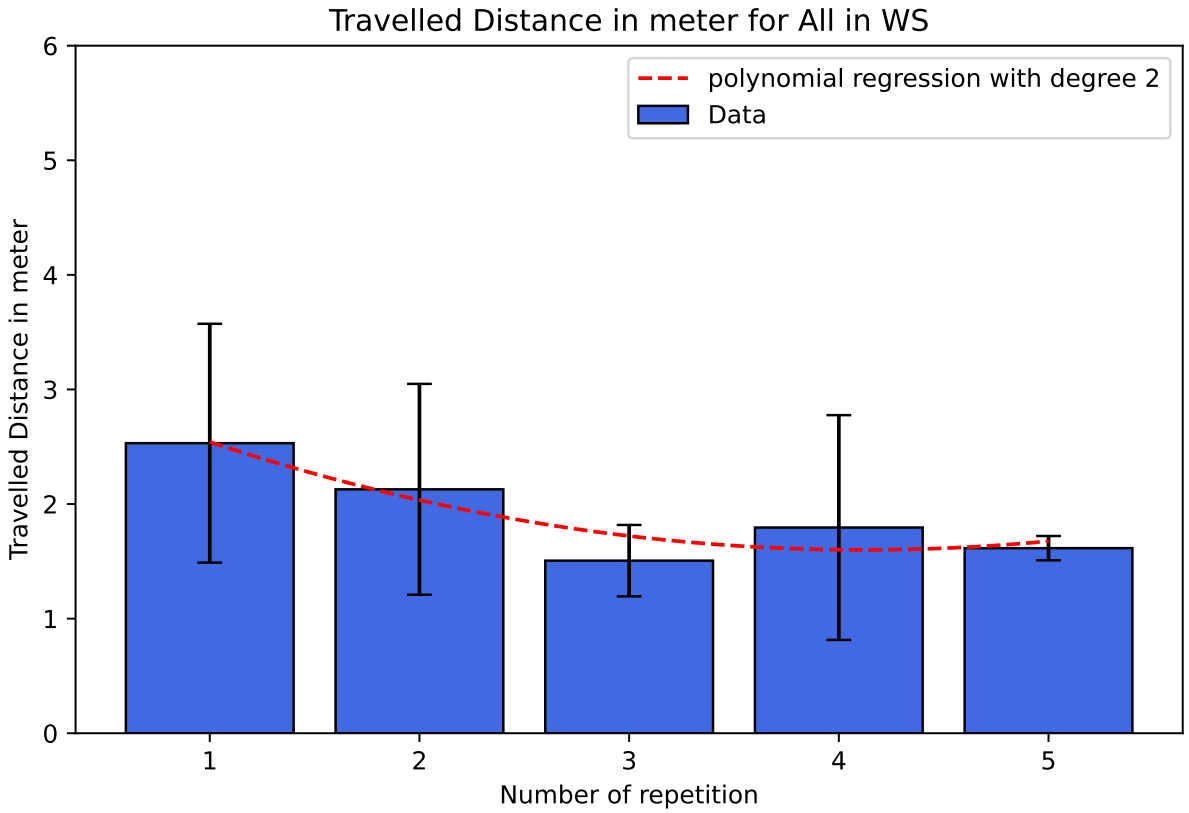

(a) The learning curve for traveled distance in the WS mode is depicted as dashed red line over all attempts.

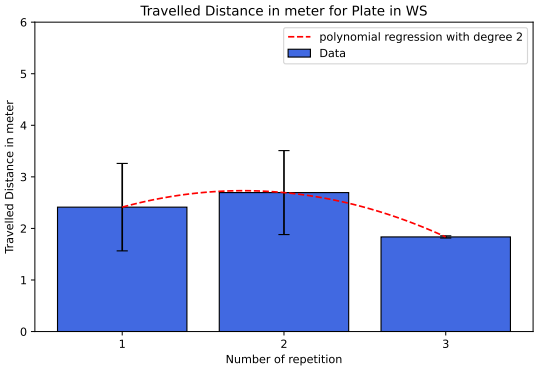

(b) The learning curve for traveled distance in the WS mode is depicted as dashed red line over the attempts performed with the plate.

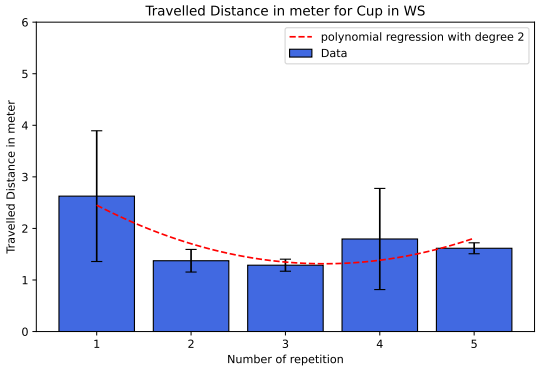

(c) The learning curve for traveled distance in the WS mode is depicted as dashed red line over the attempts performed with the cup.

Figure 32. The learning curves for traveled distance in the WS mode are depicted as dashed red lines, representing all successful attempts in this mode, as well as separately for attempts involving the plate and the cup.

Repetition	Number of successful trials	Object
1	9	both
2	7	both
3	5	both
4	4	both
5	2	both
1	4	Plate
2	4	Plate
3	2	Plate
1	5	Cup
2	3	Cup
3	3	Cup
4	4	Cup
5	2	Cup

Table 4. Table showing the number of successful trials per repetition for WS and all objects, as well as for tasks with the plate and the cup.

4.2 Subjective Measurements

To assess the users' subjective perceptions during the study, they were asked to complete the NASA TLX and VEQ questionnaires after performing each mode. The results are presented below.

4.2.1 NASA Task Load Index

The NASA TLX is analyzed in three different ways: considering all tasks, only the tasks involving the plate, and only tasks involving the cup. The results are normalized on a scale from 0 to 10 and averaged. Fig. 33 displays the results across all tasks, independent of the object, for the different modes (Teleop in Fig. 33a, AC in Fig. 33b, and WS in Fig. 33c). The corresponding standard deviations are shaded in the color associated with each mode. AC is the mode that received the least demanding ratings from users across all NASA TLX measures. However, for the Performance metric, AC and Teleop were rated similarly. WS was rated second best, except for Performance, where Teleop was rated less demanding than WS.

The difference in Mental Demand between Teleop and AC, as well as between AC and WS, is statistically significant ($p = 0.0355$ and $p = 0.0296$, respectively). However, no statistically significant difference was found between Teleop and WS ($p = 0.059$). For Physical Demand, a statistically significant difference was observed between Teleop

and AC (p = 0.0382) and between Teleop and WS (p = 0.008), whereas there was no significant difference observed between AC and WS (p = 0.26). Regarding Temporal Demand, a significant difference was found between Teleop and AC (p = 0.0252), but not between Teleop and WS (p = 0.796) or between AC and WS (p = 0.0741). For all other NASA TLX measures, independent of the object, no statistically significant differences were found between the modes.

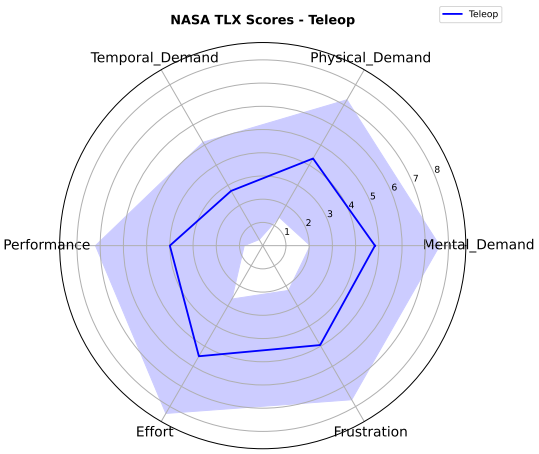

(a) Results of the NASA TLX across all tasks independent of the object for Teleop.

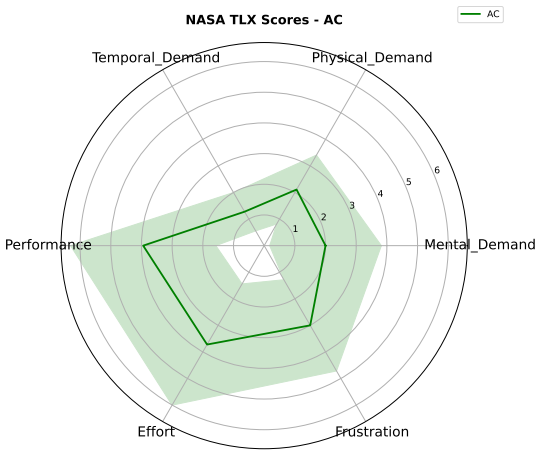

(b) Results of the NASA TLX across all tasks independent of the object for AC.

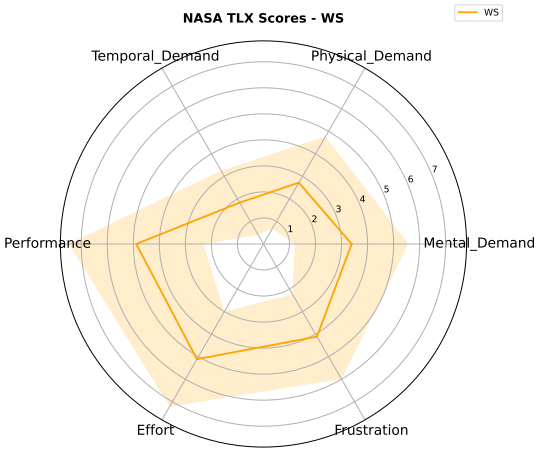

(c) Results of the NASA TLX across all tasks independent of the object for WS.

Figure 33. The NASA TLX results are presented, with solid lines indicating the mean values and shaded areas representing the standard deviations.

For tasks involving the plate (Fig. 34), AC showed the lowest ratings across all NASA TLX measures, meaning it is considered the least demanding mode. WS ranked second for Temporal Demand, Physical Demand, Mental Demand, and Frustration, while Teleop ranked second for Performance and Effort. For tasks with the plate, a statistically significant difference was found for Mental Demand between Teleop and AC (p = 0.0), Teleop and WS (p=0.03), AC and WS (p=0.041). Physical Demand is significant different between Teleop and AC (p=0), Teleop and WS (p=0.025) and AC and WS

(p=0.04). Similarly, Temporal Demand showed a significant difference between Teleop and AC (p = 0.0431), but not between any other mode comparisons. Additionally, Frustration was significantly different between Teleop and AC (p = 0.0312), whereas no significant differences were found between the other modes.

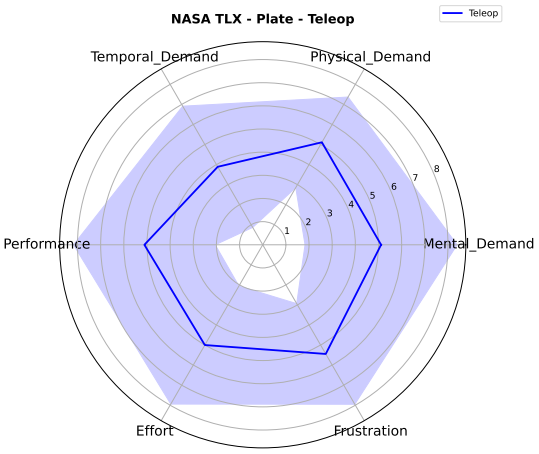

(a) Results of the NASA TLX for the tasks involving the plate for Teleop.

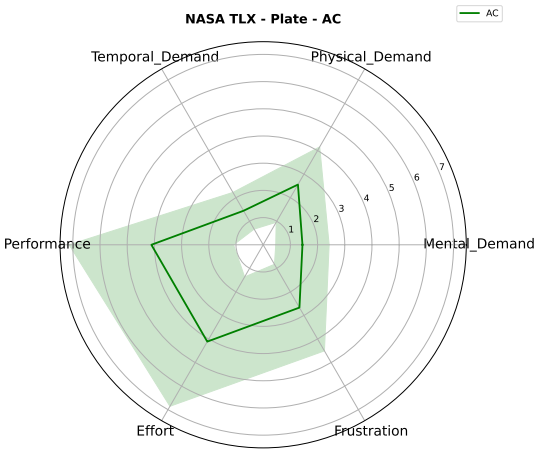

(b) Results of the NASA TLX for the tasks involving the plate for AC.

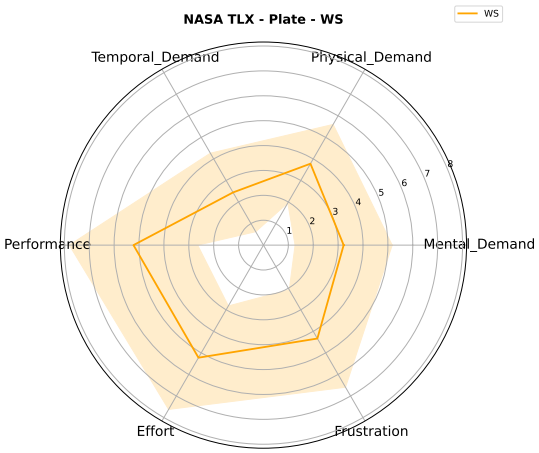

(c) Results of the NASA TLX for the tasks involving the plate for WS.

Figure 34. The NASA TLX results are presented, with solid lines indicating the mean values and shaded areas representing the standard deviations.

Tasks involving the cup (Fig. 35), results do not show a clear tendency towards any specific mode. AC was rated lowest for Mental Demand, Frustration, Effort, and Temporal Demand, while Teleop received the lowest rating for Performance. Physical Demand, AC and WS were rated similarly. However, except for Performance, Teleop received the highest ratings across all other measures, meaning it is considered the most demanding mode for these measures. The difference between Teleop and AC is significant (p=0.044) for Effort. For the other metrics no significance was found.

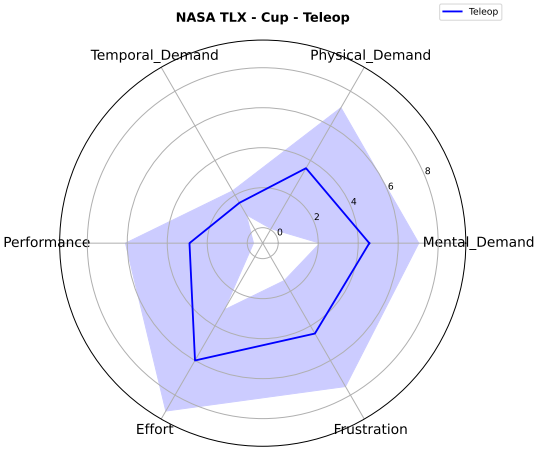

(a) Results of the NASA TLX for the tasks involving the cup for Teleop.

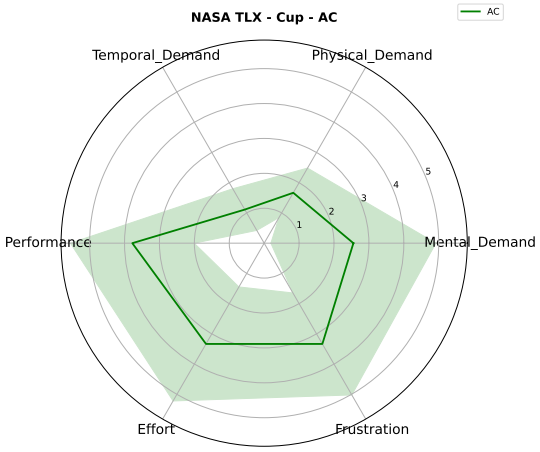

(b) Results of the NASA TLX for the tasks involving the cup for AC.

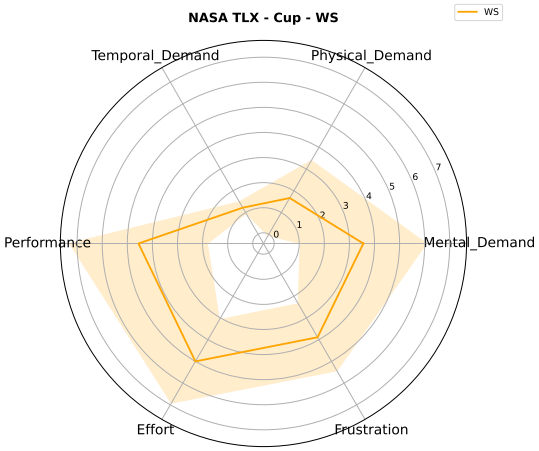

(c) Results of the NASA TLX for the tasks involving the cup for WS.

Figure 35. The NASA TLX results are presented, with solid lines indicating the mean values and shaded areas representing the standard deviations.

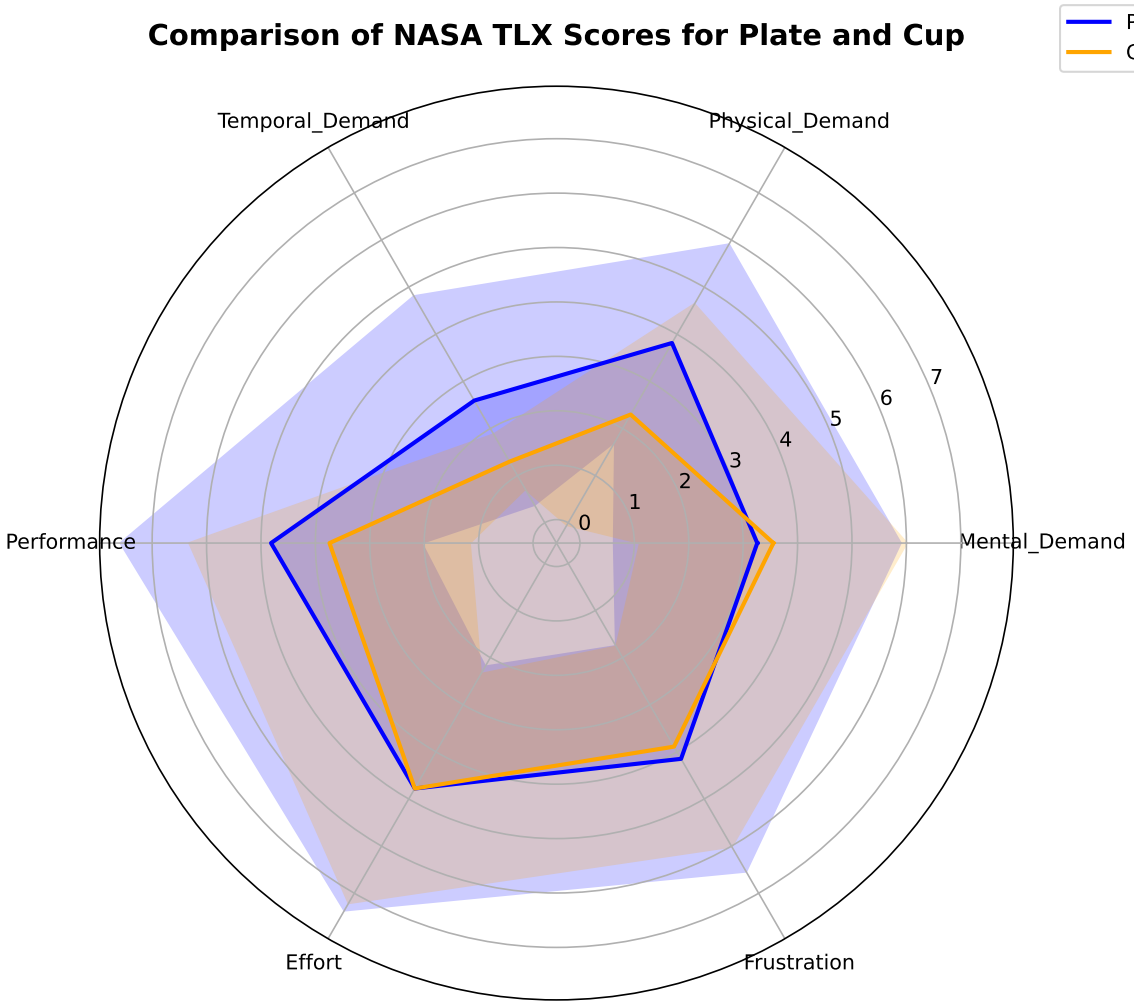

Figure 36. Result of the NASA TLX averaged across all modes for the tasks with the plate and the cup.

Fig. 36 presents the average ratings across all modes for plate and cup tasks. Cup tasks were perceived as less demanding in terms of Physical Demand, Frustration, Performance, and Temporal Demand, whereas plate tasks were rated as less demanding for Mental Demand. Effort was rated equally demanding for both objects.

4.2.2 Virtual Embodiment Questionnaire

In the following charts the results of the VEQ are presented, each mode is represented by a bar showing the average perception scores with the corresponding standard deviation shaded around the bars. The diagrams in Fig. 37 show the overall results independent of the objects, in Fig. 38 the results for the plate are illustrated and in Fig. 39 the ones for the cup tasks.

Fig. 37a shows the acceptance for all tasks independent of the object for the different modes. Descriptively, AC shows the highest acceptance for all measures, while WS shows the lowest for "It felt like robot parts were my body parts" and "It felt like the robot belonged to me". The difference between Teleop and AC for "It felt like the robot belonged to me" is significant (p=0.022), as well as between AC and WS for the same category (p=0.009).

The perceived control of the users over all tasks is illustrated in Fig. 37b. AC exhibits the highest values for all measures. WS shows the lowest values for "The movements of the robot felt like they were my movements" and Teleop for "The movements of the robot were in sync with my own movements". For the other two metrics, WS and Teleop are rated similarly.

In Fig. 37c the perceived change of all users are shown. The mode AC caused the highest change in appearance and width, while WS for weight and size. Teleop had the lowest change for size and width among the modes. WS and Teleop are similarly in terms of change of appearance and Teleop and AC in terms of weight.

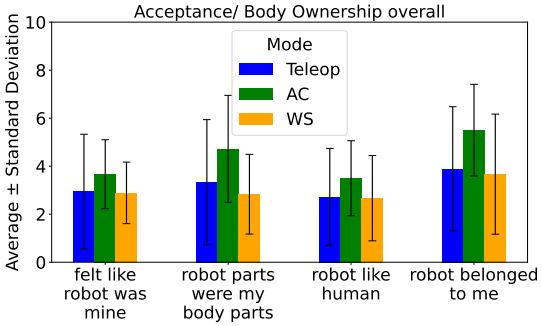

(a) Perceived acceptance over all users.

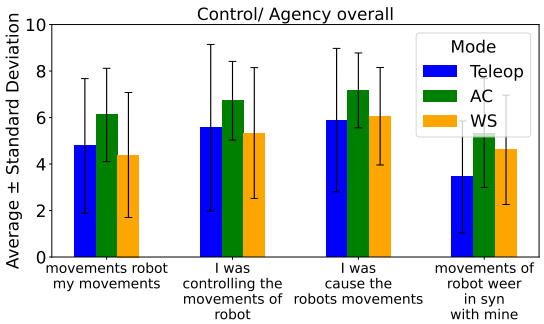

(b) Perceived control over all users.

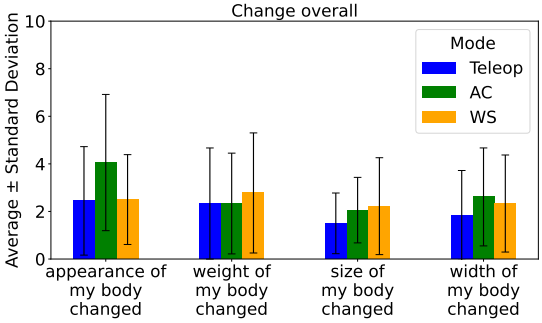

(c) Perceived change over all users.

Figure 37. Results of the VEQ over all users.

Fig. 38a illustrates the body ownership perception during the task with the plate across the different modes. The WS mode has the lowest average values, while AC shows the highest values, indicating better perceived body ownership. Teleop showed a higher value than Teleop but still lower than AC. AC scores significantly higher than WS in

the category "It felt like the robot parts were my body parts" (p=0.034). The difference between Teleop and AC for "robot belonged to me" is significant (p=0.029), as well as between AC and WS (p=0.012).

The perceived control and agency of the users for the task with the plate is displayed in Fig. 38b. AC shows the highest agency across all measurements. WS the second highest for the metrics "I felt like I was controlling the movements of the robot", "I felt like I was causing the movements of the robot" and for "The movements of the robot were in synch with my own movements". Teleop outperforms WS in the first metric "The movements of the robot felt like they were my movements". User felt significantly higher control in terms of "I felt like I was causing the movements of the robot" in AC compared to Teleop (p=0.033) and in terms of "The movements of the robot were in synch with my own movements" (p=0.039).

Fig. 38c presents the average changes in body perception, such as weight, size, and width changes, when performing the task with the plate for each mode. Descriptively, the Teleop mode generally shows the least amount of change across the measured parameters, except for the perceived change of weight, here Teleop and AC exhibit a similar height. AC indicates the highest changes in body perception for appearance size and width change. WS shows the lowest change for appearance and weight and Teleop for size and width. The perceived change in appearance between Teleop and AC and between AC and WS is significant (p=0.032 each). Also the perceived change in size is significant between Teleop and AC and between AC and WS (p=0.042 each). In Fig. 39a the acceptance of the proposed system with the task evolving the cup is illustrated. AC has the highest acceptance values over all measures. Fig. 39b displays the results of the perceived control/ agency for the cup tasks. AC has the highest perceived control for all metrics, except for "Movements of the Robot were in sync with mine", here WS show higher agency.

The diagram in Fig. 39c shows the data for change for tasks involving the cup. WS shows the highest scores over all measurements. The AC mode tends to show less change in size, and width of the body compared to Teleop. For the change in appearance of the own body and weight Teleop and WS exhibit similarly results.

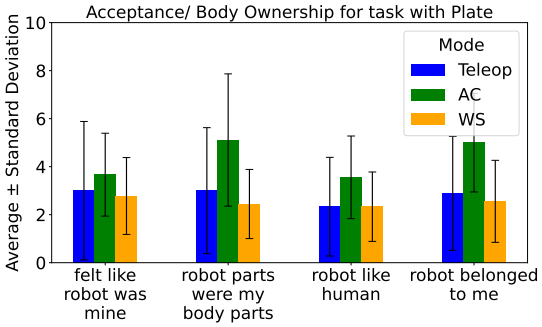

(a) Perceived acceptance of the users that performed the task with the plate.

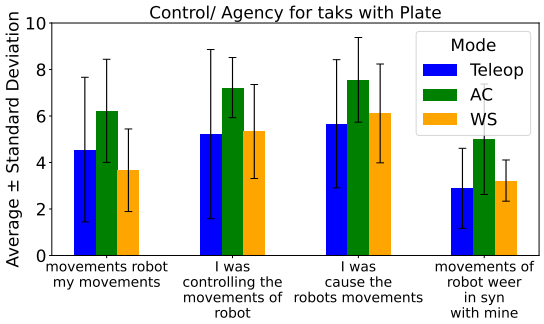

(b) Perceived control/agency of the users that performed the task with the plate.

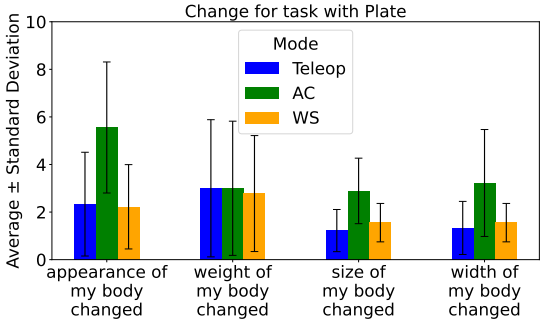

(c) Perceived change of the users that performed the task with the plate.

Figure 38. Results of the VEQ of the users that performed the task with the plate.

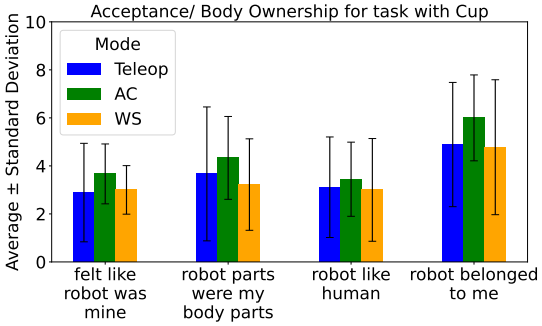

(a) Perceived acceptance of the users that performed the task with the cup.

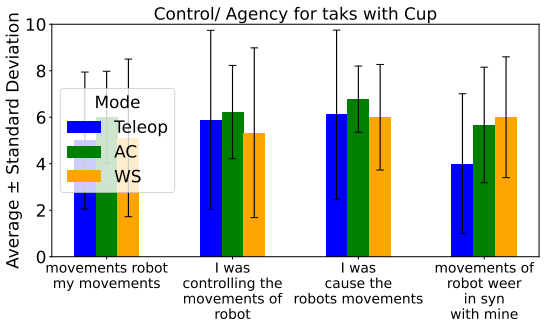

(b) Perceived control/agency of the users that performed the task with the cup.

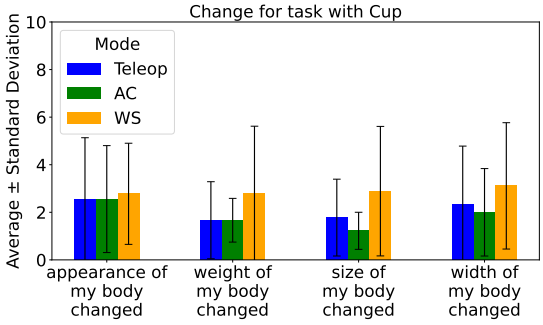

(c) Perceived change of the users that performed the task with the cup.

Figure 39. Results of the VEQ of the users that performed the task with the cup.

4.2.3 Semi Structured Interview

After completing all three control modes, participants completed a semi-structured interview consisting of seven open-ended questions (see Fig. 40 in Appendix A). Users reported difficulties in controlling the rotation of the TCP. Most participants preferred the AC mode, as it relieved them from the need to manage TCP rotation. Several users indicated that grasping the object was more challenging than moving the robot itself.

For some participants, the sEMG-based control of the gripper did not function reliably, resulting in unintended gripper movements. Although some attempted to retrain the sEMG control during the experiment, this yielded limited improvement. In contrast, other users reported that the sEMG control worked well for them.

The WS mode was often rated unfavorably due to unintuitive robot control and the inability to predict the robots optimized trajectory. Some participants mentioned experiencing a training effect throughout the experiment. Interestingly, one high-performing user expressed a preference for full manual control, as offered in the Teleop mode, and disliked the robot taking over control. Conversely, another participant reported perceiving little difference between the control modes. Finally, users found the vibration feedback distracting, stating that the task was already cognitively demanding, which limited their capacity to attend to additional sensory input.

5 Discussion

5.1 Shared Autonomy Frameworks

In total, 12 participants performed a grasping and repositioning task using either a plate or a cup in a user study. Objective metrics such as task completion time, traveled distances, and placement accuracy of the objects at a predefined position were recorded. Additionally, questionnaires were used to evaluate the modes (Teleop, AC, and WS). In this study, two distinct shared autonomy frameworks were presented: one based on AC and the other WS. These approaches were treated independently throughout the investigation. As shown in Section 4, the AC approach demonstrated beneficial assistance in certain metrics (e.g. significantly in success rates over WS and mental demand), whereas the WS mode showed advantages in others (e.g., traveled distance). [21] states that shared autonomy should be arbitrated according to the difficulty of the task and the confidence of the robot. In this study by Dragan et al. [21] arbitration is considered as the level of autonomy provided to the user. According to current knowledge, it is not clear what kind of shared autonomy is best suited for grasping and manipulation tasks. This study aims to provide a necessary starting point to identify general tendencies and guide future research.

5.1.1 Objective Measurements

Given that many attempts failed due to the object not being successfully grasped or released during transport, it is reasonable that AC performs best and significantly better in terms of success rates than WS, as it keeps the grasp once commanded by the user. The "without robot" mode exhibits the shortest completion time and shortest traveled distance, indicating that the interface to control the robot is not fully intuitive. The differences in task completion times between the modes were minimal. Therefore, no definitive conclusions can be drawn regarding the advantages of each mode.

Among the robot-assisted modes, WS results in the shortest traveled distance regardless of the handled object, likely due to its assistance strategy, which optimizes workspace efficiency by minimizing the path from the initial TCP position to the pregrasp, grasp, and final positions. No clear distinction could be observed between the Teleop and AC modes, as the influence of the cone might have been minimal and the assistance provided by the AC mode in terms of reducing the traveled distance presumably marginal.

The reduced displacement in X direction in WS can be attributed to the strong influence of the autonomous system when approaching the final position. The higher accuracy

of AC compared to Teleop could result from the assistance system, which restricts the user from opening the gripper unless the object is sufficiently close to the final position, whereas in Teleop, the object can be placed at any location during task execution.

The reason behind the differing accuracy between WS in the X direction and AC in the Y direction remains unclear. One possible explanation is that the user approaches the final position from the positive Y direction, and in WS, there is a possibility to place the object before reaching the final position in the Y direction. However, in the X direction, the user is more constrained to follow the optimal path. The greater differences observed in the plate tasks compared to the tasks with the cup could be attributed to the fact that aligning the plate correctly requires rotation around the x-axis. Since AC performs this rotation autonomously, the user can focus primarily on precise placement. In contrast, for WS and Teleop, the user must also manage this rotational adjustment to some extend.

A descriptive comparison between the plate and cup tasks, based on objective performance metrics, indicates that the plate task is more challenging. This is supported by higher success rates (under both definitions of success), shorter completion times, reduced traveled distances, and smaller average displacements in both directions for the cup task across all control modes.

Although the amount of available data, particularly beyond three repetitions, is limited, a learning effect is observable to some extent when using the proposed interface. Among the evaluated control modes, AC and WS exhibit a more pronounced learning curve compared to Teleop across all considered metrics. To see learning effects in Teleop presumable more training is necessary, as done in [46]. Furthermore, when comparing AC and WS, AC demonstrates a steeper decline in the regression curve after a few repetitions, suggesting that AC may be the more effective assistance strategy in terms of facilitating user learning during task execution with the proposed system.

5.1.2 Subjective Measurements

Given that the system targets elderly users, the finding that the AC mode significantly reduces Physical, Mental, and Temporal Demand compared to Teleop, when considering all participants, provides evidence for the effectiveness of AC. Additionally, AC is significant less mental demanding than WS. Moreover, WS is significant physically less physically demanding than Teleop, which shows the effectiveness of the assistance of the WS mode. These results, derived from the NASA-TLX workload assessment, suggest that AC is the most suitable assistance mode for elderly users among the evaluated shared autonomy strategies.

Focusing on the plate task, which, as previously discussed, represents the more complex of the two tasks, AC shows a clear advantage over Teleop in terms of reduced Mental, Physical and Temporal Demand and Frustration, all of those differences show statistically significance. Furthermore, WS out performs Teleop in terms of mental and physical demand significantly. But AC also shows significant benefits over WS for mental and physical demand. These findings highlight the effectiveness of AC over the other two modes once more.

Regarding the VEQ, trends were observed for the Acceptance/Body Ownership and Control/Agency categories across both tasks (cup and plate). AC consistently received the highest ratings in these categories, some with significant difference (see Chapter 4).

The higher ratings of AC in Acceptance/Body Ownership compared to Teleop may be explained by users reported difficulties in controlling the robot's TCP rotation in Teleop mode, which often led to unintended movements. In contrast, in AC mode these movements are autonomously managed, reducing unwanted behavior and potentially making it easier for users to identify with the robot.

For Control/Agency, it may initially seem contradictory that AC outperforms Teleop, given that Teleop offers direct user control over the robot. However, the restriction of certain movements in AC (e.g., automatic control of TCP orientation) may help users focus on higher-level aspects of the task, such as optimal grasp positioning or precise placement, thereby enhancing their perceived control. In contrast, no clear trend emerged when comparing WS with Teleop in this regard. The relatively low Control/Agency scores for Teleop may be due to users frequently executing unintentional movements, especially in the robots rotation, which is controlled via wrist motion. This interpretation is supported by user feedback from semi-structured interviews, where many participants cited rotational control as the most challenging aspect.

WSs lower scores in Control/Agency might be attributed to the strong influence of the autonomous system, particularly when the TCP is near the grasp or target position. In these moments, users were barely able to move the TCP freely, potentially reducing their sense of control. In the VEQ category Change, the results are generally less conclusive than for the other two categories. Overall, ratings in this category were relatively low, and no single mode consistently stood out. However, two notable exceptions emerged:

Participants who performed the plate task reported a significantly stronger perceived change in their appearance and size in AC mode compared to Teleop and WS. While the exact reason remains unclear, this finding may relate to the consistently higher

scores for AC in both Ownership and Agency. Prior work (e.g., [42]) suggests that higher levels of Ownership and Agency may contribute to increased perceptions of bodily change.

A similar pattern was observed for the metric "The size of my body changed", with significant differences between Teleop and AC, as well as between AC and WS. These differences may be explained in the same way as the previously discussed findings regarding changes in perceived appearance, namely, by the higher levels of Body Ownership and Agency reported in the AC condition.

5.2 Limitations

5.2.1 Technical Limitations

The proposed system is not without limitations and exhibits several technical challenges. The experiments were conducted in a laboratory environment with significant electromagnetic interference (EMF), which negatively affected the IMU by causing drift. As a result, the user's hand position was not always accurately tracked. A potential solution could involve using three IMU per segment (upper arm, lower arm, and hand) to estimate and compensate for EMF-induced drift.

The IMU were attached using Velcro straps on the arm and hand. In some cases, the IMU gradually slipped, resulting in unwanted orientation changes. This issue could potentially be resolved by employing alternative attachment methods, such as an arm sleeve with integrated IMU mounts, which would reduce the risk of slippage.

As described in Section 4.2.3, some users experienced difficulties controlling the gripper via sEMG. A definitive cause could not be identified during the study. Possible contributing factors include excessive hair on the arm or different skin moisture. These issues could be addressed in the future by increasing the number of electrodes (the Myo armband currently uses 8 electrodes) or by integrating additional sensing modalities beyond surface electrodes.

Both the HCG and CLASH grippers appeared to change their behavior over time, even when commanded to the same positions. This is likely due to the compliance in their mechanical structure, which affected the threshold used to determine whether an object was grasped. These thresholds required occasional manual adjustments.

Overall, most users appreciated the option of indexing. However, it should be noted that the current implementation only compensates for linear offsets in TCP position

and orientation. Rotational offsets of the users arm, e.g. around the z-axis, are not handled, meaning users must maintain a consistent facing direction during control.

Indexing was triggered via a button on the M5 Stick of the Fingertac. Over time, this button exhibited mechanical fatigue, occasionally failing to register presses, requiring users to verify the action via the M5 Stick display. Additionally, indexing became difficult when the users arm was fully extended, making it hard to reach the button with the opposite hand. Possible solutions include using a foot pedal to trigger indexing, though this would restrict user mobility, or implementing a secondary handheld device for indexing control. There were occasional instances where a cable detached from the Fingertac housing that holds the vibration motor in place. Implementing strain relief could mitigate this issue. During initial testing with various users prior to the main study, the angle of the virtual cone in the AC mode was increased to 45 degrees. This adjustment reduced the cones influence, making it behave more like a virtual wall behind the target position. As most users did not overshoot the target (i.e., did not navigate the TCP beyond the object or goal position from the approach direction), the effect of the cone was minimal.

During the development of the WS mode, it was observed that the robots angular velocity limits were easily exceeded, particularly when combining three disparate orientations (the current TCP orientation, the user-desired orientation, and the autonomous systems desired orientation), especially when large angular differences were present and when the weighting factor changed too rapidly. To mitigate this, the weighting factor was held constant during the experiments, and a high weight was assigned to the previous TCP orientation to ensure smoother transitions. One instance observed during the experiments in WS mode involved a user who initially grasped the plate but then decided to readjust the grasp and released it. At that point, the system had already registered a successful grasp and proceeded to assist with transporting the object to the final position, instead of continuing to support the grasping phase.

The system is designed to assist elderly individuals in ADL. However, effective use of both the overall system and the individual shared autonomy modes requires a fundamental understanding of their functionalities. This initial cognitive load may overwhelm users and hinder proper system usage. It remains unclear to what extent users need to understand the systems underlying mechanisms to operate it effectively.

5.2.2 User Study

The system is intended for use by elderly individuals; however, all participants in the study were young adults. None of the participants were elderly, making it unclear how the system would perform with the actual target user group.

Failures occurred during the study such as the object falling during the carrying phase or technical issues, such as exceeding the robots linear or angular velocity limits. During the study, a technical issue was identified while the first participant performed the task with the plate, causing the user to exceed the angular velocity threshold too easily. After resolving this issue, the participant was able to continue the experiment. Similarly, during the first trial with the cup, a malfunction in the state machine was detected. Once corrected, the participant resumed the study without further issues.

A total of only 12 users participated in the study. To draw more convincing and generalizable conclusions, a larger sample size is necessary. Notably, one participant (User 6) was unable to complete the task in any mode. While this highlights that some users may experience difficulties with the system, a valuable insight, it also introduces a flooring effect that negatively impacts the overall data quality. During the tasks involving the plate, participants were required to stand behind the rack, as this position minimized EMF from the robot. However, this positioning obstructed the users' view of the plate, which is critical for determining when the gripper fingers align with the height of the wooden block to ensure a secure grasp. In these cases, the experimenter provided verbal guidance to assist the user in achieving the correct gripper height.

If the cup was displaced by the gripper, the experimenter repositioned it to its original location. In cases where the user violated the velocity constraint at the beginning by moving too quickly into the initial position, the trial was not considered a failure and was restarted. Additionally, if the cup was placed in a tilted or fallen-over position, it was up righted to ensure accurate displacement measurement.

During the user study, drift in the IMU was observed. The extent to which this affected the outcomes of the study remains unclear. One participant suggested extending the training phase to allow for better familiarization with the system. The high standard deviations observed across several metrics indicate substantial variability among participants. One could argue that shared autonomy cannot be clearly separated into distinct approaches as done in this study. In the following chapter suggestions are explained how the proposed frameworks could be combined for future iterations.

6 Conclusion

This thesis demonstrates that shared autonomy may be a key factor in the development and application of assistive robotic systems aimed at supporting elderly individuals in ADL, particularly in light of the aforementioned requirements. Various state-of-the-art shared autonomy approaches for different robotic interfaces are presented, which serve as the motivation for the developed shared autonomy frameworks and the research question which of the proposed shared autonomy frameworks assist best in grasping and manipulation tasks with the given system. The next step involved the integration of the subsystems into a unified system through the development of the necessary software and communication architecture.

The conducted user study compared the first time according to current knowledge, to different forms of shared autonomy to investigate which is best suited for grasp and manipulation tasks. The study revealed that participants could best perform in AC mode for the given tasks and system. Moreover, AC shows the best learning progression. The subjective measurements clearly show the advantages of AC over Teleop and WS, which is particularly relevant for the target group of elderly users.

Future steps could include improvements to the hardware, such as reducing IMU drift, securing IMU on the arm using a sleeve, and enhancing sEMG-based hand pose detection by incorporating additional electrodes. This may enable more refined gripper control, such as interpolation-based opening and closing. Increasing the reliability of the HCG when controlled by humans for ADL with the given interface would also lead to further improvements of the system. Further developments should focus on improving the robustness of the state machine, minimizing occurrences of velocity violations by the robot, and establishing a more reliable and user-friendly configuration procedure at the start of control. Additionally, enabling indexing even when the user changes their orientation relative to the robot, as well as exploring alternative methods for triggering indexing, are important areas for future exploration. Moreover, integrating a vision-based system capable of detecting the position of the target object would enable a more generalizable application. Currently, object positions are hard-coded and do not update automatically if the objects location changes.

Investigating the proposed shared autonomy frameworks more detailed may also yield further insights. A combination of the advantages of AC and WS could potentially lead to further reductions in user demand and object displacement. Moreover, conducting a user study specifically with elderly participants would provide valuable feedback for tailoring the system to the target demographic.

References

[1] Oxford English Dictionary. “Definition of "autonomy"”. Accessed: 2 April 2025. [Online]. Available: https://www.oed.com/dictionary/autonomy_n?tl=true.

[2] M. Selvaggio, M. Cognetti, S. Nikolaidis, S. Ivaldi, and B. Siciliano, “Autonomy in Physical Human-Robot Interaction: A Brief Survey”, en, *IEEE Robotics and Automation Letters*, vol. 6, no. 4, pp. 7989–7996, Oct. 2021, ISSN: 2377-3766, 2377-3774. DOI: 10.1109/LRA.2021.3100603.

[3] A. E. Patterson, Y. Yuan, and W. R. Norris, “Development of user-integrated semi-autonomous lawn mowing systems: A systems engineering perspective and proposed architecture”, *AgriEngineering*, vol. 1, no. 3, pp. 453–474, 2019, Publisher: MDPI.

[4] “Old age: Responding to a rapidly ageing population”, en, pp. 47–61, Publisher: United Nations. DOI: 10.18356/39d66529-en.

[5] N. T. Loi, N. T. Dung, and H. N. Quang, “The cost effectiveness of aging in place: A literature review”, en, *HO CHI MINH CITY OPEN UNIVERSITY JOURNAL OF SCIENCE - SOCIAL SCIENCES*, vol. 11, no. 1, pp. 40–54, Jun. 2021, ISSN: 27349624. DOI: 10.46223/HCMCOUJS.soci.en.11.1.1925.2021.

[6] J. M. Beer et al., “The domesticated robot: Design guidelines for assisting older adults to age in place”, en, in *Proceedings of the seventh annual ACM/IEEE international conference on Human-Robot Interaction*, Boston Massachusetts USA: ACM, Mar. 2012, pp. 335–342, ISBN: 978-1-4503-1063-5. DOI: 10.1145/2157689.2157806.

[7] M. Pashmdarfard and A. Azad, “Assessment tools to evaluate Activities of Daily Living (ADL) and Instrumental Activities of Daily Living (IADL) in older adults: A systematic review”, *Medical Journal of the Islamic Republic of Iran*, vol. 34, p. 33, Apr. 2020, ISSN: 1016-1430. DOI: 10.34171/mjiri.34.33.

[8] E. Carmeli, H. Patish, and R. Coleman, “The Aging Hand”, *The Journals of Gerontology: Series A*, vol. 58, no. 2, pp. M146–M152, Feb. 2003, ISSN: 1079-5006. DOI: 10.1093/gerona/58.2.M146.

[9] V. K. Ranganathan, V. Siemionow, V. Sahgal, and G. H. Yue, “Effects of Aging on Hand Function”, en, *Journal of the American Geriatrics Society*, vol. 49, no. 11, pp. 1478–1484, Nov. 2001, ISSN: 0002-8614, 1532-5415. DOI: 10.1046/j.1532-5415.2001.4911240.x.

[10] Nathan Congdon, “Causes and Prevalence of Visual Impairment Among Adults in the United States”, *Archives of Ophthalmology*, vol. 122, no. 4, pp. 477–485, Apr. 2004, ISSN: 0003-9950. DOI: 10.1001/archopht.122.4.477.

[11] D. W. H. Tan, P. K. Ng, and E. E. M. Noor, “A TRIZ-BASED APPROACH IN INVESTIGATING FINGER GRIP FUNCTION DEGRADATION AMONG ELDERLIES”, en, vol. 14, no. 16,

[12] T. Mitzner, T. L. Chen, C. Kemp, and W. Rogers, “Older Adults Needs for Assistance as a Function of Living Environment”, *Proceedings of the Human Factors and Ergonomics Society Annual Meeting*, vol. 55, pp. 152–156, 2011. DOI: 10.1177/1071181311551032.

[13] L. Petrich, J. Jin, M. Dehghan, and M. Jagersand, *Assistive arm and hand manipulation: How does current research intersect with actual healthcare needs?*, en, arXiv:2101.02750 [cs], Jan. 2021.

[14] "9 Assistive robots in care: Expectations and perceptions of older people", en, in *Aging between Participation and Simulation*, J. Haltaufderheide, J. Hovemann, and J. Vollmann, Eds., De Gruyter, Apr. 2020, pp. 139–156, ISBN: 978-3-11-067748-5. DOI: 10.1515/9783110677485-009.

[15] J.-W. Jung, W.-K. Song, H. Lee, J.-S. Kim, and Z. Bien, "A STUDY ON THE ENHANCEMENT OF MANIPULATION PERFORMANCE OF WHEELCHAIR-MOUNTED REHABILITATION SERVICE ROBOT", en,

[16] C. Stanger, C. Anglin, W. Harwin, and D. Romilly, "Devices for assisting manipulation: A summary of user task priorities", en, *IEEE Transactions on Rehabilitation Engineering*, vol. 2, no. 4, pp. 256–265, Dec. 1994, ISSN: 10636528. DOI: 10.1109/86.340872.

[17] J. A. Hoppe et al., "Assistive robots in care: Expectations and pereceptions of older people", 2020.

[18] B. D. Argall, "Autonomy in Rehabilitation Robotics: An Intersection", en, *Annual Review of Control, Robotics, and Autonomous Systems*, vol. 1, no. 1, pp. 441–463, May 2018, ISSN: 2573-5144, 2573-5144. DOI: 10.1146/annurev-control-061417-041727.

[19] S. Jain and B. Argall, "An Approach for Online User Customization of Shared Autonomy for Intelligent Assistive Devices", en,

[20] D. Gopinath, S. Jain, and B. D. Argall, "Human-in-the-Loop Optimization of Shared Autonomy in Assistive Robotics", en, *IEEE Robotics and Automation Letters*, vol. 2, no. 1, pp. 247–254, Jan. 2017, ISSN: 2377-3766, 2377-3774. DOI: 10.1109/LRA.2016.2593928.

[21] A. D. Dragan and S. S. Srinivasa, "A policy-blending formalism for shared control", en, *The International Journal of Robotics Research*, vol. 32, no. 7, pp. 790–805, Jun. 2013, ISSN: 0278-3649, 1741-3176. DOI: 10.1177/0278364913490324.

[22] L. Peternel, N. Tsagarakis, D. Caldwell, and A. Ajoudani, "Robot adaptation to human physical fatigue in humanrobot co-manipulation", en, *Autonomous Robots*, vol. 42, no. 5, pp. 1011–1021, Jun. 2018, ISSN: 0929-5593, 1573-7527. DOI: 10.1007/s10514-017-9678-1.

[23] A. Broad, I. Abraham, T. Murphey, and B. Argall, "Data-driven Koopman operators for model-based shared control of humanmachine systems", en, *The International Journal of Robotics Research*, vol. 39, no. 9, pp. 1178–1195, Aug. 2020, ISSN: 0278-3649, 1741-3176. DOI: 10.1177/0278364920921935.

[24] S. Jain and B. Argall, "Probabilistic Human Intent Recognition for Shared Autonomy in Assistive Robotics", en, *ACM Transactions on Human-Robot Interaction*, vol. 9, no. 1, pp. 1–23, Mar. 2020, ISSN: 2573-9522. DOI: 10.1145/3359614.

[25] N. Mehr, R. Horowitz, and A. D. Dragan, "Inferring and assisting with constraints in shared autonomy", in *2016 IEEE 55th Conference on Decision and Control (CDC)*, Dec. 2016, pp. 6689–6696. DOI: 10.1109/CDC.2016.7799299.

[26] G. Quere et al., “Shared Control Templates for Assistive Robotics”, en, in *2020 IEEE International Conference on Robotics and Automation (ICRA)*, Paris, France: IEEE, May 2020, pp. 1956–1962, ISBN: 978-1-72817-395-5. DOI: 10.1109/ICRA40945.2020.9197041.

[27] S. A. Bowyer, B. L. Davies, and F. Rodriguez y Baena, “Active Constraints/Virtual Fixtures: A Survey”, *IEEE Transactions on Robotics*, vol. 30, no. 1, pp. 138–157, Feb. 2014, Conference Name: IEEE Transactions on Robotics, ISSN: 1941-0468. DOI: 10.1109/TRO.2013.2283410.

[28] D. Rakita, B. Mutlu, M. Gleicher, and L. M. Hiatt, “Shared controlbased bimanual robot manipulation”, en, *Science Robotics*, vol. 4, no. 30, eaaw0955, May 2019, ISSN: 2470-9476. DOI: 10.1126/scirobotics.aaw0955.

[29] A. AlbuSchäffer, S. Haddadin, C. Ott, A. Stemmer, T. Wimböck, and G. Hirzinger, “The DLR lightweight robot: Design and control concepts for robots in human environments”, *Industrial Robot: An International Journal*, vol. 34, no. 5, C. Loughlin, Ed., pp. 376–385, Jan. 2007, Publisher: Emerald Group Publishing Limited, ISSN: 0143-991X. DOI: 10.1108/01439910710774386.

[30] S. D’Avella, A. M. Sundaram, W. Friedl, P. Tripicchio, and M. A. Roa, “Multimodal Grasp Planner for Hybrid Grippers in Cluttered Scenes”, *IEEE Robotics and Automation Letters*, vol. 8, no. 4, pp. 2030–2037, Apr. 2023, Conference Name: IEEE Robotics and Automation Letters, ISSN: 2377-3766. DOI: 10.1109/LRA.2023.3247221.

[31] W. Friedl, H. Höppner, F. Schmidt, M. A. Roa, and M. Grebenstein, “CLASH: Compliant Low Cost Antagonistic Servo Hands”, in *2018 IEEE/RSJ International Conference on Intelligent Robots and Systems (IROS)*, ISSN: 2153-0866, Oct. 2018, pp. 6469–6476. DOI: 10.1109/IROS.2018.8593903.

[32] M. Sierotowicz, M. Connan, and C. Castellini, “Human-In-The-Loop Assessment of an Ultralight, Low-Cost Body Posture Tracking Device”, en, *Sensors*, vol. 20, no. 3, p. 890, Jan. 2020, Number: 3 Publisher: Multidisciplinary Digital Publishing Institute, ISSN: 1424-8220. DOI: 10.3390/s20030890.

[33] T. Hulin et al., “FingerTac A Wearable Tactile Thimble for Mobile Haptic Augmented Reality Applications”, en, in *Virtual, Augmented and Mixed Reality. Design and Interaction*, J. Y. C. Chen and G. Fragomeni, Eds., Cham: Springer International Publishing, 2020, pp. 286–298, ISBN: 978-3-030-49695-1. DOI: 10.1007/978-3-030-49695-1_19.

[34] D. Rakita, B. Mutlu, and M. Gleicher, “Effects of Onset Latency and Robot Speed Delays on Mimicry-Control Teleoperation”, en, in *Proceedings of the 2020 ACM/IEEE International Conference on Human-Robot Interaction*, Cambridge United Kingdom: ACM, Mar. 2020, pp. 519–527, ISBN: 978-1-4503-6746-2. DOI: 10.1145/3319502.3374838.

[35] E. Coumans and Y. Bai. “Pybullet python module for physics simulation for games, robotics and machine learning”. Accessed: 2025-04-16.

[36] G. Lafruit et al., “FTV software user guidelines”, *ISO/IEC JTC1/SC29/WG11, MPEG2015, Doc. M36590*, Jun. 2015.

[37] A. Gijsberts et al., “Stable myoelectric control of a hand prosthesis using non-linear incremental learning”, English, *Frontiers in Neurorobotics*, vol. 8, Feb. 2014, Publisher: Frontiers, ISSN: 1662-5218. DOI: 10.3389/fnbot.2014.00008.

[38] M. Sierotowicz, M.-A. Scheidl, and C. Castellini, “Adaptive Filter for Biosignal-Driven Force Controls Preserves Predictive Powers of sEMG”, en, in *2023 International Conference on Rehabilitation Robotics (ICORR)*, Singapore, Singapore: IEEE, Sep. 2023, pp. 1–6, ISBN: 9798350342758. DOI: 10.1109/ICORR58425.2023.10304772.

[39] N. Parajuli et al., “Real-Time EMG Based Pattern Recognition Control for Hand Prostheses: A Review on Existing Methods, Challenges and Future Implementation”, en, *Sensors*, vol. 19, no. 20, p. 4596, Jan. 2019, Number: 20 Publisher: Multidisciplinary Digital Publishing Institute, ISSN: 1424-8220. DOI: 10.3390/s19204596.

[40] Oliver Porges, Daniel Leidner, and Máximo A. Roa, *Planning Fail-Safe Trajectories for Space Robotic Arms*, en, Nov. 2021.

[41] L. E. Staveland, “Development of NASA-TLX (Task Load Index): Results of Empirical and Theoretical Research”, en, in *Advances in Psychology*, ISSN: 0166-4115, Elsevier, 1988, pp. 139–183. DOI: 10.1016/s0166-4115(08)62386-9.

[42] D. Roth and M. E. Latoschik, “Construction of the virtual embodiment questionnaire (veq)”, *IEEE Transactions on Visualization and Computer Graphics*, vol. 26, no. 12, pp. 3546–3556, 2020.

[43] C. Krueger and L. Tian, “A comparison of the general linear mixed model and repeated measures anova using a dataset with multiple missing data points”, *Biological research for nursing*, vol. 6, no. 2, pp. 151–157, 2004.

[44] Z. Yu, M. Guindani, S. F. Grieco, L. Chen, T. C. Holmes, and X. Xu, “Beyond t test and anova: Applications of mixed-effects models for more rigorous statistical analysis in neuroscience research”, *Neuron*, vol. 110, no. 1, pp. 21–35, 2022.

[45] F. Isik, J. Holland, C. Maltecca, F. Isik, J. Holland, and C. Maltecca, “A review of linear mixed models”, *Genetic Data Analysis for Plant and Animal Breeding*, pp. 49–86, 2017.

[46] M. Connan et al., “Learning to teleoperate an upper-limb assistive humanoid robot for bimanual daily-living tasks”, en, *Biomedical Physics & Engineering Express*, vol. 8, no. 1, p. 015 022, Dec. 2021, Publisher: IOP Publishing, ISSN: 2057-1976. DOI: 10.1088/2057-1976/ac3881.

Appendices

A Appendix

A.1 Semi Structured Interview

Semi-structured interview

1. *Describe how you felt about controlling the robot.*
   → What worked well and what was challenging?

2. How did you experience the different control modes?
   →What were differences?

3. *How did your control of the robot develop throughout the phases?*
   →Were there moments when you felt a significant improvement or situations that caused frustration?

4. *Which aspects of the control interface (EMG-bracelet, orientation sensors and vibration motors) supported you during control and which ones tended to distract you?*

5. *Which interactions with the robot were easy and which were more difficult to perform?*
   → If errors or unexpected movements occurred, what did you do to correct them?

6. *What would you change to make the experience and operation more enjoyable or effective for you?*
   → What improvements would you suggest? E.g. training breaks, tutorials, feedback, technical implementations

7. Do you have any other feedback?

Figure 40. Semi Structured Interview

A.2 Detailed Results of Linear Mixed Models

Success Rates all

Linear Mixed Model für: success_rates_all_objects

Mixed Linear Model Regression Results

Model:	MixedLM	Dependent Variable:	Q("Success Rate")
No. Observations:	36	Method:	REML
No. Groups:	12	Scale:	0.0409
Min. group size:	3	Log-Likelihood:	-7.6283
Max. group size:	3	Converged:	Yes
Mean group size:	3.0		

	Coef.	Std.Err.	z	P>|z|	[0.025	0.975]
Intercept	0.633	0.095	6.659	0.000	0.447	0.820
C(Mode)[T.Teleop]	-0.110	0.083	-1.329	0.184	-0.272	0.052
C(Mode)[T.WS]	-0.163	0.083	-1.975	0.048	-0.325	-0.001
Group Var	0.068	0.210				

=== Mixed Linear Model für: success_rates_all_objects ===

Mixed Linear Model Regression Results

Model:	MixedLM	Dependent Variable:	Q("Success Rate")
No. Observations:	36	Method:	REML
No. Groups:	12	Scale:	0.0409
Min. group size:	3	Log-Likelihood:	-7.6283
Max. group size:	3	Converged:	Yes
Mean group size:	3.0		

	Coef.	Std.Err.	z	P>|z|	[0.025	0.975]
Intercept	0.524	0.095	5.505	0.000	0.337	0.710
C(Mode)[T.AC]	0.110	0.083	1.329	0.184	-0.052	0.272
C(Mode)[T.WS]	-0.053	0.083	-0.646	0.518	-0.215	0.108
Group Var	0.068	0.210				

Success Rates Plate

```
Linear Mixed Model für: success_rates_plate
            Mixed Linear Model Regression Results
=================================================================
Model:            MixedLM Dependent Variable: Q("Success Rate")
No. Observations: 18      Method:             REML
No. Groups:       6       Scale:              0.0478
Min. group size:  3       Log-Likelihood:     -5.6127
Max. group size:  3       Converged:          Yes
Mean group size:  3.0
-----------------------------------------------------------------
                    Coef.  Std.Err.   z    P>|z| [0.025 0.975]
-----------------------------------------------------------------
Intercept            0.521    0.145  3.596 0.000  0.237  0.806
C(Mode)[T.Teleop]   -0.083    0.126 -0.654 0.513 -0.330  0.165
C(Mode)[T.WS]       -0.088    0.126 -0.698 0.485 -0.336  0.159
Group Var            0.078    0.334
=================================================================
```

```
=== Mixed Linear Model für: success_rates_plate ===
            Mixed Linear Model Regression Results
=================================================================
Model:            MixedLM Dependent Variable: Q("Success Rate")
No. Observations: 18      Method:             REML
No. Groups:       6       Scale:              0.0478
Min. group size:  3       Log-Likelihood:     -5.6127
Max. group size:  3       Converged:          Yes
Mean group size:  3.0
-----------------------------------------------------------------
                   Coef.   Std.Err.    z     P>|z|  [0.025  0.975]
-----------------------------------------------------------------
Intercept           0.439     0.145   3.027  0.002   0.155   0.723
C(Mode)[T.AC]       0.083     0.126   0.654  0.513  -0.165   0.330
C(Mode)[T.WS]      -0.006     0.126  -0.044  0.965  -0.253   0.242
Group Var           0.078     0.334
=================================================================
```

Success Rates Cup

```
Linear Mixed Model für: success_rates_cup
            Mixed Linear Model Regression Results
================================================================
Model:            MixedLM Dependent Variable: Q("Success Rate")
No. Observations: 18      Method:             REML
No. Groups:       6       Scale:              0.0387
Min. group size:  3       Log-Likelihood:     -3.8124
Max. group size:  3       Converged:          Yes
Mean group size:  3.0
----------------------------------------------------------------
                    Coef.  Std.Err.   z    P>|z| [0.025 0.975]
----------------------------------------------------------------
Intercept            0.745    0.126  5.898 0.000  0.497  0.993
C(Mode)[T.Teleop]   -0.137    0.114 -1.205 0.228 -0.360  0.086
C(Mode)[T.WS]       -0.238    0.114 -2.095 0.036 -0.461 -0.015
Group Var            0.057    0.275
================================================================


=== Mixed Linear Model für: success_rates_cup ===
            Mixed Linear Model Regression Results
================================================================
Model:            MixedLM Dependent Variable: Q("Success Rate")
No. Observations: 18      Method:             REML
No. Groups:       6       Scale:              0.0387
Min. group size:  3       Log-Likelihood:     -3.8124
Max. group size:  3       Converged:          Yes
Mean group size:  3.0
----------------------------------------------------------------
                   Coef.   Std.Err.    z     P>|z|  [0.025  0.975]
----------------------------------------------------------------
Intercept           0.608     0.126   4.814  0.000   0.361   0.856
C(Mode)[T.AC]       0.137     0.114   1.205  0.228  -0.086   0.360
C(Mode)[T.WS]      -0.101     0.114  -0.891  0.373  -0.324   0.122
Group Var           0.057     0.275
================================================================
```

NASA TLX Plate

```
Mixed Effects Model für: Mental_Demand
           Mixed Linear Model Regression Results
============================================================
Model:            MixedLM Dependent Variable: Mental_Demand
No. Observations: 18      Method:             REML
No. Groups:       6       Scale:              2.2765
Min. group size:  3       Log-Likelihood:     -34.0803
Max. group size:  3       Converged:          Yes
Mean group size:  3.0
------------------------------------------------------------
                Coef.  Std.Err.   z    P>|z| [0.025 0.975]
------------------------------------------------------------
Intercept        5.111    0.930  5.498 0.000  3.289  6.933
C(Mode)[T.2.0]  -3.667    0.871 -4.209 0.000 -5.374 -1.959
C(Mode)[T.3.0]  -1.889    0.871 -2.168 0.030 -3.596 -0.182
Group Var        2.909    1.883
============================================================


           Mixed Linear Model Regression Results
============================================================
Model:            MixedLM Dependent Variable: Mental_Demand
No. Observations: 18      Method:             REML
No. Groups:       6       Scale:              2.2765
Min. group size:  3       Log-Likelihood:     -34.0803
Max. group size:  3       Converged:          Yes
Mean group size:  3.0
------------------------------------------------------------
               Coef.  Std.Err.    z    P>|z|  [0.025  0.975]
------------------------------------------------------------
Intercept      1.444     0.930  1.554  0.120  -0.378   3.266
C(Mode)[T.1]   3.667     0.871  4.209  0.000   1.959   5.374
C(Mode)[T.3]   1.778     0.871  2.041  0.041   0.070   3.485
Group Var      2.909     1.883
============================================================
```

Mixed Effects Model für: Physical_Demand

Mixed Linear Model Regression Results

Model:	MixedLM	Dependent Variable:	Physical_Demand
No. Observations:	18	Method:	REML
No. Groups:	6	Scale:	1.0617
Min. group size:	3	Log-Likelihood:	-29.7235
Max. group size:	3	Converged:	Yes
Mean group size:	3.0		

	Coef.	Std.Err.	z	P>|z|	[0.025	0.975]
Intercept	5.111	0.781	6.545	0.000	3.580	6.642
C(Mode)[T.2.0]	-2.556	0.595	-4.296	0.000	-3.722	-1.390
C(Mode)[T.3.0]	-1.333	0.595	-2.241	0.025	-2.499	-0.167
Group Var	2.598	2.219				

Mixed Linear Model Regression Results

Model:	MixedLM	Dependent Variable:	Physical_Demand
No. Observations:	18	Method:	REML
No. Groups:	6	Scale:	1.0617
Min. group size:	3	Log-Likelihood:	-29.7235
Max. group size:	3	Converged:	Yes
Mean group size:	3.0		

	Coef.	Std.Err.	z	P>|z|	[0.025	0.975]
Intercept	2.556	0.781	3.272	0.001	1.025	4.086
C(Mode)[T.1]	2.556	0.595	4.296	0.000	1.390	3.722
C(Mode)[T.3]	1.222	0.595	2.054	0.040	0.056	2.388
Group Var	2.598	2.219				

```
Mixed Effects Model für: Effort
          Mixed Linear Model Regression Results
============================================================
Model:             MixedLM  Dependent Variable:  Effort
No. Observations:  18       Method:              REML
No. Groups:        6        Scale:               1.4222
Min. group size:   3        Log-Likelihood:      -33.1104
Max. group size:   3        Converged:           Yes
Mean group size:   3.0
------------------------------------------------------------
               Coef.  Std.Err.   z    P>|z| [0.025 0.975]
------------------------------------------------------------
Intercept       5.000    1.105  4.526 0.000  2.835  7.165
C(Mode)[T.2.0] -0.889    0.689 -1.291 0.197 -2.238  0.461
C(Mode)[T.3.0]  0.222    0.689  0.323 0.747 -1.127  1.572
Group Var       5.901    4.141
============================================================
```

NASA TLX Cup

```
Mixed Effects Model für: Effort
          Mixed Linear Model Regression Results
============================================================
Model:             MixedLM  Dependent Variable:  Effort
No. Observations:  18       Method:              REML
No. Groups:        6        Scale:               1.4222
Min. group size:   3        Log-Likelihood:      -33.1104
Max. group size:   3        Converged:           Yes
Mean group size:   3.0
------------------------------------------------------------
               Coef.  Std.Err.   z    P>|z| [0.025 0.975]
------------------------------------------------------------
Intercept       5.000    1.105  4.526 0.000  2.835  7.165
C(Mode)[T.2.0] -0.889    0.689 -1.291 0.197 -2.238  0.461
C(Mode)[T.3.0]  0.222    0.689  0.323 0.747 -1.127  1.572
Group Var       5.901    4.141
============================================================
```

```
Mixed Effects Model für: Effort
          Mixed Linear Model Regression Results
=========================================================
Model:             MixedLM  Dependent Variable:  Effort
No. Observations:  18       Method:              REML
No. Groups:        7        Scale:               5.2574
Min. group size:   1        Log-Likelihood:      -36.4225
Max. group size:   3        Converged:           Yes
Mean group size:   2.6
---------------------------------------------------------
               Coef.  Std.Err.   z    P>|z| [0.025 0.975]
---------------------------------------------------------
Intercept       6.000    0.938  6.397 0.000  4.162  7.839
C(Mode)[T.2.0] -2.667    1.324 -2.014 0.044 -5.261 -0.072
C(Mode)[T.3.0] -1.000    1.324 -0.755 0.450 -3.595  1.595
Group Var       0.002    0.785
=========================================================
```

```
        Mixed Linear Model Regression Results
=========================================================
Model:             MixedLM Dependent Variable: Effort
No. Observations:  18      Method:             REML
No. Groups:        7       Scale:              5.2574
Min. group size:   1       Log-Likelihood:     -36.4225
Max. group size:   3       Converged:          Yes
Mean group size:   2.6
---------------------------------------------------------
               Coef. Std.Err.   z   P>|z| [0.025 0.975]
---------------------------------------------------------
Intercept      3.333    0.938 3.554 0.000  1.495  5.172
C(Mode)[T.1]   2.667    1.324 2.014 0.044  0.072  5.261
C(Mode)[T.3]   1.667    1.324 1.259 0.208 -0.928  4.262
Group Var      0.002    0.785
=========================================================
```

```
Mixed Effects Model für: Frustration
          Mixed Linear Model Regression Results
============================================================
Model:            MixedLM Dependent Variable: Frustration
No. Observations: 18      Method:             REML
No. Groups:       7       Scale:              4.6711
Min. group size:  1       Log-Likelihood:     -35.8235
Max. group size:  3       Converged:          Yes
Mean group size:  2.6
------------------------------------------------------------
               Coef.  Std.Err.   z    P>|z| [0.025 0.975]
------------------------------------------------------------
Intercept       4.450    0.901  4.940 0.000  2.684  6.215
C(Mode)[T.2.0] -1.111    1.248 -0.890 0.373 -3.557  1.335
C(Mode)[T.3.0] -0.555    1.252 -0.443 0.657 -3.009  1.899
Group Var       0.191    0.597
============================================================
```

VEQ all

```
Mixed Effects Model für: robot_belonged_to_me
              Mixed Linear Model Regression Results
================================================================
Model:            MixedLM Dependent Variable: robot_belonged_to_me
No. Observations: 36      Method:             REML
No. Groups:       12      Scale:              2.9753
Min. group size:  3       Log-Likelihood:     -75.5578
Max. group size:  3       Converged:          Yes
Mean group size:  3.0
----------------------------------------------------------------
                   Coef.   Std.Err.    z     P>|z|  [0.025  0.975]
----------------------------------------------------------------
Intercept           3.889     0.679   5.726  0.000   2.558   5.220
C(Mode)[T.2.0]      1.611     0.704   2.288  0.022   0.231   2.991
C(Mode)[T.3.0]     -0.222     0.704  -0.316  0.752  -1.602   1.158
Group Var           2.559     1.075
================================================================
```

Mixed Linear Model Regression Results

Model:	MixedLM	Dependent Variable:	robot_belonged_to_me
No. Observations:	36	Method:	REML
No. Groups:	12	Scale:	2.9753
Min. group size:	3	Log-Likelihood:	-75.5578
Max. group size:	3	Converged:	Yes
Mean group size:	3.0		

	Coef.	Std.Err.	z	P>|z|	[0.025	0.975]
Intercept	5.500	0.679	8.099	0.000	4.169	6.831
C(Mode)[T.1]	-1.611	0.704	-2.288	0.022	-2.991	-0.231
C(Mode)[T.3]	-1.833	0.704	-2.603	0.009	-3.214	-0.453
Group Var	2.559	1.075				

Mixed Effects Model für: I_was_cause_the_robots_movements

Mixed Linear Model Regression Results

Model:	MixedLM	Dependent Variable:	I_was_cause_the_robots_movements
No. Observations:	36	Method:	REML
No. Groups:	12	Scale:	2.6117
Min. group size:	3	Log-Likelihood:	-74.4463
Max. group size:	3	Converged:	Yes
Mean group size:	3.0		

	Coef.	Std.Err.	z	P>|z|	[0.025	0.975]
Intercept	5.889	0.677	8.694	0.000	4.561	7.217
C(Mode)[T.2.0]	1.278	0.660	1.937	0.053	-0.015	2.571
C(Mode)[T.3.0]	0.167	0.660	0.253	0.801	-1.126	1.460
Group Var	2.894	1.217				

Mixed Linear Model Regression Results

Model:	MixedLM	Dependent Variable:	I_was_cause_the_robots_movements
No. Observations:	36	Method:	REML
No. Groups:	12	Scale:	2.6117
Min. group size:	3	Log-Likelihood:	-74.4463
Max. group size:	3	Converged:	Yes
Mean group size:	3.0		

	Coef.	Std.Err.	z	P>|z|	[0.025	0.975]
Intercept	7.167	0.677	10.580	0.000	5.839	8.494
C(Mode)[T.1]	-1.278	0.660	-1.937	0.053	-2.571	0.015
C(Mode)[T.3]	-1.111	0.660	-1.684	0.092	-2.404	0.182
Group Var	2.894	1.217				

VEQ Plate

Mixed Effects Model für: I_was_cause_the_robots_movements

Mixed Linear Model Regression Results

Model:	MixedLM	Dependent Variable:	I_was_cause_the_robots_movements
No. Observations:	18	Method:	REML
No. Groups:	6	Scale:	2.3556
Min. group size:	3	Log-Likelihood:	-34.1873
Max. group size:	3	Converged:	Yes
Mean group size:	3.0		

	Coef.	Std.Err.	z	P>|z|	[0.025	0.975]
Intercept	5.667	0.926	6.119	0.000	3.852	7.482
C(Mode)[T.2.0]	1.889	0.886	2.132	0.033	0.152	3.626
C(Mode)[T.3.0]	0.444	0.886	0.502	0.616	-1.292	2.181
Group Var	2.790	1.804				

Mixed Linear Model Regression Results

Model:	MixedLM	Dependent Variable:	I_was_cause_the_robots_movements
No. Observations:	18	Method:	REML
No. Groups:	6	Scale:	2.3556
Min. group size:	3	Log-Likelihood:	-34.1873
Max. group size:	3	Converged:	Yes
Mean group size:	3.0		

	Coef.	Std.Err.	z	P>|z|	[0.025	0.975]
Intercept	7.556	0.926	8.159	0.000	5.741	9.371
C(Mode)[T.1]	-1.889	0.886	-2.132	0.033	-3.626	-0.152
C(Mode)[T.3]	-1.444	0.886	-1.630	0.103	-3.181	0.292
Group Var	2.790	1.804				

Mixed Effects Model für: I_was_controlling_the_movements_of_robot

Mixed Linear Model Regression Results

Model:	MixedLM	Dependent Variable:	I_was_controlling_the_movements_of_robot
No. Observations:	18	Method:	REML
No. Groups:	6	Scale:	4.3802
Min. group size:	3	Log-Likelihood:	-37.1711
Max. group size:	3	Converged:	Yes
Mean group size:	3.0		

	Coef.	Std.Err.	z	P>|z|	[0.025	0.975]
Intercept	5.222	1.027	5.084	0.000	3.209	7.236
C(Mode)[T.2.0]	2.000	1.208	1.655	0.098	-0.368	4.368
C(Mode)[T.3.0]	0.111	1.208	0.092	0.927	-2.257	2.479
Group Var	1.951	1.262				

Mixed Linear Model Regression Results

Model:	MixedLM	Dependent Variable:	I_was_controlling_the_movements_of_robot
No. Observations:	18	Method:	REML
No. Groups:	6	Scale:	4.3802
Min. group size:	3	Log-Likelihood:	-37.1711
Max. group size:	3	Converged:	Yes
Mean group size:	3.0		

	Coef.	Std.Err.	z	P>|z|	[0.025	0.975]
Intercept	7.222	1.027	7.031	0.000	5.209	9.236
C(Mode)[T.1]	-2.000	1.208	-1.655	0.098	-4.368	0.368
C(Mode)[T.3]	-1.889	1.208	-1.563	0.118	-4.257	0.479
Group Var	1.951	1.262				

Mixed Effects Model für: movements_of_robot_weer_in_syn_with_mine

Mixed Linear Model Regression Results

Model:	MixedLM	Dependent Variable:	movements_of_robot_weer_in_syn_with_mine
No. Observations:	18	Method:	REML
No. Groups:	6	Scale:	3.1309
Min. group size:	3	Log-Likelihood:	-32.5315
Max. group size:	3	Converged:	Yes
Mean group size:	3.0		

	Coef.	Std.Err.	z	P>|z|	[0.025	0.975]
Intercept	2.889	0.722	3.999	0.000	1.473	4.305
C(Mode)[T.2.0]	2.111	1.022	2.067	0.039	0.109	4.113
C(Mode)[T.3.0]	0.333	1.022	0.326	0.744	-1.669	2.336
Group Var	0.000	0.467				

Mixed Linear Model Regression Results

Model:	MixedLM	Dependent Variable:	movements_of_robot_weer_in_syn_with_mine
No. Observations:	18	Method:	REML
No. Groups:	6	Scale:	3.1309
Min. group size:	3	Log-Likelihood:	-32.5315
Max. group size:	3	Converged:	Yes
Mean group size:	3.0		

	Coef.	Std.Err.	z	P>|z|	[0.025	0.975]
Intercept	5.000	0.722	6.922	0.000	3.584	6.416
C(Mode)[T.1]	-2.111	1.022	-2.067	0.039	-4.113	-0.109
C(Mode)[T.3]	-1.778	1.022	-1.740	0.082	-3.780	0.224
Group Var	0.000	0.467				

```
Mixed Effects Model für: robot_belonged_to_me
            Mixed Linear Model Regression Results
=================================================================
Model:            MixedLM Dependent Variable: robot_belonged_to_me
No. Observations: 18      Method:             REML
No. Groups:       6       Scale:              2.8098
Min. group size:  3       Log-Likelihood:     -34.0554
Max. group size:  3       Converged:          Yes
Mean group size:  3.0
-----------------------------------------------------------------
                    Coef.   Std.Err.    z     P>|z|  [0.025  0.975]
-----------------------------------------------------------------
Intercept            2.889     0.842   3.430  0.001   1.238   4.540
C(Mode)[T.2.0]       2.111     0.968   2.181  0.029   0.214   4.008
C(Mode)[T.3.0]      -0.333     0.968  -0.344  0.731  -2.230   1.563
Group Var            1.447     1.102
=================================================================
```

```
            Mixed Linear Model Regression Results
=================================================================
Model:            MixedLM Dependent Variable: robot_belonged_to_me
No. Observations: 18      Method:             REML
No. Groups:       6       Scale:              2.8098
Min. group size:  3       Log-Likelihood:     -34.0554
Max. group size:  3       Converged:          Yes
Mean group size:  3.0
-----------------------------------------------------------------
                Coef.    Std.Err.     z      P>|z|   [0.025   0.975]
-----------------------------------------------------------------
Intercept        5.000      0.842    5.936   0.000    3.349    6.651
C(Mode)[T.1]    -2.111      0.968   -2.181   0.029   -4.008   -0.214
C(Mode)[T.3]    -2.444      0.968   -2.526   0.012   -4.341   -0.548
Group Var        1.447      1.102
=================================================================
```

```
Mixed Effects Model für: robot_parts_were_my_body_parts
                Mixed Linear Model Regression Results
=================================================================================
Model:            MixedLM Dependent Variable: robot_parts_were_my_body_parts
No. Observations: 18      Method:             REML
No. Groups:       6       Scale:              4.7358
Min. group size:  3       Log-Likelihood:     -36.6394
Max. group size:  3       Converged:          Yes
Mean group size:  3.0
---------------------------------------------------------------------------------
                     Coef.     Std.Err.      z       P>|z|    [0.025    0.975]
---------------------------------------------------------------------------------
Intercept             3.000       0.959     3.129    0.002     1.121     4.879
C(Mode)[T.2.0]        2.111       1.256     1.680    0.093    -0.351     4.574
C(Mode)[T.3.0]       -0.556       1.256    -0.442    0.658    -3.018     1.907
Group Var             0.780       0.840
=================================================================================
```

```
                 Mixed Linear Model Regression Results
=========================================================================
Model:            MixedLM Dependent Variable: robot_parts_were_my_body_parts
No. Observations: 18      Method:             REML
No. Groups:       6       Scale:              4.7358
Min. group size:  3       Log-Likelihood:     -36.6394
Max. group size:  3       Converged:          Yes
Mean group size:  3.0
-------------------------------------------------------------------------
                 Coef.   Std.Err.     z      P>|z|   [0.025   0.975]
-------------------------------------------------------------------------
Intercept         5.111     0.959    5.331  0.000    3.232    6.990
C(Mode)[T.1]     -2.111     1.256   -1.680  0.093   -4.574    0.351
C(Mode)[T.3]     -2.667     1.256   -2.122  0.034   -5.129   -0.204
Group Var         0.780     0.840
=========================================================================
```

VEQ Cup

```
Mixed Effects Model für: appearance_of_my_body_changed
                 Mixed Linear Model Regression Results
=========================================================================
Model:            MixedLM Dependent Variable: appearance_of_my_body_changed
No. Observations: 18      Method:             REML
No. Groups:       6       Scale:              2.1136
Min. group size:  3       Log-Likelihood:     -33.9249
Max. group size:  3       Converged:          Yes
Mean group size:  3.0
-------------------------------------------------------------------------
                 Coef.   Std.Err.     z      P>|z|   [0.025   0.975]
-------------------------------------------------------------------------
Intercept         2.556     0.949    2.692  0.007    0.695    4.416
C(Mode)[T.2.0]    0.000     0.839    0.000  1.000   -1.645    1.645
C(Mode)[T.3.0]    0.222     0.839    0.265  0.791   -1.423    1.867
Group Var         3.294     2.130
=========================================================================


                 Mixed Linear Model Regression Results
=========================================================================
Model:            MixedLM Dependent Variable: appearance_of_my_body_changed
No. Observations: 18      Method:             REML
No. Groups:       6       Scale:              2.1136
Min. group size:  3       Log-Likelihood:     -33.9249
Max. group size:  3       Converged:          Yes
Mean group size:  3.0
-------------------------------------------------------------------------
                 Coef.   Std.Err.     z      P>|z|   [0.025   0.975]
-------------------------------------------------------------------------
Intercept         2.556     0.949    2.692  0.007    0.695    4.416
C(Mode)[T.1]      0.000     0.839    0.000  1.000   -1.645    1.645
C(Mode)[T.3]      0.222     0.839    0.265  0.791   -1.423    1.867
Group Var         3.294     2.130
=========================================================================
```

Mixed Effects Model für: felt_like_robot_was_mine

Mixed Linear Model Regression Results

Model:	MixedLM	Dependent Variable:	felt_like_robot_was_mine
No. Observations:	18	Method:	REML
No. Groups:	6	Scale:	2.0691
Min. group size:	3	Log-Likelihood:	-30.0409
Max. group size:	3	Converged:	Yes
Mean group size:	3.0		

	Coef.	Std.Err.	z	P>|z|	[0.025	0.975]
Intercept	2.889	0.614	4.705	0.000	1.686	4.092
C(Mode)[T.2.0]	0.778	0.830	0.937	0.349	-0.850	2.406
C(Mode)[T.3.0]	0.111	0.830	0.134	0.894	-1.517	1.739
Group Var	0.193	0.475				

Mixed Linear Model Regression Results

Model:	MixedLM	Dependent Variable:	felt_like_robot_was_mine
No. Observations:	18	Method:	REML
No. Groups:	6	Scale:	2.0691
Min. group size:	3	Log-Likelihood:	-30.0409
Max. group size:	3	Converged:	Yes
Mean group size:	3.0		

	Coef.	Std.Err.	z	P>|z|	[0.025	0.975]
Intercept	3.667	0.614	5.972	0.000	2.463	4.870
C(Mode)[T.1]	-0.778	0.830	-0.937	0.349	-2.406	0.850
C(Mode)[T.3]	-0.667	0.830	-0.803	0.422	-2.294	0.961
Group Var	0.193	0.475				

Mixed Effects Model für: I_was_cause_the_robots_movements

Mixed Linear Model Regression Results

Model:	MixedLM	Dependent Variable:	I_was_cause_the_robots_movements
No. Observations:	18	Method:	REML
No. Groups:	6	Scale:	3.1655
Min. group size:	3	Log-Likelihood:	-36.3458
Max. group size:	3	Converged:	Yes
Mean group size:	3.0		

	Coef.	Std.Err.	z	P>|z|	[0.025	0.975]
Intercept	6.111	1.065	5.738	0.000	4.024	8.198
C(Mode)[T.2.0]	0.667	1.027	0.649	0.516	-1.347	2.680
C(Mode)[T.3.0]	-0.111	1.027	-0.108	0.914	-2.124	1.902
Group Var	3.639	2.044				

Mixed Linear Model Regression Results

Model:	MixedLM	Dependent Variable:	I_was_cause_the_robots_movements
No. Observations:	18	Method:	REML
No. Groups:	6	Scale:	3.1655
Min. group size:	3	Log-Likelihood:	-36.3458
Max. group size:	3	Converged:	Yes
Mean group size:	3.0		

	Coef.	Std.Err.	z	P>|z|	[0.025	0.975]
Intercept	6.778	1.065	6.364	0.000	4.690	8.865
C(Mode)[T.1]	-0.667	1.027	-0.649	0.516	-2.680	1.347
C(Mode)[T.3]	-0.778	1.027	-0.757	0.449	-2.791	1.236
Group Var	3.639	2.044				

Mixed Effects Model für: movements_robot_my_movements

Mixed Linear Model Regression Results

Model:	MixedLM	Dependent Variable:	movements_robot_my_movements
No. Observations:	18	Method:	REML
No. Groups:	6	Scale:	3.0766
Min. group size:	3	Log-Likelihood:	-36.8057
Max. group size:	3	Converged:	Yes
Mean group size:	3.0		

	Coef.	Std.Err.	z	P>|z|	[0.025	0.975]
Intercept	5.000	1.156	4.323	0.000	2.733	7.267
C(Mode)[T.2.0]	1.000	1.013	0.987	0.323	-0.985	2.985
C(Mode)[T.3.0]	0.111	1.013	0.110	0.913	-1.874	2.096
Group Var	4.948	2.638				

Mixed Linear Model Regression Results

Model:	MixedLM	Dependent Variable:	movements_robot_my_movements
No. Observations:	18	Method:	REML
No. Groups:	6	Scale:	3.0766
Min. group size:	3	Log-Likelihood:	-36.8057
Max. group size:	3	Converged:	Yes
Mean group size:	3.0		

	Coef.	Std.Err.	z	P>|z|	[0.025	0.975]
Intercept	6.000	1.156	5.188	0.000	3.733	8.267
C(Mode)[T.1]	-1.000	1.013	-0.987	0.323	-2.985	0.985
C(Mode)[T.3]	-0.889	1.013	-0.878	0.380	-2.874	1.096
Group Var	4.948	2.638				

```
Mixed Effects Model für: movements_of_robot_weer_in_syn_with_mine
                    Mixed Linear Model Regression Results
================================================================================
Model:            MixedLM Dependent Variable: movements_of_robot_weer_in_syn_with_mine
No. Observations: 18      Method:             REML
No. Groups:       6       Scale:              3.1259
Min. group size:  3       Log-Likelihood:     -36.5622
Max. group size:  3       Converged:          Yes
Mean group size:  3.0
--------------------------------------------------------------------------------
                     Coef.       Std.Err.         z         P>|z|       [0.025       0.975]
--------------------------------------------------------------------------------
Intercept             4.000          1.106       3.618       0.000        1.833        6.167
C(Mode)[T.2.0]        1.667          1.021       1.633       0.103       -0.334        3.667
C(Mode)[T.3.0]        2.000          1.021       1.959       0.050       -0.001        4.001
Group Var             4.207          2.300
================================================================================
```

```
                    Mixed Linear Model Regression Results
================================================================================
Model:            MixedLM Dependent Variable: movements_of_robot_weer_in_syn_with_mine
No. Observations: 18      Method:             REML
No. Groups:       6       Scale:              3.1259
Min. group size:  3       Log-Likelihood:     -36.5622
Max. group size:  3       Converged:          Yes
Mean group size:  3.0
--------------------------------------------------------------------------------
                    Coef.        Std.Err.         z          P>|z|       [0.025       0.975]
--------------------------------------------------------------------------------
Intercept            5.667          1.106       5.126       0.000        3.500        7.833
C(Mode)[T.1]        -1.667          1.021      -1.633       0.103       -3.667        0.334
C(Mode)[T.3]         0.333          1.021       0.327       0.744       -1.667        2.334
Group Var            4.207          2.300
================================================================================
```

```
Mixed Effects Model für: robot_belonged_to_me
             Mixed Linear Model Regression Results
=====================================================================
Model:            MixedLM Dependent Variable: robot_belonged_to_me
No. Observations: 18      Method:             REML
No. Groups:       6       Scale:              3.4815
Min. group size:  3       Log-Likelihood:     -36.1647
Max. group size:  3       Converged:          Yes
Mean group size:  3.0
---------------------------------------------------------------------
                   Coef.   Std.Err.    z     P>|z|  [0.025  0.975]
---------------------------------------------------------------------
Intercept           4.889     0.994   4.917  0.000   2.940   6.838
C(Mode)[T.2.0]      1.111     1.077   1.031  0.302  -1.000   3.223
C(Mode)[T.3.0]     -0.111     1.077  -0.103  0.918  -2.223   2.000
Group Var           2.449     1.499
=====================================================================
```

Mixed Linear Model Regression Results

Model:	MixedLM	Dependent Variable:	robot_belonged_to_me
No. Observations:	18	Method:	REML
No. Groups:	6	Scale:	3.4815
Min. group size:	3	Log-Likelihood:	-36.1647
Max. group size:	3	Converged:	Yes
Mean group size:	3.0		

	Coef.	Std.Err.	z	P>|z|	[0.025	0.975]
Intercept	6.000	0.994	6.035	0.000	4.051	7.949
C(Mode)[T.1]	-1.111	1.077	-1.031	0.302	-3.223	1.000
C(Mode)[T.3]	-1.222	1.077	-1.135	0.257	-3.334	0.889
Group Var	2.449	1.499				

Mixed Effects Model für: robot_like_human

Mixed Linear Model Regression Results

Model:	MixedLM	Dependent Variable:	robot_like_human
No. Observations:	18	Method:	REML
No. Groups:	6	Scale:	2.5728
Min. group size:	3	Log-Likelihood:	-33.2591
Max. group size:	3	Converged:	Yes
Mean group size:	3.0		

	Coef.	Std.Err.	z	P>|z|	[0.025	0.975]
Intercept	3.111	0.794	3.918	0.000	1.555	4.667
C(Mode)[T.2.0]	0.333	0.926	0.360	0.719	-1.482	2.148
C(Mode)[T.3.0]	-0.111	0.926	-0.120	0.904	-1.926	1.704
Group Var	1.210	0.998				

Mixed Linear Model Regression Results

Model:	MixedLM	Dependent Variable:	robot_like_human
No. Observations:	18	Method:	REML
No. Groups:	6	Scale:	2.5728
Min. group size:	3	Log-Likelihood:	-33.2591
Max. group size:	3	Converged:	Yes
Mean group size:	3.0		

	Coef.	Std.Err.	z	P>|z|	[0.025	0.975]
Intercept	3.444	0.794	4.338	0.000	1.888	5.001
C(Mode)[T.1]	-0.333	0.926	-0.360	0.719	-2.148	1.482
C(Mode)[T.3]	-0.444	0.926	-0.480	0.631	-2.260	1.371
Group Var	1.210	0.998				

Mixed Linear Model Regression Results

Model:	MixedLM	Dependent Variable:	robot_parts_were_my_body_parts
No. Observations:	18	Method:	REML
No. Groups:	6	Scale:	4.7702
Min. group size:	3	Log-Likelihood:	-35.7382
Max. group size:	3	Converged:	No
Mean group size:	3.0		

	Coef.	Std.Err.	z	P>|z|	[0.025	0.975]
Intercept	3.667	0.895	4.099	0.000	1.913	5.420
C(Mode)[T.2.0]	0.667	1.261	0.529	0.597	-1.805	3.138
C(Mode)[T.3.0]	-0.444	1.261	-0.352	0.724	-2.916	2.027
Group Var	0.031	0.759				

Mixed Linear Model Regression Results

Model:	MixedLM	Dependent Variable:	robot_parts_were_my_body_parts
No. Observations:	18	Method:	REML
No. Groups:	6	Scale:	4.7702
Min. group size:	3	Log-Likelihood:	-35.7382
Max. group size:	3	Converged:	No
Mean group size:	3.0		

	Coef.	Std.Err.	z	P>|z|	[0.025	0.975]
Intercept	4.333	0.895	4.844	0.000	2.580	6.087
C(Mode)[T.1]	-0.667	1.261	-0.529	0.597	-3.138	1.805
C(Mode)[T.3]	-1.111	1.261	-0.881	0.378	-3.583	1.360
Group Var	0.031	0.759				